

AD-A139 910	VIBRATION CONTROL OF SPACE STRUCTURES VCOSS B: MOMENTUM EXCHANGE AND TRUS. (U) TRW SPACE AND TECHNOLOGY GROUP REDONDO BEACH CA L BRADY ET AL. JUL 83	1/2
UNCLASSIFIED	AFMIL-TR-83-3075 F33615-81-C-3235	F/G 20/11 NL

AD-A139 910	VIBRATION CONTROL OF SPACE STRUCTURES VCOSS B: MOMENTUM EXCHANGE AND TRUS. (U) TRW SPACE AND TECHNOLOGY GROUP REDONDO BEACH CA L BRADY ET AL. JUL 83	1/2
UNCLASSIFIED	AFMIL-TR-83-3075 F33615-81-C-3235	F/G 20/11 NL

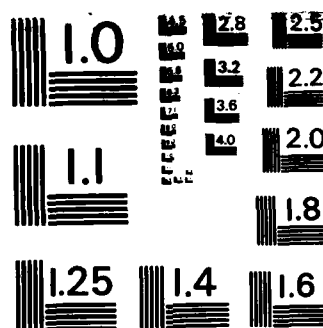
AD-A139 910	VIBRATION CONTROL OF SPACE STRUCTURES VCOSS B: MOMENTUM EXCHANGE AND TRUS. (U) TRW SPACE AND TECHNOLOGY GROUP REDONDO BEACH CA L BRADY ET AL. JUL 83	1/2
UNCLASSIFIED	AFMIL-TR-83-3075 F33615-81-C-3235	F/G 20/11 NL

UNCLASSIFIED AFWAL-TR-83-3075 F33615-81-C-3235 F/G 20/11 NL

UNCLASSIFIED AFWAL-TR-83-3075 F33615-81-C-3235 F/G 20/11 NL

UNCLASSIFIED AFWAL-TR-83-3075 F33615-81-C-3235 F/G 20/11 NL

UNCLASSIFIED AFWAL-TR-83-3075 F33615-81-C-3235 F/G 20/11 NL



MICROCOPY RESOLUTION TEST CHART  
NATIONAL BUREAU OF STANDARDS-1963-A

AD **A139910**

AFWAL-TR-83-3075

12



# Vibration Control of Space Structures VCOSS B: Momentum Exchange and Truss Dampening

TRW Space and Technology Group  
One Space Park  
Redondo Beach, CA 90278

July 1983

Final Report for Period August 1981 to July 1983

Approved for public release; distribution unlimited

DTIC FILE COPY

DTIC

APR 10 84

A

Flight Dynamics Laboratory  
Air Force Wright Aeronautical Laboratories  
Air Force Systems Command

84 04 09 110

NOTICE

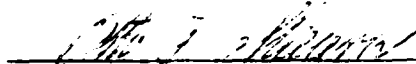
When Government drawings, specifications, or other data are used for any purpose other than in connection with a definitely related Government procurement operation, the United States Government thereby incurs no responsibility nor any obligation whatsoever; and the fact that the government may have formulated, furnished, or in any way supplied the said drawings, specifications, or other data, is not to be regarded by implication or otherwise as in any manner licensing the holder or any other person or corporation, or conveying any rights or permission to manufacture, use, or sell any patented invention that may in any way be related thereto.

This report has been reviewed by the Information Office (OI) and is releasable to the National Technical Information Service (NTIS). At NTIS, it will be available to the general public, including foreign nations.

This technical report has been reviewed and is approved for publication.




JEROME PEARSON, Project Engineer  
Engineering Technology Group  
Structural Vibration Branch



OTTO F. MAURER, Acting Technical Manager  
Engineering Technology Group  
Structural Vibration Branch

FOR THE COMMANDER



RALPH L. KUSTER, JR., Colonel, USAF  
Chief, Structures and Dynamics Division

"If your address has changed, if you wish to be removed from our mailing list, or if the addressee is no longer employed by your organization please notify AFWEL/FIBG, W-PAFB, OH 45433 to help us maintain a current mailing list".

Copies of this report should not be returned unless return is required by security considerations, contractual obligations, or notice on a specific document.

SECURITY CLASSIFICATION OF THIS PAGE (When Data Entered)

DD FORM 1473 EDITION OF 1 NOV 65 IS OBSOLETE

SECURITY CLASSIFICATION OF THIS PAGE (When Data Is Available)

UNCLASSIFIED

SECURITY CLASSIFICATION OF THIS PAGE(When Data Entered)

- (3) Graphic representation of system performance (LOS errors).
- (4) Comparison of active controlled to stiffness controlled model.

During this phase an emphasis was placed on development of control hardware and its impact on spacecraft power and weight budgets. A preliminary estimate of the implementation costs associated with the chosen design was also made. An evaluation of the selected hardware is presented.

It was determined that the mission requirements could be met and that the hardware necessary to achieve these requirements is essentially existing and state of the art in nature. Based on the presented comparison between the active and the stiffness controlled models, it appears that there is a substantial payoff in active control.

UNCLASSIFIED

SECURITY CLASSIFICATION OF THIS PAGE(When Data Entered)

## FOREWORD

The work reported herein was performed by TRW Spacecraft Engineering Division. The study was supported by the Defense Advanced Research Projects Agency of the Department of Defense and Air Force Wright Aeronautical Laboratories. It was monitored by AFWAL/FIBG, Wright-Patterson Air Force Base as part of the Contract No. F33615-81-C-3235. This report covers the period from 1 August 1981 through 1 July 1983. The technical monitor was Jerome Pearson of AFWAL/FIBG.

Milton H. Gran was the Project Manager. The study was performed within the Control Sensors and Systems Laboratory, Dr. I. J. Williams, Manager. The contributors to this report were Mr. John Kern, Dr. Frank Tung, Mr. Lee Brady, Mr. Leroy Keranen and Ms. Gloria Franco.

Distribution	
Available to	
Approved for	
Dist	Special
A-1	



# CONTENTS

<u>Section</u>		<u>Page</u>
I	INTRODUCTION	1
	1. DESIGN GOALS	1
II	CONTROL SYSTEM DESIGN METHODOLOGY	2
	1. POSITIVITY DESIGN APPROACH	2
	2. MULTIVARIABLE FREQUENCY DOMAIN TECHNIQUES	6
III	CONTROL SYSTEM DESIGN RESULTS	9
	1. VCOSS CONTROL PROBLEM	9
	2. DESIGN ITERATIONS	11
	3. VCOSS STRUCTURE WITH MAGNETIC ISOLATOR	13
	4. INTERACTIVE CONTROL SYSTEM DESIGN SOFTWARE	16
	5. ACTUATOR AND SENSOR MODELING	19
	6. VCOSS DESIGN RESULTS	19
IV	GENERAL HARDWARE CONSIDERATIONS	34
	1. MOMENTUM EXCHANGE	34
	2. TRUSS DAMPENING	34
	3. ACTIVE ISOLATION	34
	4. HARDWARE DESIGN PHILOSOPHY	35
	5. SUMMARY OF SELECTED HARDWARE	36
V	ACTUATORS	37
	1. ACTUATOR SELECTION	37
	2. COMPONENT LEVEL REQUIREMENTS	38
	3. CONTROL DEVICE LOCATIONS	39
	4. CANDIDATE ACTUATORS	40
	5. CONTROL DEVICES	43
	6. PERFORMANCE SUMMARY	47
VI	SENSORS	51
	1. REQUIREMENTS	51
	2. SENSOR GOALS	51
	3. CANDIDATE SENSOR CONCEPTS	52
	4. COMPONENTS SPECIFICATIONS	57
	5. RISK ASSESSMENT	57
VII	CONTROL ELECTRONICS	60
	1. ELECTRONICS REQUIREMENTS	60
	2. GOALS ESTABLISHED FOR VCOSS ELECTRONICS	62
	3. CANDIDATES FOR ELECTRONICS	62



## CONTENTS (Concluded)

<u>Section</u>	<u>Page</u>
4. CANDIDATE SELECTION	64
5. ELECTRONICS RISK ASSESSMENT	71
VIII CONCLUSIONS	74
APPENDIXES	
A SENSOR CONFIGURATION, GENERAL CONSIDERATIONS	75
B FIBER ELONGATION SENSOR	87
REFERENCES	99

## ILLUSTRATIONS (Concluded)

<u>Figure</u>		<u>Page</u>
A-5	SAMS breadboard objectives lens holder	84
A-6	SAMS DRA breadboard receiver	85
A-7	SAMS DRA breadboard receiver aft optics	85
B-1	Structural member containing F.O.I.	89
B-2	F.O.I. schematic	89

# TABLES

<u>Table</u>		<u>Page</u>
I	VCOSS Control System Design Iterations	12
II	Structure modes of VCOSS structure with magnetic isolation	14
III	Effect of individual mode to LOS and defocus errors	17
IV	Matrices $V(j\omega)$ and $H_a$	25
V	Error budget	33
VI	Summary of selected hardware	36
VII	Component level requirements	38
VIII	Candidate actuators	40
IX	Capabilities vs requirements	48
X	Actuator control parameters	49
XI	Sensor requirements summary	52
XII	Selected component specifications	58
XIII	Sensor risk assesement	59
XIV	Control electronics requirements	60
XV	Characteristics of control electronics	61
XVI	Electronic candidates	63
XVII	Candidate selections	64
XVIII	Electronics risk assessment	72
XIX	Electronics risk assessment	72
XX	Summary of active control system performance	73
XXI	Stiffness controlled performance	74

## ILLUSTRATIONS (Concluded)

<u>Figure</u>		<u>Page</u>
A-5	SAMS breadboard objectives lens holder	84
A-6	SAMS DRA breadboard receiver	85
A-7	SAMS DRA breadboard receiver aft optics	85
B-1	Structural member containing F.O.I.	89
B-2	F.O.I. schematic	89

## TABLES

<u>Table</u>		<u>Page</u>
I	VCOSS Control System Design Iterations	12
II	Structure modes of VCOSS structure with magnetic isolation	14
III	Effect of individual mode to LOS and defocus errors	17
IV	Matrices $V(j\omega)$ and $H_a$	25
V	Error budget	33
VI	Summary of selected hardware	36
VII	Component level requirements	38
VIII	Candidate actuators	40
IX	Capabilities vs requirements	48
X	Actuator control parameters	49
XI	Sensor requirements summary	52
XII	Selected component specifications	58
XIII	Sensor risk assesement	59
XIV	Control electronics requirements	60
XV	Characteristics of control electronics	61
XVI	Electronic candidates	63
XVII	Candidate selections	64
XVIII	Electronics risk assessment	72
XIX	Electronics risk assessment	72
XX	Summary of active control system performance	73
XXI	Stiffness controlled performance	74

## SECTION I

### INTRODUCTION

Increasing recent interest has developed in precise control of large space structures which contain payloads requiring extremely precise positioning of distributed elements. Large, distributed antennas and mirrors require careful, active structural damping and stiffness designs to maintain surface figure accuracy and element-to-element precision during steady state as well as slewing operations. The objective of this study is to apply modern control techniques and state-of-the-art hardware concepts to an active vibration controlled spacecraft design (Draper Model 2, Rev. 3) and compare its effectiveness to that of a purely passive, stiffness oriented design. Then assuming that the active control system design compares favorably with the passive structural design, the second objective is to define a follow-on program for developing/testing promising hardware technology.

#### 1. DESIGN GOALS

The goal is to reduce the response of the payload to disturbances such that the closed loop line-of-sight errors are  $0.05 \mu\text{rad}$  (x and y axis) and focus errors are  $25 \mu\text{m}$ . This constitutes a reduction of the open loop errors by a factor of 70,000. A constraint on the TRW design is that the disturbance on node 37 cannot be isolated through vibration compensation. Other goals implicit in design process include:

- o Use physically realizable control devices with reasonable performance parameters.
- o Emphasize active control design (particularly for active structural design vs. beam control).
- o Acknowledge impact of solution on other control functions such as slew, absolute line-of-sight pointing (as opposed to vibrations induced), overall optical alignment requirements and thermal orbital disturbance effects on design.

## SECTION II

### CONTROL SYSTEM DESIGN METHODOLOGY

A stability ensuring control system design methodology was developed at TRW during previous LSS technology studies (Refs. 1, 2) (e.g., ACOSS-8, ACOSS-14 and IRAD). It is a combination of the positivity method and the multivariable frequency domain (MFD) method. Each method has merits and shortcomings. A general design process that can best utilize the advantages of both methods is depicted in Figure 1. The positivity approach is used in the first design iteration. It is a conservative design that ensures the stabilities of the closed-loop system. The positivity design is then checked to ensure that it meets the required performance. If so, a design is constituted. Otherwise, system identification techniques may be needed to remove the plant uncertainties so that the multivariable frequency domain method can be safely applied to "tune" the controller for high performance.

This control system design methodology was used in the VCOSS design. The positivity approach was applied first and the resulting design was too conservative to meet ambitious VCOSS performance goals. The positivity design is documented in the interim report (Ref. 3). Since VCOSS assumes the structural model is fairly accurate, this allows use of multivariable frequency domain (MFD) techniques. The MFD design that can be shown to satisfy the performance requirements is presented in Section 3 of this report.

The remainder of this section reviews the positivity method and the MFD method.

#### 1. POSITIVITY DESIGN APPROACH

The positivity approach is briefly reviewed here and the details can be found in reference 1. The primary reason of using the positivity concept in the LSS controller design is that an LSS with collocated, ideal (infinite bandwidth) rate sensors and force actuators can be modeled by a positive operator. The Positivity Theorem states that a positive plant, such as an LSS, and a positive controller in a negative feedback configuration results in a stable, closed-loop system, if at least one of them is

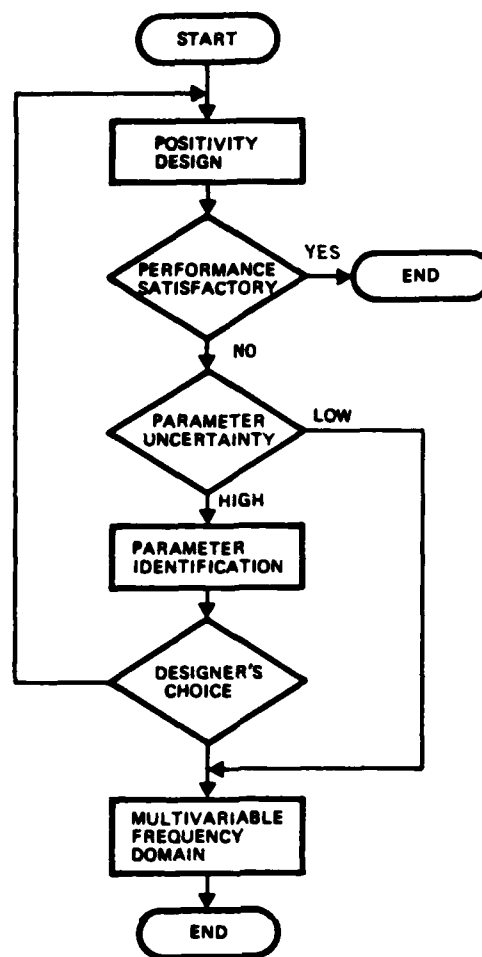


Figure 1. Flowchart of the TRW LSS design approach.

strictly positive. This is true regardless of system parameter uncertainties.

The positivity of a square operator with Laplace transform  $G(s)$  can be determined by first computing the positivity

$$\delta_s(\omega) \triangleq \lambda_{\min} \frac{1}{2} [G(j\omega) + G^*(j\omega)] , \omega \in (0, \infty)$$

where

$\lambda_{\min} \{\cdot\}$  denotes "minimum-eigenvalue-of" and "\*" denotes conjugate-transpose.

If

$\delta(\omega) > 0$  for all  $\lambda$  defined above, then  $G$  is strictly positive real

$\delta(\omega) = 0$  for all  $\lambda$  defined above, then  $G$  is positive real

$\delta(\omega) < 0$  for some  $\lambda$  in the defined range, then  $G$  is not positive



The conditions imposed by the Positivity Theorem are often too restrictive in practice. For example when actuator and sensor dynamics are accounted for, or when actuators and sensors are not collocated, the LSS will no longer be positive. Therefore, the technique of operator embedding is introduced in order to enlarge the class of plants that can be treated by the theorem. Embedding transformations are sets of block diagram manipulations which do not alter a system's stability property.

Two types of embedding transformations are considered: "F" embedding refers to the cascade transformation in Figure 2. "D" embedding refers to the parallel transformation in Figure 3. The important thing to realize about embedding transformations is that they are only mathematical and are not physically implemented. The embedding may impose conditions on the controller which is to be physically implemented. For example, constant "F" embedding may impose that the gain of the controller must be less than some number at all frequencies.

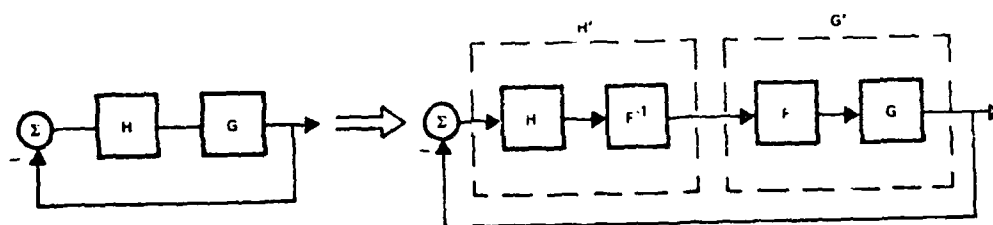


Figure 2. "F" embedding.

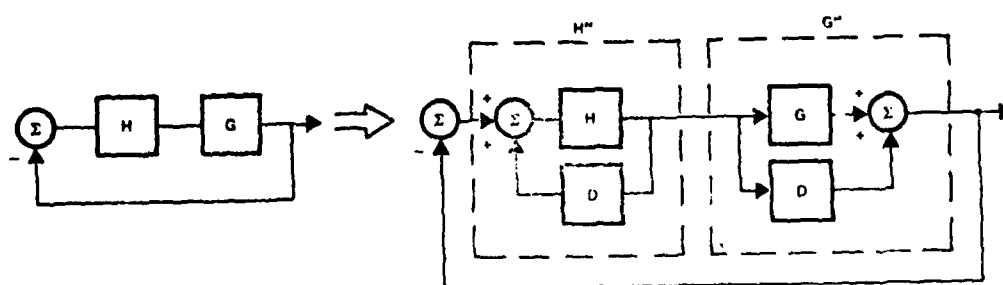


Figure 3. "D" embedding.

Generally, embedding requires some knowledge of the plant to be controlled. For example, constant "D" embedding will require that the norm of the mode shapes and damping ratio of the high frequency modes have been estimated. If additional knowledge of the plant is available, more complex embedding can be used to yield less conservative stability conditions. In a gross manner, embedding permits quantifying stability conditions as a function of system knowledge.

The positivity approach can incorporate some frequency domain compensation techniques in order to meet stability and performance objectives. The two are combined by first determining the characteristic gains and positivity index of the plant and shaping them using techniques similar to those of MacFarlane [Refs. 4, 5]. The shaping network is a precompensator  $M(s)$  which is designed for performance. Once the design of  $M(s)$  is completed, the D embedding operator that makes the precompensated plant positive can be determined. This is typically done by determining the positivity index  $\delta(\omega)$  of the precompensated plant, finding its most negative peak  $\delta_{\min}$ , and choosing  $D = \delta_0 I$ ,  $\delta_0 > -\delta_{\min} > 0$ . The "H" part of the controller consists then merely of gains that must be set to less than or equal to  $1/\delta_0$ . The actually implemented controller satisfying the positivity design is then given by  $(1/\delta_0) M(s)$  (see Figure 4). The actual steps are:

- 1) Determine the characteristic gains  $\lambda(\omega)$  and positivity index  $\delta(\omega)$  of the plant + actuators + sensors.
- 2) Shape characteristic gains and positivity index (cascade compensator  $M(s)$ ) using Nyquist/Bode approach and CAD filter design program
  - o Design for damping
  - o Design for nonmodal sensitivity
  - o Design for noise and disturbance rejection
  - o Design high frequency roll-off characteristics
  - o  $\delta(\omega)$  is shaped for modal sensitivity
- 3) Evaluate positivity index  $\delta(\omega)$  for entire precompensated system and determine  $\delta_{\min}$  (maximum negative peak)
- 4) Implement controller as  $1/\delta_0 * M(s)$  where  $\delta_0 > -\delta_{\min} > 0$

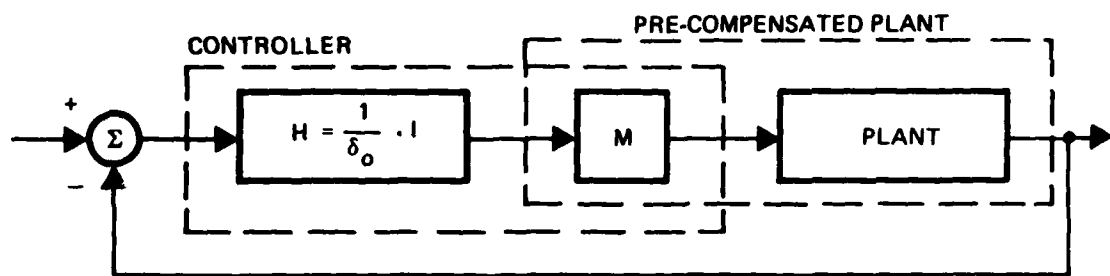


Figure 4. "D" embedding a precompensated plant.

## 2. MULTIVARIABLE FREQUENCY DOMAIN TECHNIQUES

For a square system (equal number of actuators and sensors; non-square system can be squared down [2] to a square one), the feedback control system can be designed using multivariable frequency domain techniques. They are extensions of the classical Nyquist/Bode techniques to the appropriate multivariable case. The key to the development is the characteristic gains  $\lambda(s)$  which are the eigenvalues of the open-loop transfer function  $G(s)$ , i.e.,

$$\text{DET} [\lambda(s) \cdot I - G(s)] = 0; s \in (0, j, \infty, j)$$

The  $m$  by  $m$  matrix-valued complex function  $G(s)$  can be expressed in the dyadic form

$$G(s) = \sum_{i=1}^m \lambda_i(s) w_i(s) v_i^T(s)$$

where

$\{w_i(s); i = 1, 2, \dots, m\}$  are eigenvectors of  $G(s)$ , and

$\{v_i^T(s); i = 1, 2, \dots, m\}$  are the corresponding dual eigenvectors

The importance of the characteristic gains stem from the fact that the closed-loop characteristic gains of a unity feedback system are related to the open-loop values in a manner analogous to single-input-single-output

systems. Consider the disturbance rejection properties of the closed-loop system shown in Figure 5. The transfer function from disturbance  $u$  to output  $y$  can be found to be:

$$\begin{aligned} \frac{y}{u} &= G_c(s) = [I + G(s)]^{-1} \\ &= \sum_{i=1}^m \frac{1}{1 + \lambda_i(s)} w_i(s) v_i^T(s) \end{aligned}$$

For disturbance rejection, it is desirable that all the characteristic gains have large magnitude over the disturbance frequency band.

Other results using this technique are:

- 1) Closed-loop stability occurs if and only if the net sum of counter-clockwise encirclements of the  $(-1,0)$  point by the characteristic gains is equal to the number of open-loop unstable poles.
- 2) In frequency bands of low interaction, the notions of gain margin and phase margin may be applied as a qualitative assessment of performance.
- 3) There is a relationship between tracking accuracy and the magnitude of the characteristic gains. Under the appropriate assumptions the relationship is analogous to the single-input-single-output case.

Frame alignment--Although the relations between open-loop and closed-loop characteristic gains are well understood, the problem of how to manipulate characteristic gains individually remains a difficult one. In the VCOSS controller design the method of approximately-commutative controller with real frame alignment (Ref. 5) is used.

Let  $W(s)$  and  $V(s)$  be a pair of matrices having  $\{W_i(s)\}$  and  $\{V_i(s)\}$  as columns and rows, respectively. The column vector of  $W(s)$  is normalized to

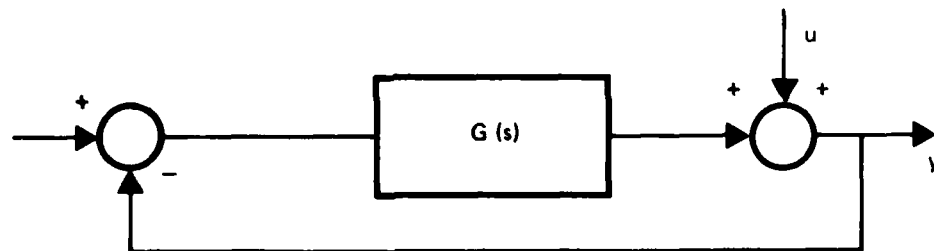


Figure 5. Unity feedback system.

have unit length. The matrices  $W(s)$  and  $V(s)$  are, in general, complex valued. To approximate  $V(s)$  [or  $W(s)$ ] at a specified value of  $s$  by a real matrix  $A$  is referred to as the frame alignment problem.

The column vector of  $A$ ,  $\{A_i\}$  is chosen so as to minimize the quotient

$$\phi_i = \frac{|(V_i, A_i)|^2}{\sum_{\substack{j=1 \\ j \neq i}}^m |(V_j, A_i)|^2}$$

where  $(.,.)$  denotes vector inner product.

It follows that  $A_i$  is the eigenvector corresponding to the maximum eigenvalue of the generalized eigenvalue problem

$$C_i A_i = \lambda_i D_i A_i$$

where

$$C_i = \alpha_i \alpha_i^T + \beta_i \beta_i^T$$

$$D_i = \sum_{\substack{j=1 \\ j \neq i}}^m \alpha_j \alpha_j^T + \beta_j \beta_j^T$$

$\alpha_i$  and  $\beta_i$  are the real and imaginary parts of  $V_i$ , i.e.,  $V_i = \alpha_i + j\beta_i$

A computer program, ALIGN, has been developed at TRW by R.J. Benhabib to carry out the alignment of a complex matrix by a real one. The procedure of controller design using frame alignment is as follows:

- 1) Compute  $W(j\omega)$  and  $V(j\omega)$  at angular frequency involved.
- 2) Compute a real matrix  $H_a$  which approximates  $W(j\omega)$ , using ALIGN.
- 3) Compute a real matrix  $H_b$  which approximates the dual matrix  $V(j\omega)$ , using ALIGN.
- 4) The controller  $H(s)$  is taken to be of the form

$$H(s) = H_a \Lambda(s) H_b$$

where  $\Lambda(s)$  is a diagonal matrix. Its diagonal elements are chosen by the designer to shape the characteristic gains of the combined system.

## SECTION III

### CONTROL SYSTEM DESIGN RESULTS

The control system design methodology described in the previous section is applied to the VCOSS vibration control problem. The design process and results are presented in this section.

#### 1. VCOSS CONTROL PROBLEM

The structure used in the VCOSS design problem is the Draper model #2 revision 3 (see Figure 6 for geometry and Ref. 6 for detail material). The structure consists of a flexible optical support structure ("clean structure") and an equipment section ("dirty box") connected to the clean structure through isolators. The optical system and the line-of-sight (LOS) path are also shown in Figure 6.

The structure is subjected to disturbances acting on nodes 37 and 46. The control system design goal is then to reduce the response of the payload to these disturbances such that the closed-loop LOS errors are less than 0.05  $\mu$ rad (X and Y axes) and focus error is less than 25  $\mu$ m. Furthermore, the control system is to be designed with the following constraints:

- o Disturbance at node 37 cannot be isolated.
- o Actuators cannot be placed on the mirrors.
- o Use physically realizable control devices with reasonable performance parameters (bandwidth, output force).
- o Emphasize active design.

The disturbance is defined in Reference 7. It consists of a broadband disturbance (see Figure 7) and three discrete disturbances at 8, 10 and 20 Hz. Identical but independent disturbances are applied to mode 37 and 46. The broadband disturbances PSD function is modeled as

$$S_{xx}(s) = \frac{G W_c^2}{W_c^2 - s^2}$$

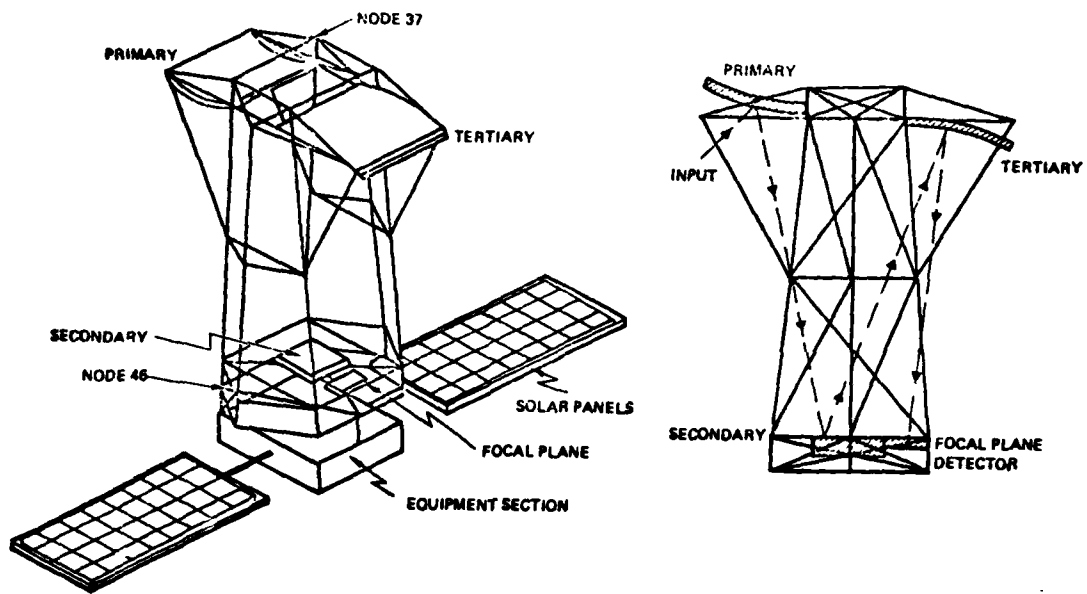


Figure 6. Draper example structure model #2.

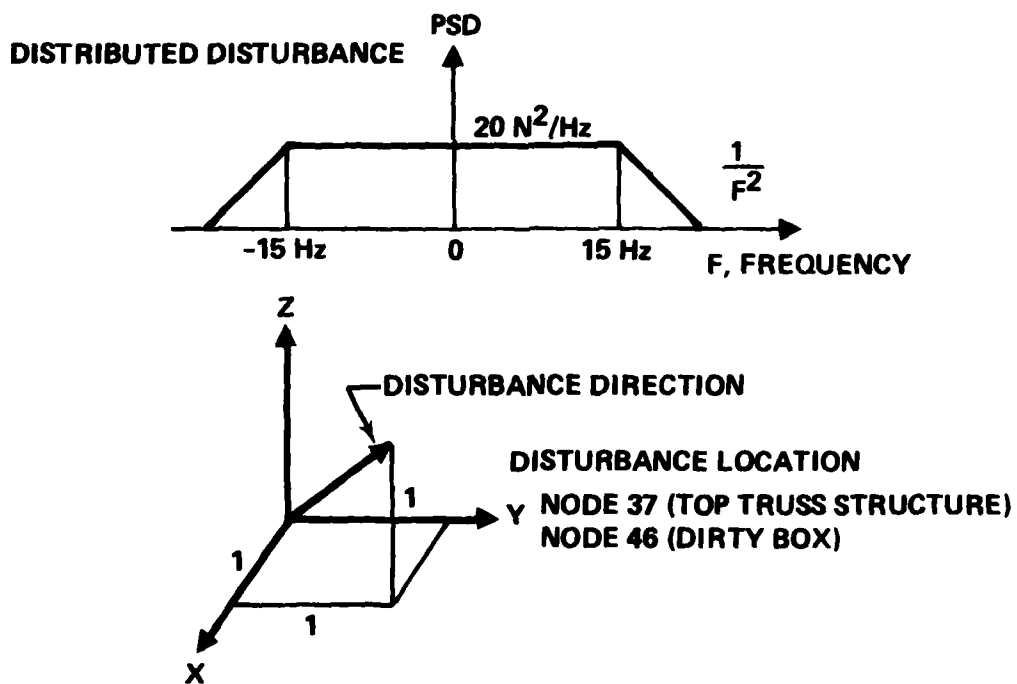


Figure 7. VCOSS broadband disturbance model.

where

$$G = 20 \text{ N-s}$$

$$W_C = 2\pi f_C$$

$$f_C = 15 \text{ Hz}$$

The three discrete disturbances are

$$F_i = 10 \sin(2\pi f_i t) \text{ N}$$

where

$$f_1 = 8 \text{ Hz}$$

$$f_2 = 10 \text{ Hz}$$

$$f_3 = 20 \text{ Hz}$$

For simplicity, it is assumed that the direction of the disturbance makes an equal angle with all three axes at each location. The projection of the input disturbance on each axis is the disturbance given above.

## 2. DESIGN ITERATIONS

The control system has gone through several design iterations. The major steps are listed in Table I. The interim design is the one presented in the interim report (Ref. 3) with the exception that the rigid body modes and the beam control system are omitted. Trusses and isolators are damped using passive dampers that have theoretically infinite bandwidth but currently available hardware can only produce about  $10^4$  to  $10^5$  N-s/m damping. Momentum exchange actuators (MEAs) coupled with accelerometers are used to counteract the disturbance at node 37. The angular motions of the dirty box are controlled by control moment gyros (CMGs). The interim design, because of the deletion of the beam control system, has LOS error of 163  $\mu$ rad and focus error of 2  $\mu$ m.

The interim design was modified in order to improve its performance.

- o Active damper was used for truss and isolator control. It consists of an electromagnetic linear force actuator and a relative rate/position sensor. Assuming actuator bandwidth of 660 Hz and sensor bandwidth of 1000 Hz, the active damper can produce  $10^6$  -  $10^7$  N-s/m damping that is about 2 orders of magnitude higher than the passive one. The active damper also permits position error feedback to



TABLE I. VCOSS CONTROL SYSTEM DESIGN ITERATIONS

Design	Control Systems	LOS/Defocus ( $\mu\text{rad}/\mu\text{m}$ )	Remark
Interim	Truss Damper Isolator MEA (Node 37) CMG	163/2	Beam control loop and rigid body modes are removed
Modified Interim	Truss Damper (Active) Isolator (Active) MEA (Solar Panel) CMG	10/1	Performance is limited by the ability to control symmetric solar panel modes
Reduced Isolator Spring	MEA (Metering Truss) Truss Damper (Active) Isolator (Active)	0.03/0.9	

improve the performance at lower frequencies. The number of truss dampers was increased from 6 to 15 and the locations were also rearranged.

- o It was noticed from CSDL modal data that the bulk of the LOS errors were due to modes having strong coupling with the solar panels, e.g., modes 7, 9, 13, 14 and 15 (0.114, 0.150, 0.196, 0.615 and 0.636 Hz, respectively). Thus, momentum exchange actuators and accelerometers are collocated at the midpoint (nodes 50 and 55) of the solar panels in the Y and Z direction (four pairs in total). Since the momentum exchange actuator has limited travel and the accelerometer has high noise level at low frequencies, the feedback loop is then assumed to have low frequency cutoff at 1 Hz. Although this is higher than the modes it is intended to control, all influential solar panel modes are controlled to some degree. Significant reduction in LOS error is achieved, but it is still far from the goal.
- o The control moment gyro system with some modifications was carried over from interim design. The momentum exchange controller at node 37 was deleted.

The modified interim design reduced LOS and focus errors to 10  $\mu\text{rad}$  and 1  $\mu\text{m}$ , respectively.

Examining the LOS error PSDs showed that the solar panel modes were still the major source of error. They had to be either controlled or isolated from the precision structure. Solar panel vibrations were

difficult to control -- the momentum exchange actuator is limited by its capabilities at lower frequencies, and truss dampers on the solar panels have even less effect since the motions are perpendicular to the truss axial direction. Attention was then turned to the isolator springs. It was felt that the isolator springs were too stiff (5790 N/m), allowing the transmission of the solar panel vibrations to the precision structure. The isolator springs were therefore replaced by magnetic isolation systems which were modeled as very soft springs (10 N/m).

The magnetic isolator greatly reduced the influence of the solar panel modes. The control strategy was to use active truss dampers and momentum exchange actuators to provide stiffness and damping to the precision structure, and to use LOS and defocus information (from optical sensors) and active isolator controller to control LOS and defocus. The performance goal was met with this approach. The design details are presented in the remainder of this section.

### 3. VCOSS STRUCTURE WITH MAGNETIC ISOLATOR

Magnetic isolators were used in order to attenuate the transmission of solar panel vibrations to the precision structure. It was assumed that the magnetic isolator has very weak position control within a properly designed deadband and has position and rate control comparable to the isolator spring it replaced outside the deadband. Thus, in normal operations, the magnetic isolator acts as a very soft spring. Switching to magnetic isolators required a reduction of the isolator spring constant in the finite element model. Since a lightweight structure finite element model was not readily available (TRW has only the modal data), a computer program was developed to modify the existing Revision 3 modal data so that it represents a structure with low isolator spring constant.

The first 24 structure modes and their descriptions are listed in Table II. As expected, all the isolator modes now have much lower frequencies than the solar panel modes. However the price paid is very high in initial open loop LOS and focus errors. A comparison of open loop performance is given in Figure 8 which also shows that the degradation of open loop performance is almost completely due to isolator modes. All higher frequency modes remain unchanged.

TABLE II. STRUCTURE MODES OF VCOSS STRUCTURE WITH MA JETI ISOLATION

MODE	FREQ (RAD/Hz)	DESCRIPTION
7	.043/.0068	ISOLATOR Y - ROT
8	.094/.0149	ISOLATOR Z - ROT
9	.115/.0183	ISOLATOR Z - TRANS
10	.155/.0247	ISOLATOR Y - TRANS
11	.169/.0269	ISOLATOR X - TRANS
12	.173/.0275	ISOLATOR X - ROT
13	.958/.152	S.P. Y - SYM
14	.979/.159	S.P. Z - SYM
15	2.195/.349	S.P. Y - ASYM
16	2.815/.448	S.P. Z - ASYM
17	5.095/.811	S.P. 2ND Y - SYM
18	5.103/.812	S.P. 2ND Z - SYM
19	5.174/.823	S.P. X - ASYM. ROT
20	5.421/.863	S.P. X - SYM. ROT
21	5.630/.896	S.P. 2ND Y - ASYM
22	6.673/1.062	S.P. 2ND Z - ASYM
23	9.381/1.493	STRUCTURE Y - TORSION
24	10.140/1.614	STRUCTURE Z - TORSION

The selection of modes to be included in the design and evaluation models is based upon their individual influence on the LOS or focus errors. The three discrete disturbances are relatively insignificant in comparison with the broadband disturbance. Thus, only the influences due to broadband disturbance are evaluated. Assuming mode  $n$  is the only structural mode, let  $P_{n,LOS}$  denote the LOS error due to mode  $n$ . Then,

$$P_{n,LOS}^2 = \frac{1}{2\pi} \int_{-\infty}^{\infty} S_{xx}(\omega) \frac{|\phi_n^2|}{|\omega_n^2 - \omega^2 + 2\zeta\omega_n\omega|} d\omega$$

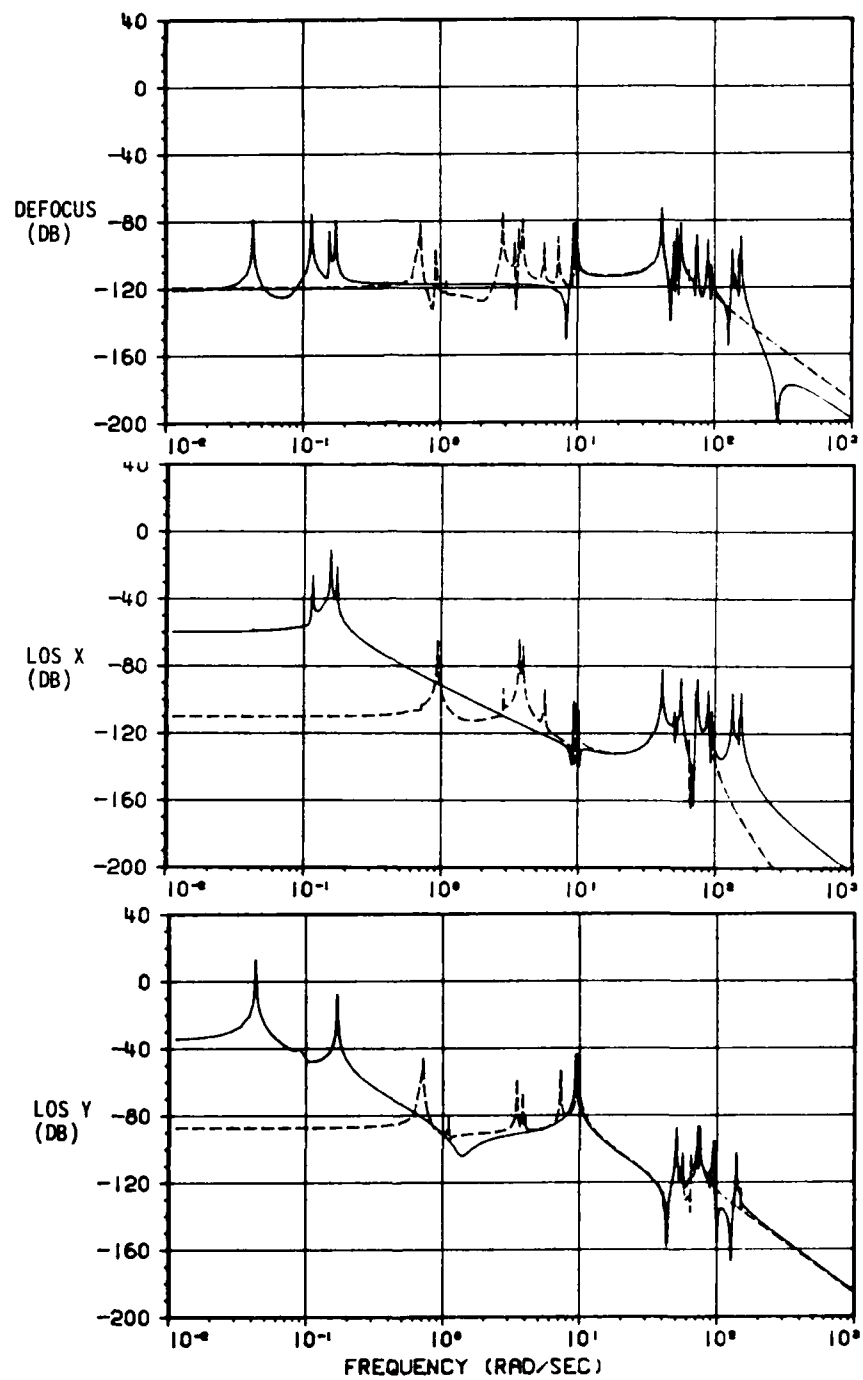
where

$S_{xx}(\omega)$  = the broadband disturbance PSD

$\omega_n$  = mode  $n$  modal frequency

$\zeta$  = damping ratio

$\phi_n^2 = A^2 + B^2 + C^2 + D^2$



----- Revision 3  
 ——— Soft Isolator

Figure 8. LOS and focus errors of revision 3 structure and one with magnetic isolation.

$$A = \phi_{37}^{(n)} \phi_{LOSX}^{(n)}$$

$$B = \phi_{37}^{(n)} \phi_{LOSY}^{(n)}$$

$$C = \phi_{46}^{(n)} \phi_{LOSX}^{(n)}$$

$$D = \phi_{46}^{(n)} \phi_{LOSY}^{(n)}$$

$$\phi_{37}^{(n)} = \phi_{37,X}^{(n)} + \phi_{37,Y}^{(n)} + \phi_{37,Z}^{(n)}$$

$$\phi_{46}^{(n)} = \phi_{46,X}^{(n)} + \phi_{46,Y}^{(n)} + \phi_{46,Z}^{(n)}$$

$$\phi_{i,j}^{(n)} = \text{nth mode shape at node } i \text{ direction } j$$

Each mode's individual contribution to LOS and focus errors are listed in Table III. Two groups of modes are selected. The first group of modes makes up the design model which consists of 18 modes in the lower frequency region. The second group has four higher frequency modes that are added to the design model to form the evaluation model.

The number of modes included in the design and evaluation models were a tradeoff between two factors: (1) the modes included should accurately represent the response of the Draper model #2 to the disturbances, generally, and (2) the analysis programs in use at TRW have a limit on the number of states that can be handled in a time and cost efficient manner.

#### 4. INTERACTIVE CONTROL SYSTEM DESIGN SOFTWARE

Most of the required computer programs have already been developed from previous LSS studies. They were applied to the VCOSS problem with only minor modifications. The relations among these programs are shown in Figure 9, and their main functions are listed below:

- o BMODAL selects modes and actuator/sensor locations from modal data in either NASTRAN or TRWSAP form. It can also compute the G-factors between two nodes at a modal frequency of interest.
- o TOPLOG is a system topology program that permits one to specify the interconnections among subsystem (e.g., LSS structure and controller) and determines the state space representation of the connected system.

TABLE III. EFFECT OF INDIVIDUAL MODE TO LOS AND DEFOCUS ERRORS

LOS/DEFOCUS ERROR OF EACH MODE DUE TO DISTURBANCE AT NODES 27 AND 46

MODE	LOS (URAD)	DEFOCUS (UM)	MODE	LOS (URAD)	DEFOCUS (UM)
● 7	4.23E+04	1.09E+00	● 37	1.58E+01	2.88E+01
● 8	9.67E+02	6.67E-02	38	2.48E+00	7.64E-01
● 9	8.21E+02	2.70E+00	● 39	4.85E+00	1.11E-01
● 10	5.11E+03	9.28E+03	● 40	1.94E+01	5.47E+00
● 11	7.76E+03	9.48E-02	41	1.95E-07	7.03E-09
● 12	1.79E+03	1.99E+00	42	2.23E-07	1.24E-07
13	6.03E-01	8.43E-03	43	7.18E-08	5.36E-08
14	5.23E-03	2.15E-03	44	1.71E-05	7.88E-06
15	5.10E-03	5.99E-04	● 45	2.51E+01	1.49E-01
16	6.54E-01	1.04E-02	46	1.98E+00	1.23E+00
17	1.08E-03	1.98E-04	● 47	8.40E+00	1.13E+01
18	1.30E-04	2.06E-04	● 48	8.03E+00	1.96E+00
19	2.01E-19	2.64E-23	49	3.67E-02	8.21E-01
20	1.52E-03	1.01E-03	50	9.17E-01	2.45E-01
21	2.19E-03	7.12E-05	51	7.08E-01	5.11E-01
22	3.73E-01	6.01E-03	52	1.58E-08	1.87E-08
● 23	3.13E+02	1.08E+01	53	2.11E-09	3.97E-11
● 24	1.56E+01	1.95E+00	54	5.02E-09	1.45E-08
25	3.53E-19	3.94E-23	55	4.06E-07	2.60E-06
26	8.69E-06	7.98E-06	○ 56	8.65E+00	7.37E+00
27	2.54E-17	3.46E-21	57	4.14E-25	3.39E-25
28	1.41E-05	1.32E-05	○ 58	4.27E+00	7.92E-01
29	1.41E-05	3.17E-05	○ 59	1.26E+00	4.48E+00
30	1.09E-06	1.15E-05	60	1.23E-05	4.21E-05
31	1.44E-05	1.22E-07	61	3.37E-01	1.98E-01
32	1.67E-03	4.14E-06	○ 62	9.13E+00	1.95E+01
● 33	2.31E+01	6.82E+01	63	1.64E+00	9.97E-02
● 34	1.41E+01	7.02E+00	64	4.14E+00	1.34E+00
● 35	8.01E-01	1.84E+01	65	1.15E+00	1.02E+00
● 36	4.51E-01	6.31E+00	66	7.12E-01	7.51E-01

● MODE SELECTED FOR DESIGN

○ ADDITIONAL MODE INCLUDED IN PERFORMANCE EVALUATION

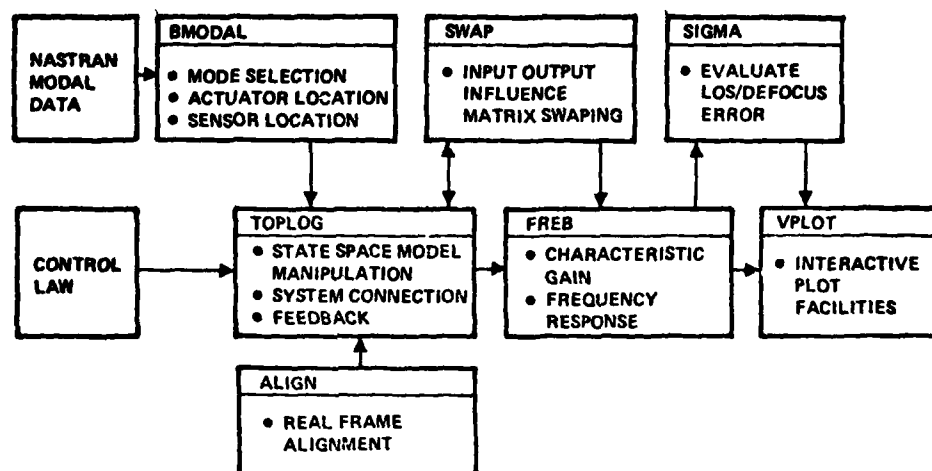


Figure 9. Computer software used in control system design.

- o ALIGN performs the frame alignment algorithm discussed in Section II.2.
- o SWAP allows changes to be made to input and output influence matrices - a program designed to save memory space.
- o FREB computes frequency response, characteristic gains and positivity index function of a multi-input, multi-output system.
- o SIGMA evaluates LOS and focus errors from system frequency responses and disturbance spectrum.
- o VPLOT is an interactive plotting program.

Other programs used to aid the design include:

- o SPRING reduces isolator spring constant and writes a new NASTRAN tape.
- o DISTB evaluates LOS and focus errors associated with each mode under VCOSS broadband disturbance.
- o STRAIN evaluates and sorts for each mode the longitudinal deformation of each truss.

These programs are developed in modular form so that a specific task can be accomplished by executing a sequence of programs. For example, the programs BMODAL, TOPLOG, FREB and VPLOT are run to obtain open loop characteristic gains or positivity index so that feedback gains can be

determined. Return can then be made to TOPLOG to close the loop and execute FREB, SIGMA and VPLOTT to evaluate the performance.

## 5. ACTUATOR AND SENSOR MODELING

One of the requirements in the VCOSS problem is to include realistic control device models in the controller design. Two parameters considered in this study were bandwidth and output force. The bandwidth has direct impact on the controller design and system performance. Disturbance rejection design usually calls for high loop gains which, for stability reasons, are limited by the available actuator and sensor bandwidth. The output force does not enter the design directly. It is estimated afterward and used as one of the requirements in selecting actual hardware.

The actuator used is the linear force type manufactured by Kimco. It is modeled as a first order system:

$$H(s) = \frac{4000}{s + 4000}$$

The bandwidth of a typical Kimco actuator is about 4000-6000 rad/s. Bandwidth of 4000 rad/s was assumed in the design.

Three comments about this model:

- 1) The laboratory experiments of a similar type of actuator show that the attenuation rate at high frequency is about 6 db/decade which is much slower than the 20 db/decade attenuation rate of a first order system.
- 2) The transfer function is a command voltage to output force relation. If the actuator is regulated to follow a current command, the effective bandwidth can be higher.
- 3) The actuator has limit travel. When it is used as a momentum exchange device, it cannot have any effect on the "dc" level. To avoid saturation, the open loop response should have at least two zeros at the origin; otherwise, additional zeros at the origin should be included in the actuator model.

The bandwidth of a sensor is determined not only from its dynamic response time, but also from the signal-to-noise level. The optical sensors such as the triangulation sensor (TAS) and the fiber optical interferometer have very short response times, but their noise levels increase in proportion to the frequency. The actual bandwidth was determined from analysis of signal and



noise. However, it is reasonable to assume that they have a bandwidth of 6000 rad/s and can be modeled as:

$$H(s) = \frac{6000}{s + 6000}$$

The accelerometer has dynamic limit at high frequencies and high noise level at low frequencies, thus it was modeled as a second order system with both high and low frequency cut-offs:

$$H(s) = \frac{s (6000)}{(s + 6) (s + 6000)}$$

## 6. VCOSS DESIGN RESULTS

The VCOSS vibration control baseline design consists of three independent control systems - truss dampening, momentum exchange and active isolation. The locations of control devices are shown in Figure 10. The truss dampening controller provides stiffness and damping to upper and lower support structures. The momentum exchange controller damps the metering truss vibrations, particularly in the X direction. After these two control loops are closed, the precision structure becomes rather stiff. This permits the use of a high bandwidth active isolation controller to drastically reduce the LOS and focus errors.

For each of these designs, a block diagram, characteristic gain plot and plots comparing open-loop and closed-loop performance are presented as well as a more detailed design process description.

a. Truss member damper design--The locations of truss dampers were selected on the basis of their effectiveness in controlling critical modes. A computer program STRAIN was developed to compute for a given mode, the axial direction deformation of each truss member. Besides all the existing truss members, all possible connections between two nodes that do not interfere with the optical path were also considered. The best locations for each critical mode was tabulated, and 12 truss elements, 7 existing ones and 5 additional, were selected. The truss damper locations and control system block diagram are shown in Figure 11.

Force actuators were placed in series with selected truss elements. They have some kind of brake or caging mechanism to provide rigidity in case of actuator failure. However, to model this correctly would require the releasing of the axial constraint of the truss elements involved and

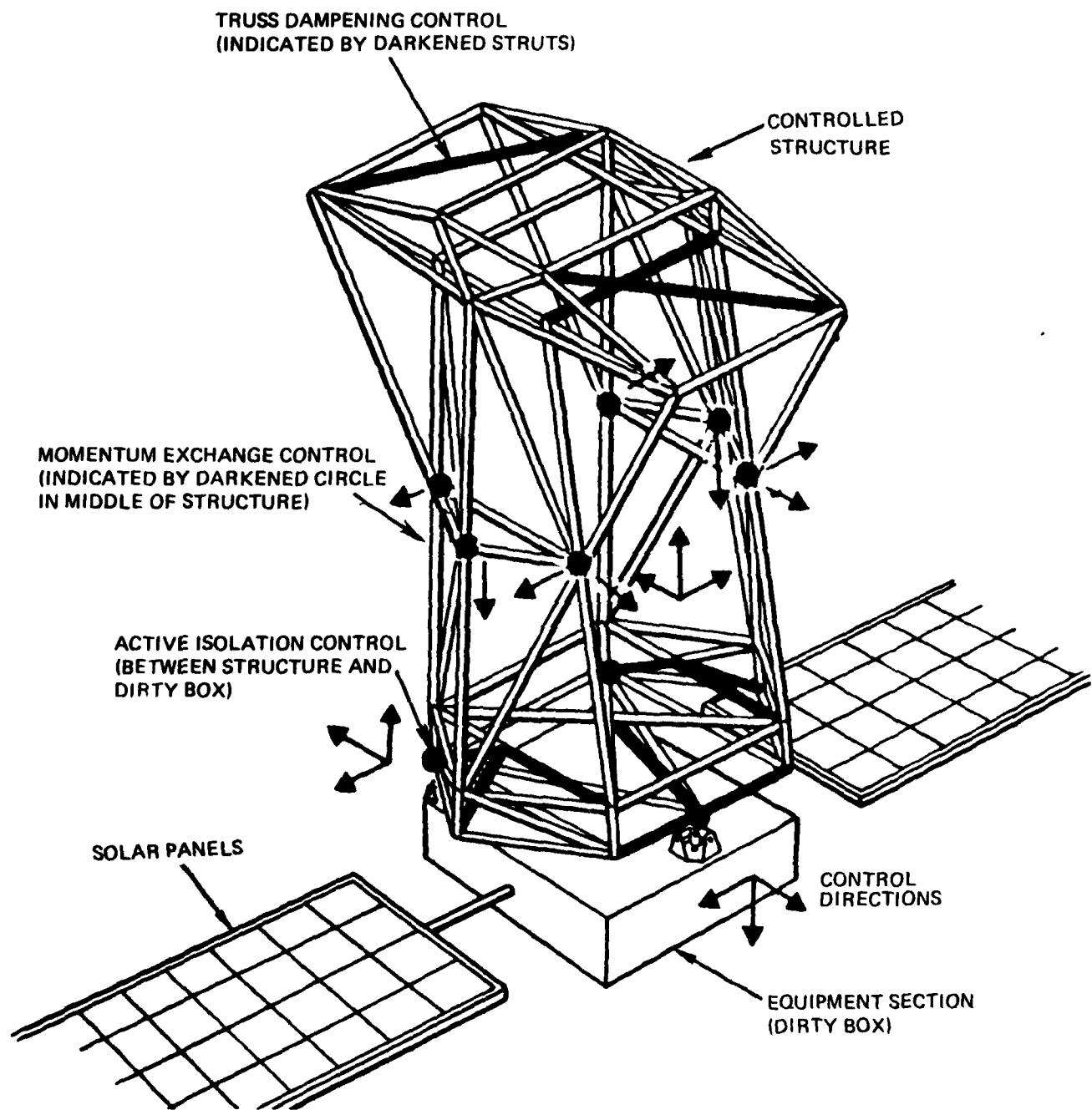
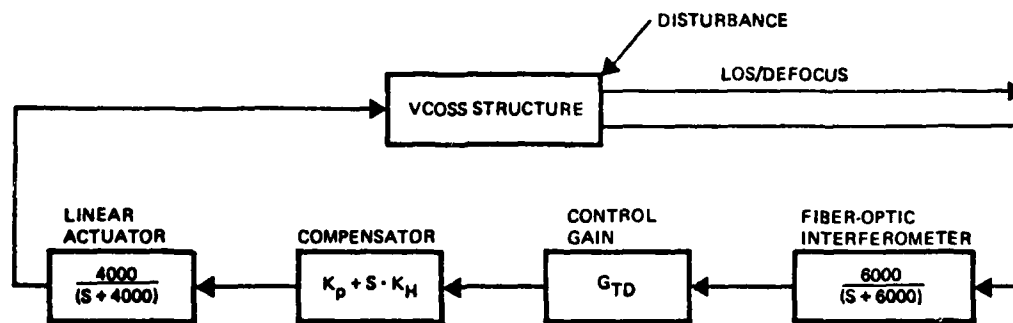


Figure 10. Control device locations.



• Collocated Linear Actuator and F-O Interferometers

<u>Truss</u>	<u>Node A</u>	<u>Node B</u>
4	2	4
6	4	5
32	9	910
39	11	1112
60	27	29
203	3	910
205	6	1112
413*	38	32
415*	37	35
419*	1	910
421*	7	1112
423*	4	40

\* ADDED TRUSS

Figure 11. Truss dampening control system block diagram.

rerunning of the NASTRAN program. Thus, for simplicity, in this study the truss dampers of existing truss elements were modeled as if the actuators were placed in parallel with the truss elements. This would be equivalent to increasing the position feedback gain that represents the stiffness of the corresponding truss element.

The axial direction deformation of the truss element is measured by fiber-optic interferometer with its fiber fixed at the two ends of the truss element. Further details of this sensing system are discussed later in the section on hardware systems.

The controller consists of decoupled position plus rate compensator and control gain matrix  $G_{TD}$  which is computed using the frame alignment procedure. The effect of frame alignment can be seen by comparing the characteristic gain plots shown in Figures 12 and 13. In both cases the compensator gains are temporarily set to  $K_p = 400$  and  $K_R = 1$ . Figure 12 shows the case without frame alignment ( $G_{TD} = I$ ). Some of the modes having low characteristic gains over the controller frequency band will not be controlled by the truss damper. Figure 13 shows the case

$$G_{TD} = H_a \Lambda H_b$$

where

$H_a$  is in alignment with eigenvector,  $V(j\omega)$ , of the open loop transfer function at frequency of 3000 rad/s

$H_b$  is in alignment with the corresponding dual eigenvector  $W(j\omega)$ , and  $\Lambda$  is a diagonal matrix with diagonal elements (1., 1., 2., 2.5., 3., 7., 12., 43., 65., 123., 1000., 500.)

Matrices  $V(j\omega)$  and  $H_a$  are shown in Table IV.

The Nichols plot of the characteristic gain of the open loop system with alignment is shown in Figure 14. A desirable operating point is

$$K_p = 5.6 \times 10^8 \text{ N/m}$$

$$K_R = 1.2 \times 10^6 \text{ N-s/m}$$

The open-loop and closed-loop LOS and focus errors are compared in Figure 15.

b. Momentum exchange controller design--The momentum exchange controller consists of collocated momentum exchange actuators and accelerometers. The objective of this control loop is to reduce the vibrations of the metering truss. The control device locations and the control system block diagram are shown in Figure 16. The control gain  $G_{ME}$  is a diagonal matrix with diagonal elements (50., 1., 12.5, 1.4, 1., 12.5, 1.4, 50.). This means that all the control devices are decoupled and the control law can be implemented by simple analog electronics.

The Nichols plot of the open loop (truss damper loop closed) characteristic gains is shown in Figure 17. A gain of  $K_R = 1000$  is necessary to

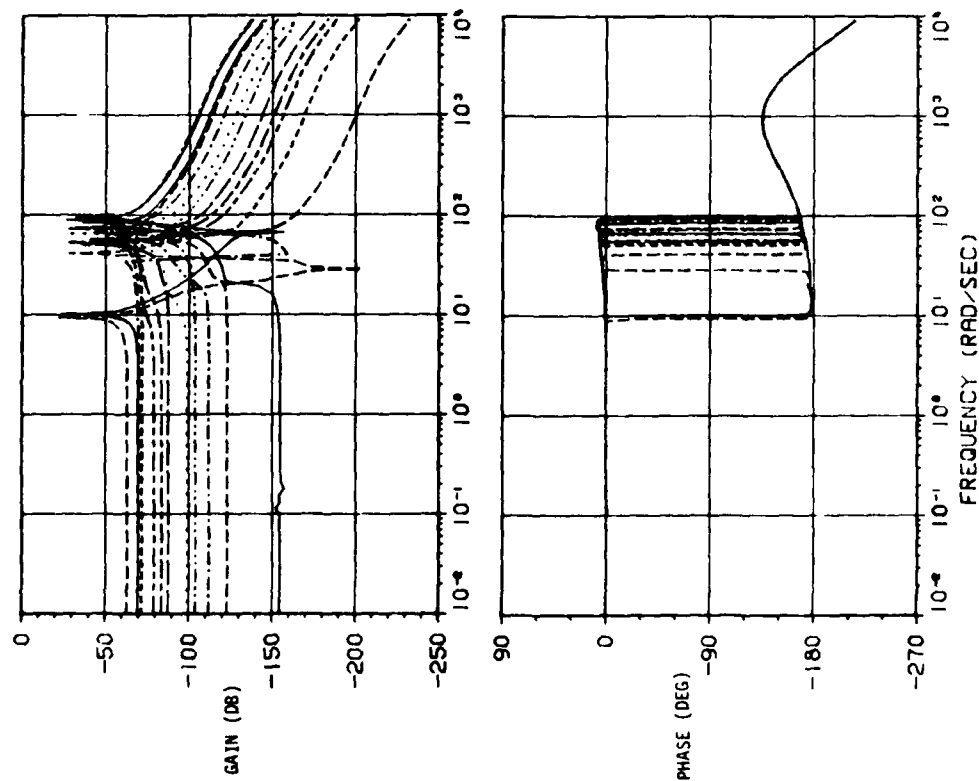


Figure 12. Characteristic gains of truss dampening control system with out frame alignment.

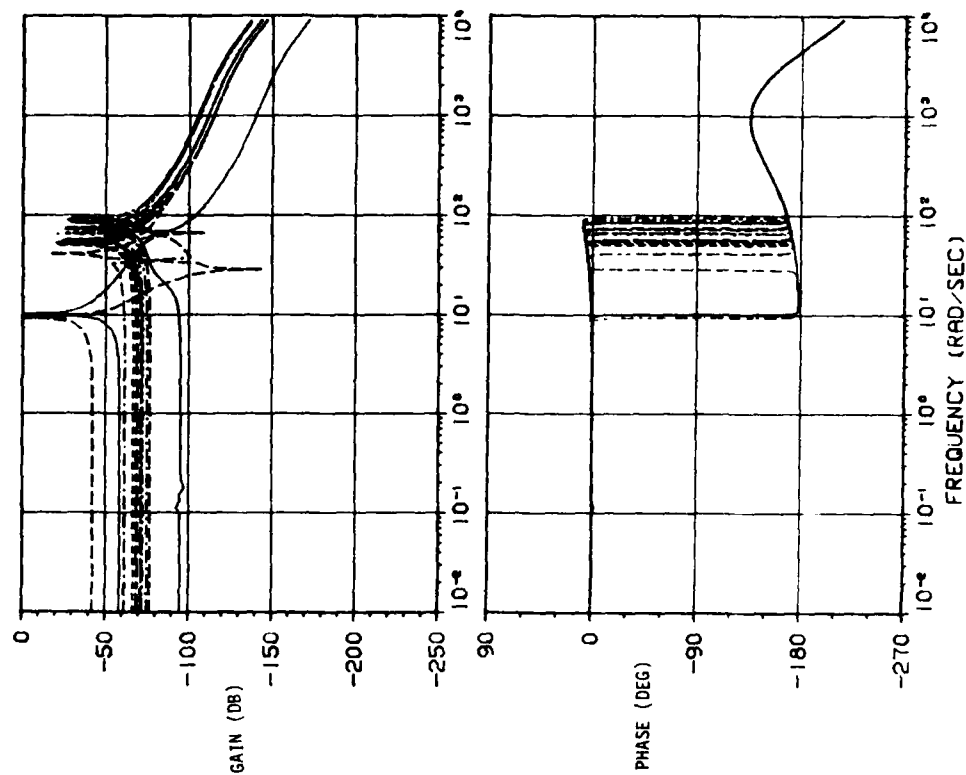


Figure 13. Characteristic gains of truss dampening control system with frame alignment.

TABLE IV. MATRICES  $V(j)$  and  $H_a$ 

1			2			3		
1	( 2.76E-03, 2.26E-06)	(-1.92E-01, 2.37E-06)	(-2.91E-01, 6.10E-05)					
2	( 1.32E-03, 1.70E-06)	(-2.00E-01, 2.43E-06)	(-2.67E-01, 5.64E-05)					
3	( 6.82E-02, 1.40E-05)	( 1.26E-01, -1.18E-06)	( 1.73E-01, -3.57E-05)					
4	( 1.35E-02, 2.78E-06)	( 1.11E-01, -1.58E-06)	( 1.78E-01, -3.53E-05)					
5	( 5.90E-02, 1.42E-05)	( 3.13E-03, 5.51E-07)	( 2.20E-02, -3.40E-06)					
6	( 3.06E-01, 6.75E-05)	(-3.11E-01, 5.12E-06)	( 9.66E-02, -2.13E-05)					
7	(-2.87E-01, -6.01E-05)	(-2.82E-01, 6.04E-07)	( 1.20E-01, -2.62E-05)					
8	( 1.49E-01, 3.63E-05)	(-1.05E-01, 1.18E-06)	( 2.63E-02, -2.43E-06)					
9	( 5.75E-03, -2.88E-06)	(-5.59E-02, 1.98E-06)	( 1.50E-03, -2.47E-06)					
10	( 6.69E-01, 1.45E-04)	(-4.85E-01, 9.51E-06)	( 2.88E-01, -6.16E-05)					
11	(-5.87E-01, -1.20E-04)	(-5.75E-01, 1.35E-06)	( 3.77E-01, -7.95E-05)					
12	( 2.07E-02, 1.58E-06)	( 3.73E-01, -4.71E-06)	( 7.30E-01, -1.53E-04)					
4			5			6		
1	(-2.64E-03, 1.81E-06)	( 4.81E-02, -4.07E-06)	( 9.77E-02, 1.99E-06)					
2	( 1.24E-03, 1.48E-06)	( 2.86E-02, -2.27E-06)	( 1.87E-01, 2.20E-06)					
3	(-2.25E-01, 2.00E-05)	( 4.36E-01, -3.19E-05)	( 2.22E-01, -5.22E-08)					
4	( 1.95E-01, -1.50E-05)	(-3.38E-01, 2.48E-05)	( 8.71E-01, 1.22E-05)					
5	( 2.24E-01, -1.80E-05)	(-6.92E-02, 2.13E-06)	( 4.98E-02, 1.61E-06)					
6	(-9.54E-02, 4.78E-06)	( 1.03E-01, -9.60E-06)	(-4.48E-02, -2.67E-07)					
7	(-5.83E-02, 4.94E-06)	(-1.22E-01, 1.27E-05)	( 6.59E-02, 2.04E-06)					
8	( 7.79E-01, -6.64E-05)	(-2.42E-01, 1.05E-05)	(-2.66E-01, -9.61E-06)					
9	(-4.77E-01, 2.90E-05)	(-7.70E-01, 6.12E-05)	(-1.73E-01, -9.84E-07)					
10	(-9.92E-02, 3.19E-06)	( 1.48E-02, -1.31E-06)	( 6.95E-02, 9.30E-07)					
11	( 5.92E-02, -3.02E-06)	( 9.66E-02, -8.01E-06)	(-1.40E-04, -1.38E-06)					
12	( 1.99E-03, -3.91E-06)	(-2.80E-02, 1.86E-06)	(-1.82E-01, -3.18E-06)					
7			8			9		
1	( 1.25E-01, 1.85E-05)	( 9.33E-02, 4.01E-07)	(-1.59E-01, -3.99E-05)					
2	( 1.66E-02, 5.75E-06)	(-5.06E-01, -3.04E-06)	(-1.03E-01, -3.31E-05)					
3	( 7.07E-01, 9.95E-05)	( 8.14E-02, 2.53E-06)	( 3.70E-01, 9.29E-05)					
4	(-1.43E-02, -1.55E-08)	( 6.41E-02, 5.08E-07)	(-1.14E-01, -2.26E-05)					
5	( 2.66E-01, 4.07E-05)	(-2.30E-01, 5.48E-07)	(-8.33E-02, -3.40E-05)					
6	( 2.45E-01, 3.42E-05)	( 3.65E-01, 1.07E-06)	(-7.25E-01, -1.80E-04)					
7	(-1.72E-01, -2.64E-05)	( 6.28E-01, 1.08E-06)	( 2.87E-01, 5.95E-05)					
8	( 3.29E-01, 4.49E-05)	( 1.10E-01, 2.09E-06)	( 1.78E-01, 4.73E-05)					
9	( 3.61E-01, 4.73E-05)	(-9.46E-02, 2.16E-06)	( 6.10E-02, 1.84E-05)					
10	(-2.53E-01, -3.64E-05)	(-1.58E-01, -1.18E-06)	( 3.38E-01, 8.42E-05)					
11	( 1.16E-01, 1.77E-05)	(-2.87E-01, -5.13E-07)	(-6.45E-02, -1.09E-05)					
12	(-9.29E-02, -1.35E-05)	(-1.21E-01, -8.59E-07)	(-2.16E-01, -5.92E-05)					
10			11			12		
1	(-7.93E-02, 2.06E-05)	(-9.00E-01, 6.27E-06)	( 9.04E-03, -3.61E-06)					
2	( 4.83E-01, -1.18E-04)	( 8.20E-02, -5.20E-07)	( 5.88E-01, -7.27E-20)					
3	( 1.21E-01, -3.06E-05)	(-3.31E-03, -4.32E-08)	( 4.59E-02, 6.52E-06)					
4	( 5.54E-02, -8.89E-06)	( 1.31E-02, -8.03E-08)	(-1.54E-01, -2.75E-06)					
5	(-7.92E-01, 1.90E-04)	( 9.51E-02, -4.63E-07)	( 4.15E-01, -5.17E-06)					
6	( 8.08E-02, -1.37E-05)	( 2.30E-01, -1.56E-06)	( 2.92E-02, -1.45E-05)					
7	(-5.32E-03, -2.93E-06)	( 1.79E-02, -2.53E-08)	( 5.42E-01, 7.65E-06)					
8	( 2.75E-01, -6.65E-05)	(-2.84E-02, 8.94E-08)	(-3.41E-02, 4.72E-06)					
9	( 4.19E-02, -1.07E-05)	(-2.16E-02, 9.24E-08)	(-3.72E-02, 1.62E-06)					
10	(-8.00E-02, 1.65E-05)	(-8.32E-02, 5.70E-07)	(-5.07E-02, 6.74E-06)					

TABL IV. CONC UDED

11 (-3.45E-02, 9.35E-06) ( 2.47E-03, -7.11E-08) (-2.61E-01, -2.46E-06)					
12 ( 1.56E-01, -3.80E-05) (-3.34E-01, 2.36E-06) ( 2.96E-01, -2.93E-06)					
2.76E-03	-1.92E-01	-2.91E-01	-2.64E-03	-4.81E-02	-9.77E-02
1.32E-03	-2.00E-01	-2.67E-01	1.24E-03	-2.86E-02	-1.87E-01
6.82E-02	1.26E-01	1.73E-01	-2.25E-01	-4.36E-01	-2.22E-01
1.35E-02	1.11E-01	1.78E-01	1.95E-01	3.38E-01	-8.71E-01
5.90E-02	3.13E-03	2.20E-02	2.24E-01	6.92E-02	-4.98E-02
3.06E-01	-3.11E-01	9.66E-02	-9.54E-02	-1.03E-01	4.48E-02
-2.87E-01	-2.82E-01	1.20E-01	-5.83E-02	1.22E-01	-6.59E-02
1.49E-01	-1.05E-01	2.63E-02	7.79E-01	2.42E-01	2.66E-01
5.75E-03	-5.59E-02	1.50E-03	-4.77E-01	7.70E-01	1.73E-01
6.69E-01	-4.85E-01	2.88E-01	-9.92E-02	-1.48E-02	-6.95E-02
-5.87E-01	-5.75E-01	3.77E-01	5.92E-02	-9.66E-02	1.40E-04
2.07E-02	3.73E-01	7.30E-01	1.99E-03	2.80E-02	1.82E-01
-1.25E-01	-9.33E-02	1.59E-01	-7.93E-02	9.00E-01	9.04E-03
-1.66E-02	5.06E-01	1.03E-01	4.83E-01	-8.20E-02	5.88E-01
-7.07E-01	-8.14E-02	-3.70E-01	1.21E-01	3.31E-03	4.59E-02
1.43E-02	-6.41E-02	1.14E-01	5.54E-02	-1.31E-02	-1.54E-01
-2.66E-01	2.30E-01	8.33E-02	-7.92E-01	-9.51E-02	4.15E-01
-2.45E-01	-3.65E-01	7.25E-01	8.08E-02	-2.30E-01	2.92E-02
1.72E-01	-6.28E-01	-2.87E-01	-5.32E-03	-1.79E-02	5.42E-01
-3.27E-01	-1.10E-01	-1.78E-01	2.75E-01	2.84E-02	-3.41E-02
-3.61E-01	9.46E-02	-6.10E-02	4.19E-02	2.16E-02	-3.72E-02
2.53E-01	1.58E-01	-3.38E-01	-8.00E-02	8.32E-02	-5.07E-02
-1.16E-01	2.87E-01	6.45E-02	-3.45E-02	-2.47E-03	-2.61E-01
9.29E-02	1.21E-01	2.16E-01	1.56E-01	3.34E-01	2.96E-01

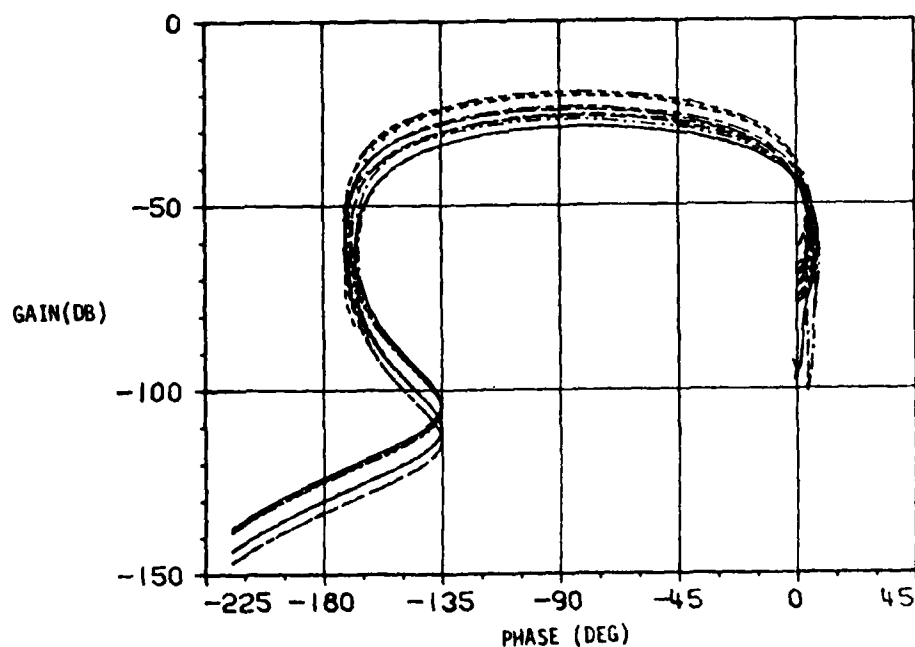
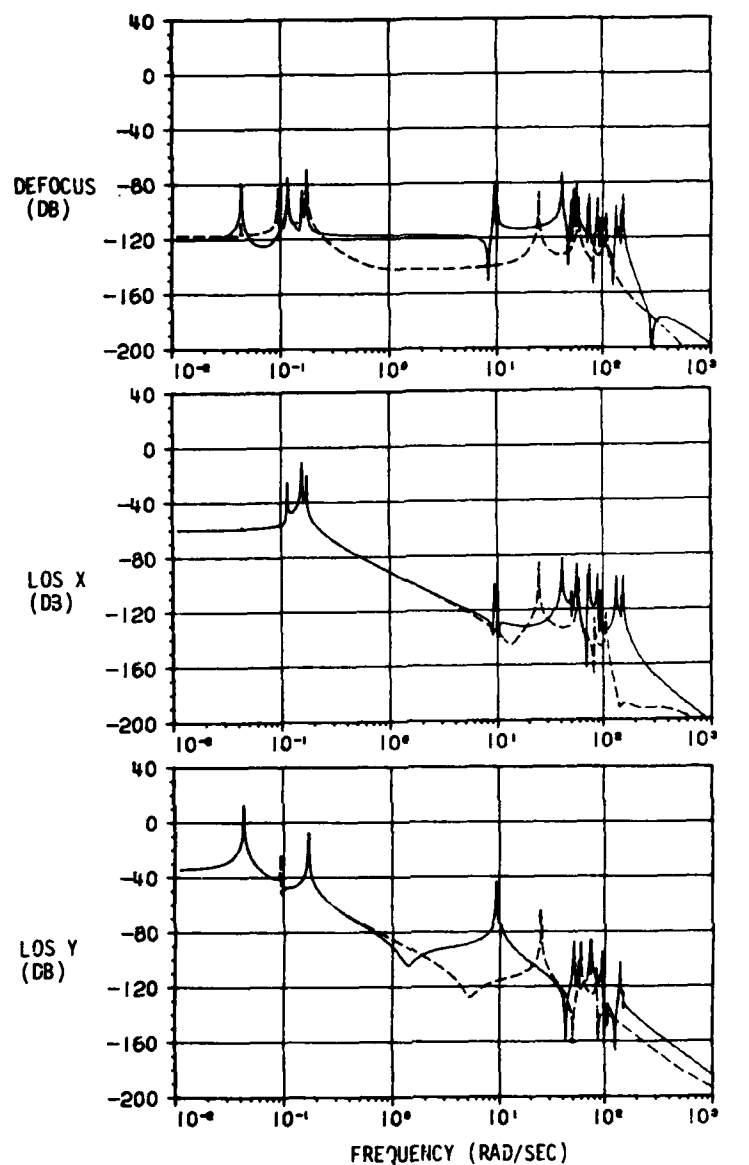


Figure 14. Nichols plot of characteristic gains of truss dampening control system with frame alignment.



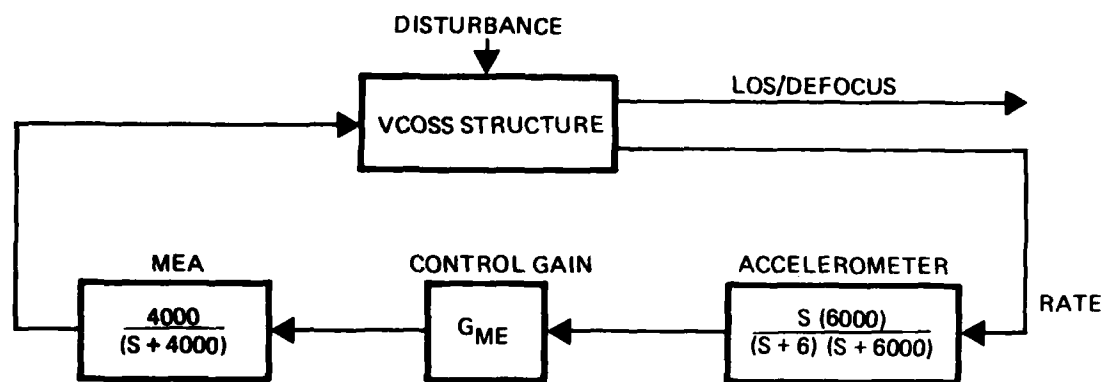
— Open Loop  
 - - - Truss Dampening Control Loop Closed

#### DISTRIBUTED/DISCRETE

	LOS X ( $\mu\text{rad}$ )	LOS Y ( $\mu\text{rad}$ )	DEFOCUS ( $\mu\text{m}$ )
Node 37	3393/.42	26781/1.26	14/.77
Node 46	2167/.003	36091/.004	7/.002
RSS	5812	44942	16

Figure 15. Comparison of open and closed loop LOS and focus errors for truss dampening control system.





• COLLOCATED MOMENTUM EXCHANGE ACTUATOR AND ACCELEROMETER

NODE	DIRECTION
14	Z
15	X
15	Y
16	X
17	X
17	Y
18	X
19	Z

Figure 16. Momentum exchange control system block diagram.

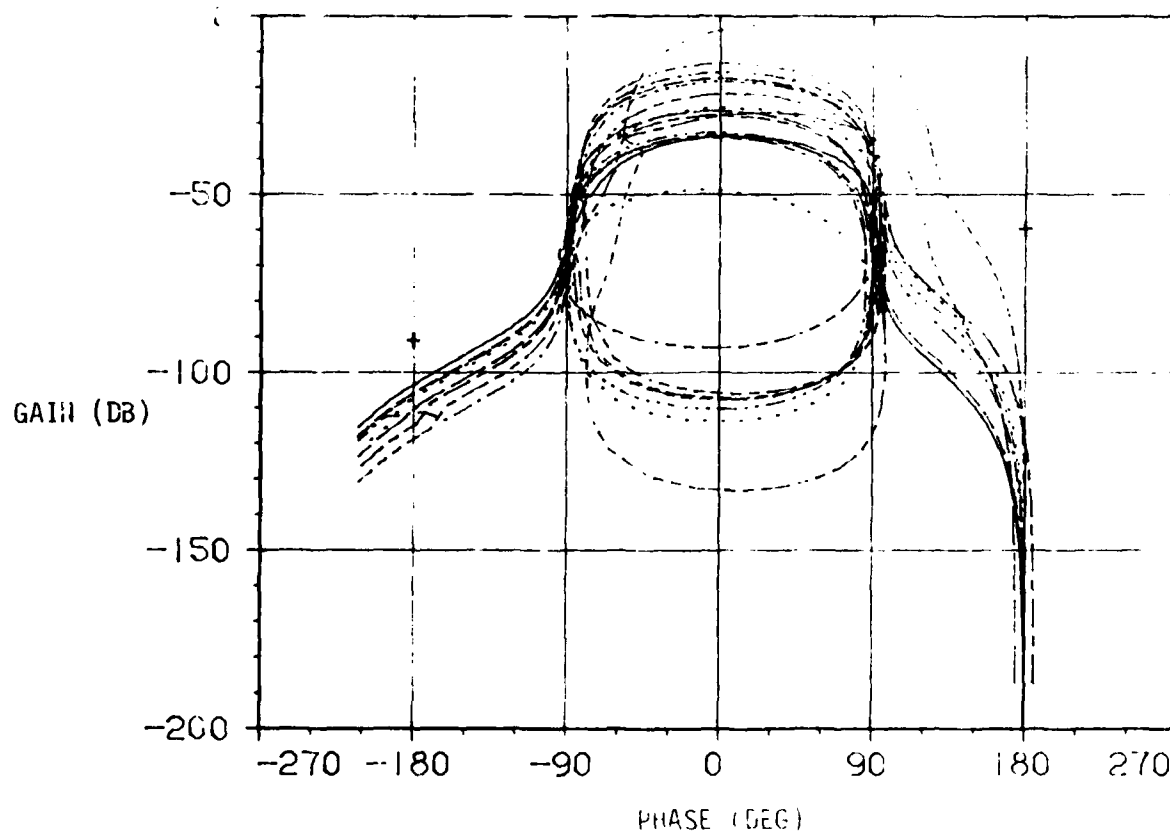


Figure 17. Nichols plot of characteristic gains of momentum exchange control system.

shift the Nichols plot to a desirable operating point. Figure 18 compares the closed-loop (both truss damper and momentum exchange loops closed) and open-loop performance.

c. Active isolator controller design--The control system block diagram is shown in Figure 19. The active isolator is a noncollocated system. The tilt in the X and Y axes of the detector and the three mirrors is measured by four triangulation sensors (TAS); see section on hardware systems for details. These measurements are used to estimate the LOS errors. There are also four accelerometers mounted on the back of the detector and the mirrors. The defocus is estimated from the accelerometer and the TAS measurements. However, in the controller design the LOS and the defocus estimation matrices are not actually implemented, but rather the LOS and defocus information contained in the structural modal data are used directly.

The active isolator was designed with the truss damping and momentum exchange control loops closed. The control signals are distributed to nine actuators in a manner given by the resolver matrix  $G_{IS}$  which is the pseudo-inverse of the 'dc' transfer matrix from actuators to LOS/defocus. With the choice of  $K_{PL} = 400$ ,  $K_{RL} = 1$ ,  $K_{PD} = 0.2$  and  $K_{RD} = 1$ , the characteristic gains of the open loop (active isolation only, truss dampening and momentum loops closed) system are shaped into a desirable form. Their Nichols plots are shown in Figure 20 which indicates a feedback gain of 50 db can be safely added to the system. This leads to the following compensator parameters:

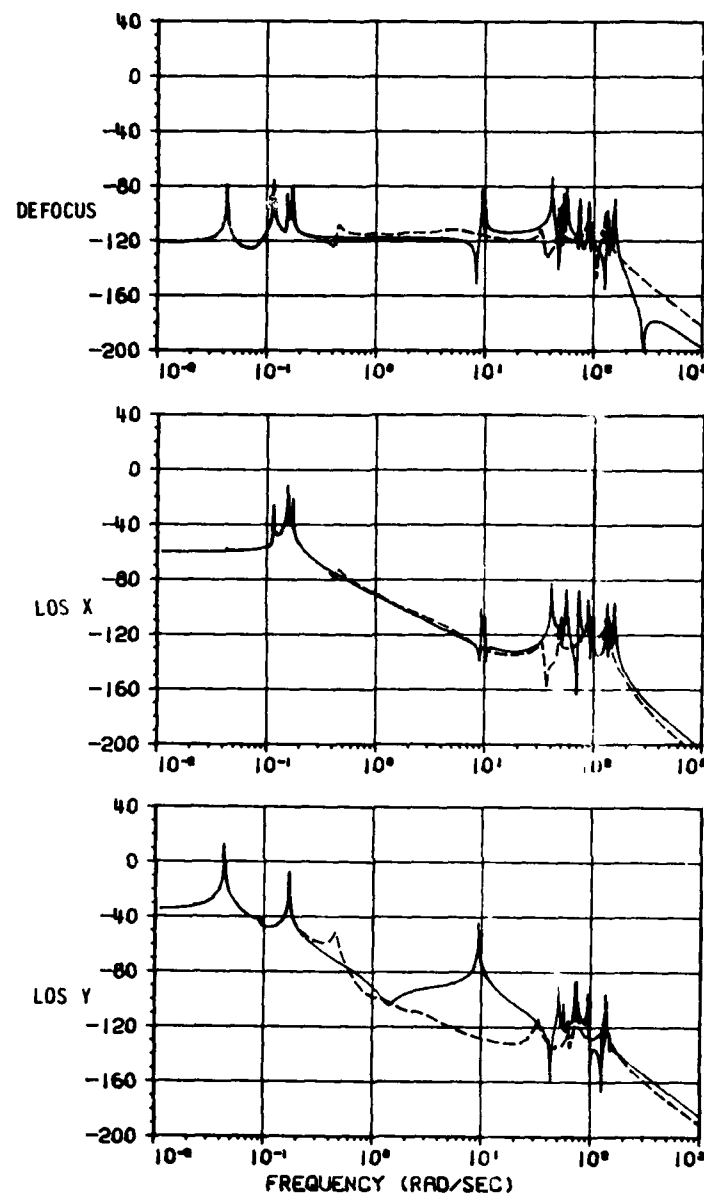
$$K_{PL} = 126400 \text{ N/rad}$$

$$K_{RL} = 316 \text{ N/rad}$$

$$K_{PD} = \text{N/m}$$

$$K_{RD} = 316 \text{ N-s/m}$$

Figure 21 compares the LOS/defocus PSDs for the open-loop (no control) system, the system with truss dampening and momentum exchange loops closed, and the system with all three control loops closed. The active isolator is



— Open loop  
 ----- Truss dampening and momentum exchange loop closed  
 DISTRIBUTED/DISCRETE (RSS)

	<u>LOS-X (<math>\mu</math>RAD)</u>	<u>LOS-Y (<math>\mu</math>RAD)</u>	<u>DEFOCUS (<math>\mu</math>M)</u>
NODE 37	5508/.01	26964/.02	2/.005
NODE 46	1926/.003	35866/.004	7/—
RSS	5835	44871	7

Figure 18. Comparison of open and closed loop, LOS and focus errors

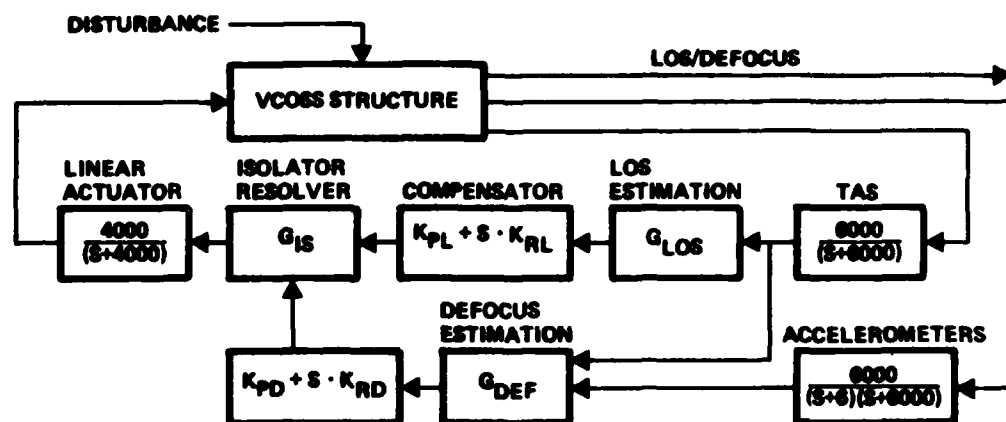


Figure 19. Active isolation control system block diagram.

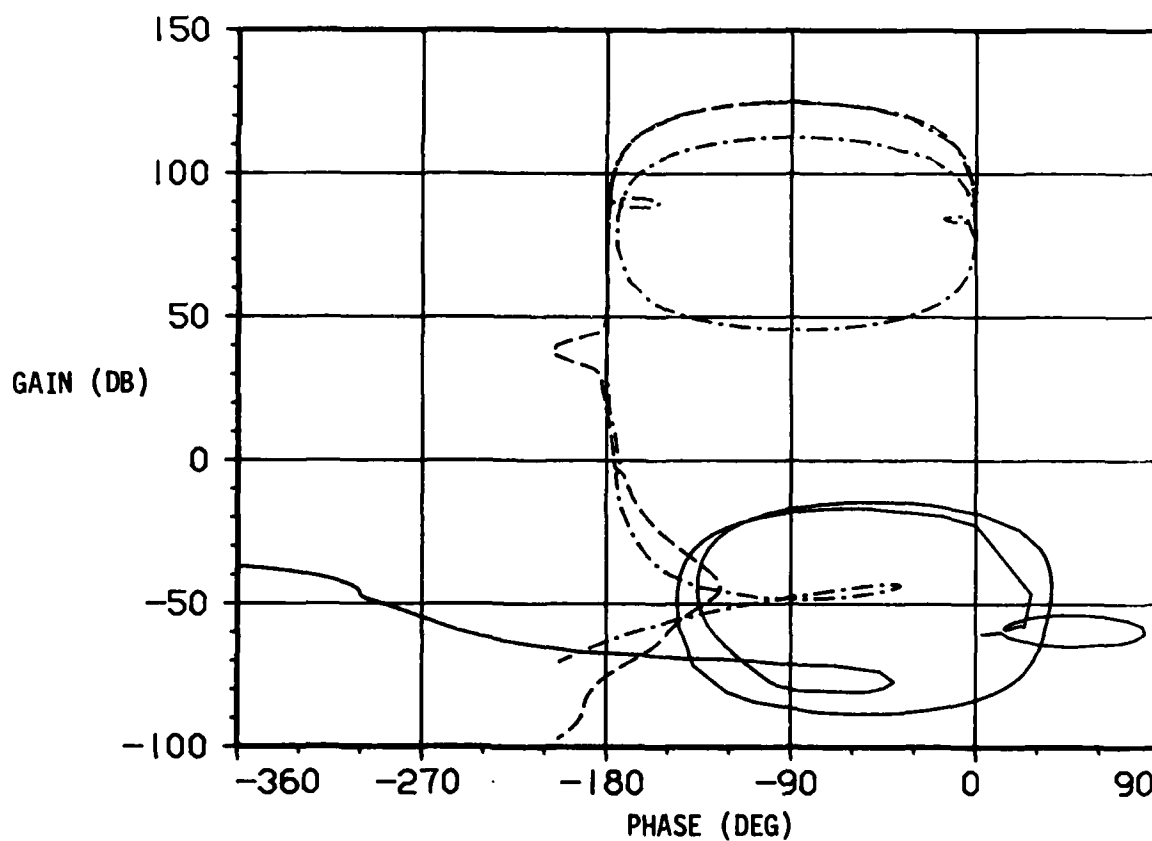
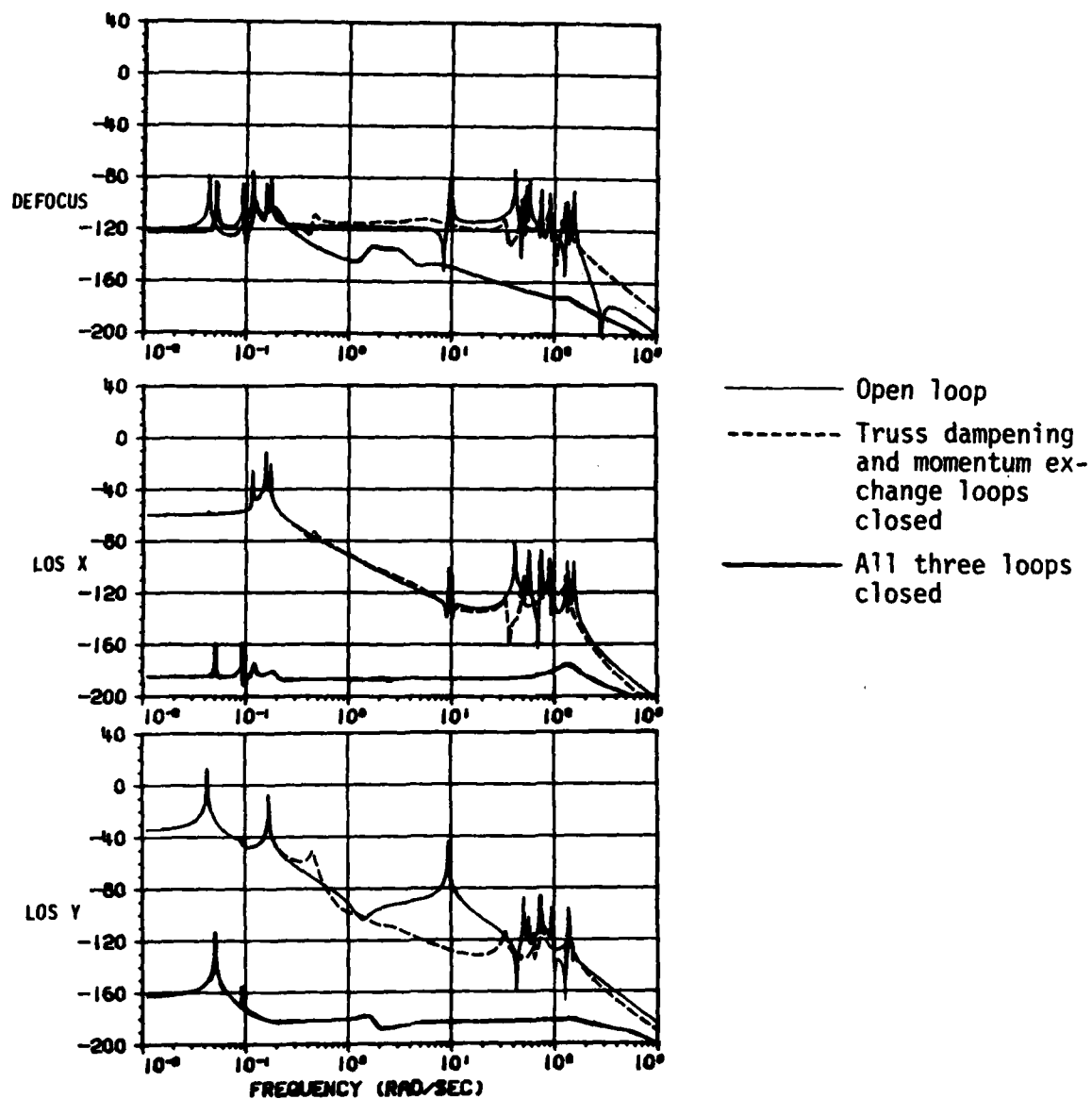


Figure 20. Nichols plot of active isolation control system open-loop (truss damping and momentum exchange loops closed) characteristic gains.



DISTRIBUTED/DISCRETE (RSS)

	<u>LOS-X (<math>\mu</math>RAD)</u>	<u>LOS-Y (<math>\mu</math>RAD)</u>	<u>DEFOCUS (<math>\mu</math>M)</u>
NODE 37	.013/.002	.021/.001	.43/.006
NODE 46	.002/—	.026/—	.78/.002
RSS	.012	.033	.9

Figure 21. Comparison of open and closed loop LOS and focus errors.

very effective in reducing the LOS error but it has almost no control over the defocus error. The LOS/defocus goals can be met with all three control systems active.

d. Design summary--An error budget which roughly accounts for all error sources is listed in Table V. The error due to disturbances was obtained from the above design analysis considering 22 structural modes. Since the characteristics of the hardware noises, including sensor, actuator and electronics, are not available at the present time, certain errors were allocated in the budget to account for their effects on LOS and defocus. The total RSS system errors were 0.052  $\mu$ rad for LOS and 2  $\mu$ m for defocus.

TABLE V. ERROR BUDGET

Source of Error	LOS/Defocus ( $\mu$ rad)/( $\mu$ m)	Basis of Estimate
Disturbance	0.036/0.9	System Analysis
Sensor Noise F-0 Interferometer Accelerometers TAS	0.010/1.0	Allocation
Actuator Noise MED Strut Dampeners Isolators	0.031/1.0	Allocation
Electronics Analog Digital	0.010/1.0	Allocation
Total	0.052/2.0	RSS

## SECTION IV

### GENERAL HARDWARE CONSIDERATIONS

In VCOSS, as with any other controlled design, there are three elements which make up the functional system: sensors, actuators, and an electronic controller. Each has been selected to perform a specific function. The system design is divided into three control categories: momentum exchange, truss dampening and active isolation.

#### 1. MOMENTUM EXCHANGE

Motion sensing is performed using accelerometers placed at nodes 14 through 19 along the appropriate axes (see Figure 10). Signal outputs are processed by an analog controller circuit which in turn drives a momentum exchange actuator.

#### 2. TRUSS DAMPENING

In the case of truss dampening the desired motion to be measured is the elongation of individual structural members. This measurement is performed using a TRW developed fiber optic interferometer. Its output is processed by a serial arithmetic unit. Control signals are then sent to an electromagnetic motor installed in series with the member to be controlled.

#### 3. ACTIVE ISOLATION

The ultimate goal of the VCOSS control system is to minimize line of sight (LOS) and defocus errors in the spacecraft's optical system. To achieve this function it is necessary to measure these errors. A combination of two sensors is required to perform this task.

The LOS, as defined by Henderson (Ref. 6) is a function of mirror (primary, secondary and tertiary) decentrations, radii of curvature (ROC), tilts, separations and effective focal length (EFL). Defocus is a function of axial translations, tilts, separations, ROC and EFL. To measure LOS parameters, TRW-developed triangulation sensors (TAS) are employed. Assuming knowledge of separations, EFL and ROC, they measure decentrations and tilts of all three optical components.

Axial translations of all optics and the focal plane detector array are measured with accelerometers. This combined with tilts measured by TAS give defocus information. Due to the complex nature of these errors, a digital processor is employed to control this loop. Its output drives three, three-axis, electromagnetic isolators located between the structure and the dirty box.

All hardware designs for the entire control system have been system optimized in terms of weight, power consumption and cost. More complete details on the individual components are given in the following sections.

#### 4. HARDWARE DESIGN PHILOSOPHY

During the VCOSS program a design philosophy was adopted which would direct the design effort in a consistent manner. By implementing such an approach, each individual performer would have a set of guidelines in which to make trade decisions. These guidelines were allocated by control system element.

a. Actuator --(details in section V)--During Phase I of this program, different types of actuators were investigated, including several original TRW concepts. Careful review of such devices showed the possibility of no more than a factor of two improvement in performance over the off-the-shelf variety. To improve performance by an order of magnitude would require an extended design effort (outside the scope of VCOSS). It was decided to constrain the actuators to catalog items. Not only would they meet the control system requirements but in doing so, if the VCOSS II control design changed appreciably, a greater flexibility would be afforded in selecting new actuators.

b. Sensors --(details in section VI)--Since a fundamental goal of this program was to achieve better performance by active vibration control rather than by stiffness control, considerations of weight and power consumption were of interest. Once performance requirements were established for each sensor, their designs were constrained to minimize both weight and power consumption.

An additional constraint was placed on the hardware. If required performance could be achieved, the hardware must be available in the time



frame of VCOSS II. This would allow a rollover of the design effort of this program to VCOSS II. Both of these goals were achieved.

c. Electronic controller--(details in section VII)--Three constraints were placed on the electronics design. It must be the simplest design that could meet the control requirements. This implied that different control electronics could be applied to the individual control methods (truss dampening, momentum exchange and active isolation). The electronic designs themselves must be highly reliable. Emphasis was placed on existing hardware that had previously been flight tested. Finally, past experience has shown how expensive these types of hardware really are when made flight worthy. Since VCOSS II was to be a ground-based demonstration, it was desirable to make VCOSS I hardware scalable to a cost effective VCOSS II design.

#### 5. SUMMARY OF SELECTED HARDWARE

Table VI summarizes the selected hardware for the VCOSS control system. The design requirements and performance specifications, including risk assessment, are covered in more detail in the following sections.

TABLE VI. SUMMARY OF SELECTED HARDWARE

Control Approach	Type of Actuator	No. Required	Type of Sensor	No. Required	Type of Electronics	No. Required
Truss Dampening	Electromagnetic (Kimco-LA40-52)	12	Elongation (TRW F-0 Interferometer)	12	Hybrid	12
Momentum-Exchange	Electromagnetic (Kimco-LA40-52)	8	Accelerometer (Sundstrand QA-2000)	8	Analog	8
Isolation Control	Electromagnetic (Kimco-LA20-26)	9	Angular Displacement (TRW TAS)	8	Microprocessor	1
			Accelerometer (Sundstrand QA-2000)	4		

## SECTION V

### ACTUATORS

#### 1. ACTUATOR SELECTION

The function of the actuators in VCOSS is to actively minimize vibration inputs propagating through the structure to the optical train. This is achieved by selectively placing the actuators at key points within the structure. They apply an equal but opposite vibrational force to counteract the disturbance.

Several methods for reducing these vibrations were considered and are listed below:

<u>Method</u>	<u>Description</u>	<u>Advantages</u>	<u>Disadvantages</u>
Vibration Isolation	Active damping with variable stiffness between disturbance and structure	Isolate disturbance at source, effective at low and high frequency, performance improvement possible	Higher force requirement
Truss Dampening	Active augment damping or stiffness of individual truss	Permits tuneable structural resonances, effective for random disturbances	Performance improvement limited (software dependent)
Momentum Exchange	Reaction mass to counteract disturbance	Very efficient against discrete sinusoidal disturbances, reduces problem at source	Actuator stroke limitations
Passive	Passive dampers, change of truss element stiffness, relocation of mirror/truss interface	Inherently stable, reliable, inexpensive	Not spirit of current study, performance improvement limited
Rigid Body	Place actuators at mirror/truss interface	Provides direct control of problem, low mass of mirrors reduce torques demanded, reduced structure dynamics interaction with reaction cancellation	May create mirror figure problems

The first three methods were chosen to satisfy discrete disturbances located throughout the structure.

Vibration isolation, truss dampening, and momentum exchange methods were attractive since each have unique characteristics to best eliminate discrete disturbances throughout the structure. Passive and rigid body controls were not in the spirit of the current study since they use no actuators. Direct mirror control was not chosen because it creates mirror figure problems, although LOS could be effectively controlled.

## 2. COMPONENT LEVEL REQUIREMENTS

The task of producing hardware suitable to meet VCOSS system requirements followed three major areas of control:

- o Structure isolator control
- o Truss dampening control
- o Momentum exchange control

These control devices each have specific locations on the spacecraft and a unique set of requirements to be satisfied (see Table VII).

There are two key modes which can be employed to satisfy the active dampening requirements: force and displacement (stroke) actuation. Although each control device has a variance in these modes, a design goal to have similar hardware for all areas of control was selected. All

TABLE VII. COMPONENT LEVEL REQUIREMENTS

Device	Bandwidth (Hz)	Weight (kg)	Peak Power (watts)	Force (newtons)	Stroke (mm)
Structure Isolator Control	DC-650	3.5	37	32	1.5
Truss Dampening Control	DC-650	3.0	15	18	0.12
Momentum Exchange Device	0.1-650	5.0	49	23	30

requirements in Table VII were established on the system level, with the exception of weight, which was initially allocated and minimized upon selection.

### 3. CONTROL DEVICE LOCATIONS

Spacecraft structure control device locations may be seen in Figure 22. These locations were selected by an extensive iteration process involving system level control processes discussed earlier. For hardware purposes they were broken up into three areas of control:

- o Isolator control separates the controlled structure from the equipment section at three points, with three degrees of freedom

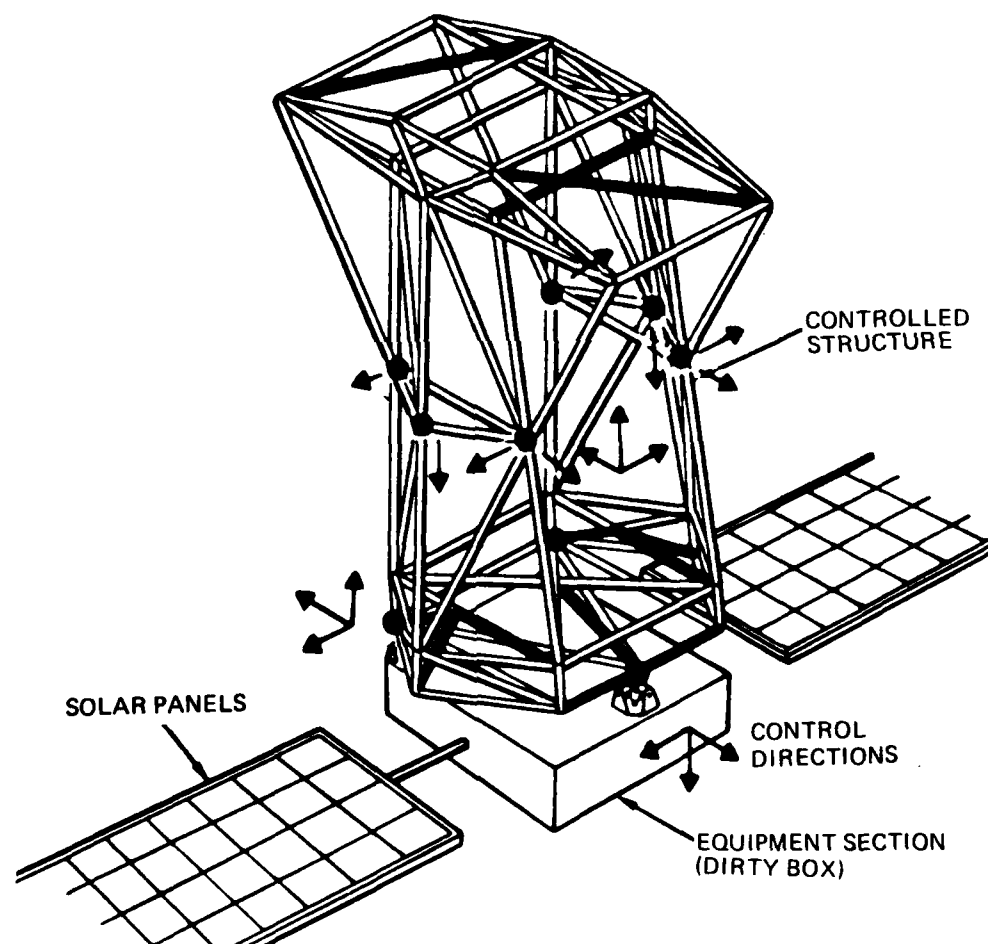


Figure 22. Draper Model 2 Structure. Darkened struts represent truss dampened control. Momentum-exchange control is located at darkened circles. Isolation control separates the structure from the dirty box.

at each point. Control at these locations primarily eliminates lower frequency modes associated with solar panel flexibility and spacecraft vibrations.

- o Truss dampening controls on the structure are placed along the twelve darkened truss locations in Figure 22. One degree of freedom is controlled along the axial direction for each truss shown. These control locations prove to be advantageous for selective structure control at the locations chosen at system level.
- o Momentum exchange controls are located in the center of the structure at six points, four control one degree of freedom while the remaining are capable of controlling two degrees of freedom. Control at these locations primarily eliminate bending modes associated with the structure.

#### 4. CANDIDATE ACTUATORS

Initially, available off-the-shelf actuators were surveyed to determine appropriateness to VCOSS component requirements. The survey reduced the perspective set to a subset of four major types of actuators shown in Table VIII and summarized below:

- o Electromechanical - The mechanical actuator chosen to best fit system requirements is an outgrowth of the ALPHA program. The configuration features a ball screw actuator with a parallel bellow spring which produces the desired frequency cut-off. The actuator

TABLE VIII. CANDIDATE ACTUATORS

Actuator	Bandwidth (Hz)	Resolution ( $\mu\text{m}$ )	Force (N)	Weight (kg)	Power (watts)	Comments
Electromechanical	10	0.4	1000	7	8	Low bandwidth and power
Electromagnetic	1000	0.1	50	5	47	High bandwidth, resolution and power
Hydraulic	150	0.3	240	2.5	20	3% hysteresis 7% linearity
Piezoelectric	1000	0.1	1000	0.25	10	Small deflections only 200V power supply

is essentially reversible by virtue of selecting the ball screws lead parameter to be greater than one third of the screw diameter. Its prime mover is a brushless DC torquer, commutated via a capacitive pick-off.

- o Electromagnetic - Voice coil actuators have been used for many years primarily to drive speakers. the Kimco actuators work on the same concept with two basic internal components: magnetic field - a high permanent flux density is created using samarium cobalt, and focused onto the coil to minimize coil windings; coil - the coil base and hobbin are a one-piece hard anodized aluminum element wound with two layers of magnet wire. The advantages are in its simplicity and structural rigidity.
- o Hydraulic - The hydraulic design is an outgrowth of a high response and alignment requirement of an optical train associated with a high energy laser system. The actuator basically consists of two flexural chambers, an insert and a hydraulic flow valve. The latter effects the command actuator displacements by metering appropriate flow rates. The actuator is also equipped with displacement and velocity transducing elements at two rod ends.
- o Piezoelectric - The configuration of the piezoelectric actuator is a stack of single piezoelectric elements connected in series to satisfy system requirements. The stacking is required since each element is limited to small deflections. Since piezoelectric devices exhibit the property of producing a force proportional to input voltage, vibration may be controlled by closing the loop with an amplified voltage signal proportional to structure acceleration.

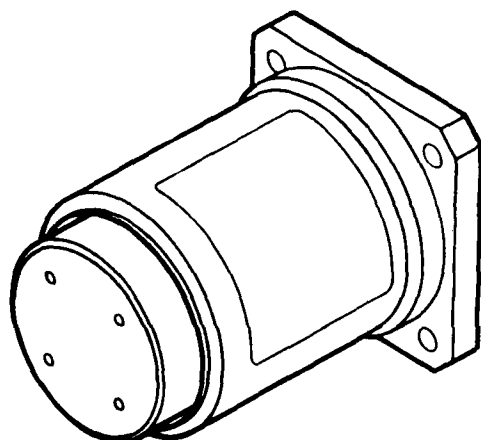
The piezoelectric actuator which initially showed the most promise, was found to have major problems: high voltage requirements, massive electronics and small deflection limitations (stacking required). The electromagnetic voice coil actuator was found to be most suited to provide the system with a single actuator, satisfying all requirements while minimizing power inputs and weights. The remaining hydraulic and electromechanical actuator types fell short of the bandwidth requirement of 650 Hz. There are a number of voice coil actuators on the market. Kimco actuators were chosen over other available actuators for four major reasons:

- o Flight qualified
- o Utilized in similar space systems
- o Designed to minimize power and weight
- o Available in "catalog type" form showing characteristics

The Kimco actuators, best suited to meet the requirements are shown in Figure 23 and listed below:

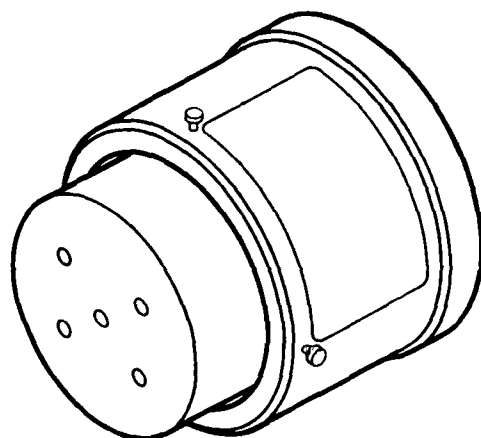
<u>Control Area</u>	<u>Kimco Actuator Model Number</u>
Structure isolator control	LA20-26
Truss dampening control	LA20-26
Momentum exchange control	LA40-52

KIMCO VOICE COIL ACTUATOR  
LA20-26



WEIGHT	0.98 KG
COST	\$2000
PEAK FORCE	49 N
BANDWIDTH	1000 HZ
PEAK POWER	47 WATTS
MEAN TIME BEFORE FAILURE	100,000 HR
PROCUREMENT TIME	12 WEEKS

KIMCO VOICE COIL ACTUATOR  
LA40-52



WEIGHT	4.2 Kg
COST	\$2500
PEAK FORCE	133 N
BANDWIDTH	1000 HZ
PEAK POWER	315 WATTS
MEAN TIME BEFORE FAILURE	100,000 HR
PROCUREMENT TIME	12 WEEKS

Figure 23. Actuator selection.

Those chosen best fit requirements while minimizing weight and power. Other model numbers could easily be selected if there is a change in future system requirements (VCOSS II).

## 5. CONTROL DEVICES

A control device is an actuator with additional integration hardware to secure a degree of freedom movement. The integration hardware for each control area was designed to best enhance actuator performance at location.

There are isolator control mounts like that of Figure 24 located at three points on the structure, with three degrees of freedom (or three actuators) controlled at each point. Each isolator mount will actively control the structure with devices having the capability of providing variable stiffness in three degrees of freedom. This enables the isolators to control both low and high frequency disturbances directly between the dirty box equipment section and the structure.

A close up of one actuator with integrating hardware (isolator control) is shown in Figure 25. Here the actuator is encased in a graphite epoxy tube with one end attached to the tube and the other attached to stainless steel shaft. The shaft is allowed to move in the axial direction only, with the use of a linear ball bushing. The use of the shaft serves two purposes: to keep the actuator coil mechanism aligned to its permanent magnet counterpart in the axial direction and to add overall stiffness to the control device. In this case, both ends of the control device are attached to a rigid surface through a spherical bearing so as not to induce any residual bending stresses through the device. One spherical bearing will be mounted in the hardware attached to the controlled structure side while the other is mounted to hardware attached to the dirty box.

Truss dampening is accomplished by placing the selected actuator in series with the truss to be controlled. This counteracts axial forces distributed through the truss due to vibrational disturbances. A control location through the neutral axis of the truss is more attractive than placing control outside of the truss for two reasons: a control location outside the truss will create unwanted residual bending with respect to the



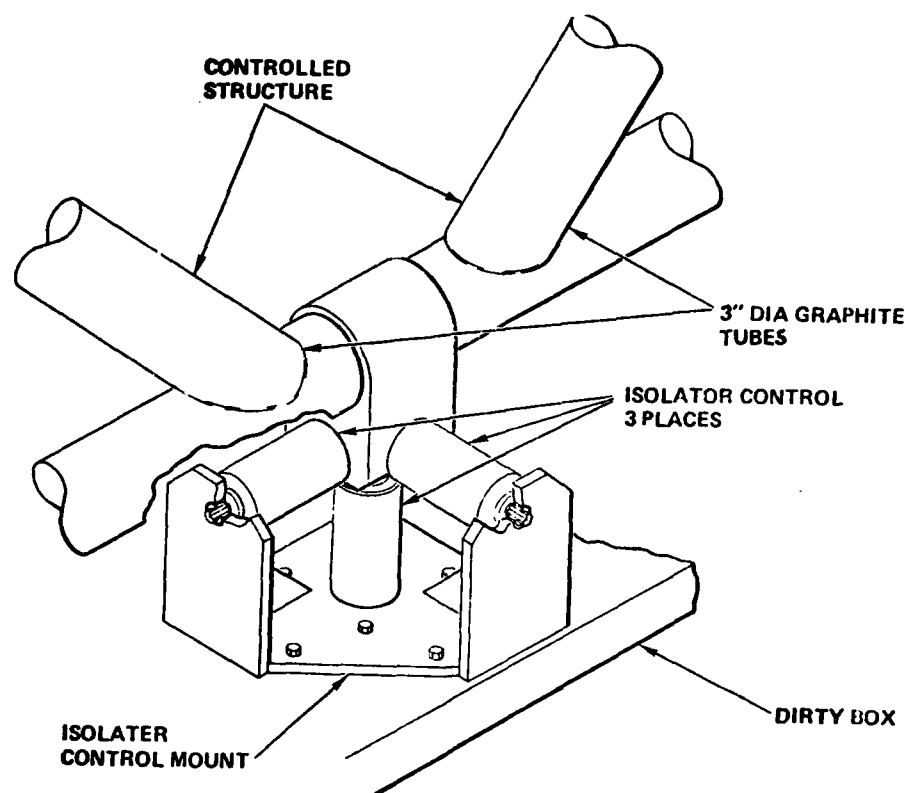


Figure 24. Isolator control mount.

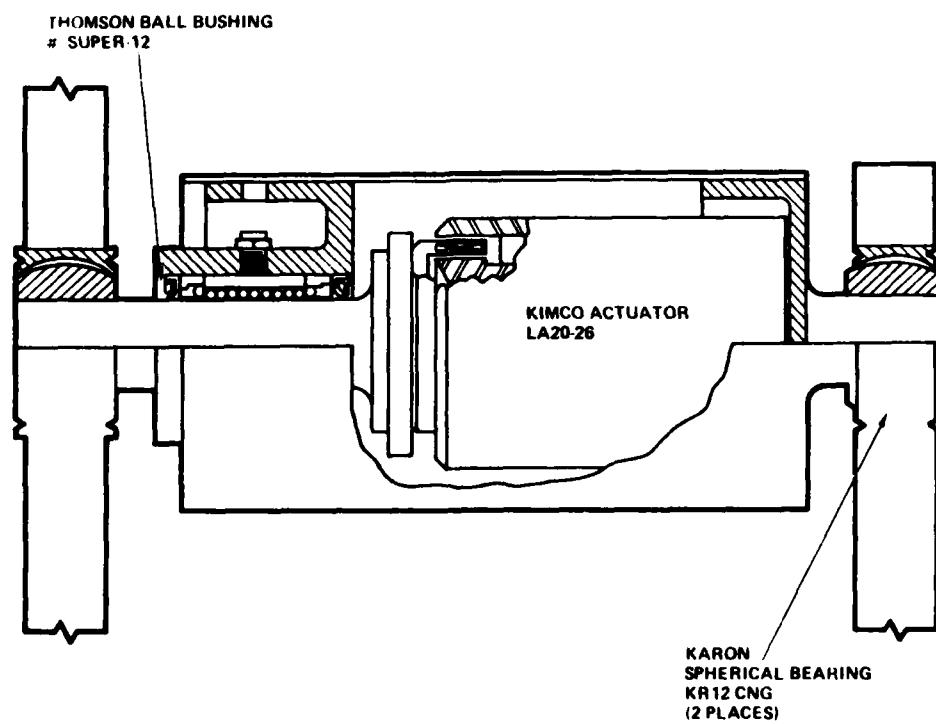


Figure 25. Isolator control.

truss neutral axis when the actuator is flexed and control located within a truss calls for less hardware, a less complicated design and an overall neater device package.

Both truss dampening and isolator control devices followed the same design path to achieve the present system. The ball bushing and shaft used for truss dampening (Figure 26) carry out the same function here as they did with the isolator control device. The load of both designs is carried through identical paths. Bending, shear and torsional loads are taken from the shaft through the ball bushing to the truss, while axial loads flow through the actuator only. The difference in the two designs occurs at the device interface. In Figure 26, the truss is separated into two sections where loads at the device interface flow from truss through device to truss again, while the isolator loads flow through the spherical bearings at each end.

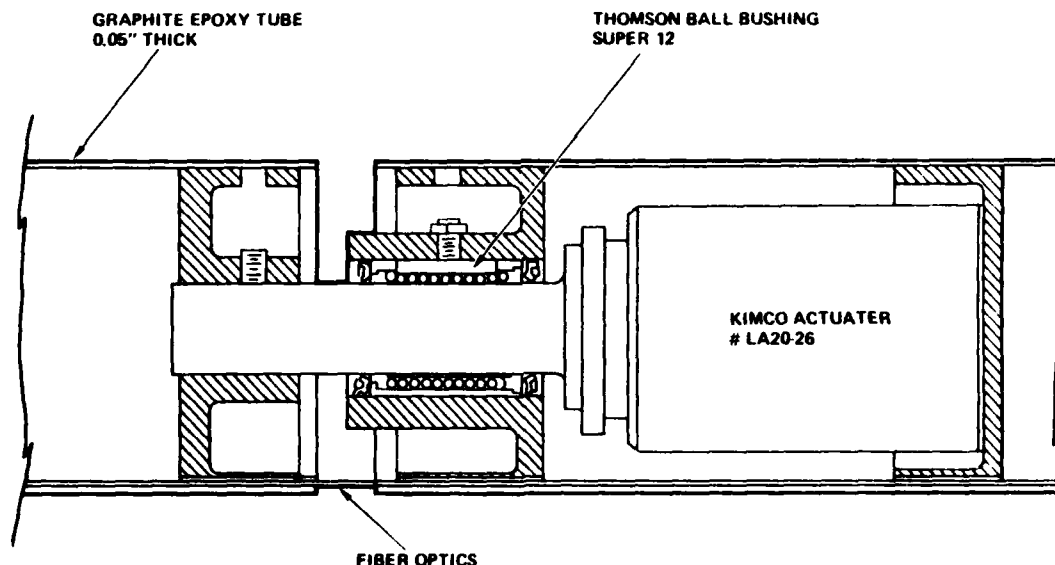


Figure 26. Truss dampening.

An area through the truss dampening device has been left free for the fiber optic sensing device to be placed. In Figure 26, it may be seen stretched along the inside wall of the truss. Control sensors are discussed in detail in the following section.

The momentum exchange device uses an accelerated mass to provide structural vibration force control needed to dampen input disturbances. There are six points chosen on the structure in which the momentum exchange device would serve. The justification for these specific devices, chosen to operate at the points defined, is that they control directions perpendicular to the truss axial direction even when there is no physical connection in that direction. Figure 27 details the Kimco actuators as they would be attached to the controlled structure through integrating aluminum hardware. As seen here, the single axis and dual axis controls are identically mounted with the exception of the extra face and components on the dual axis control (the orthogonal third axis is controlled by truss dampening, there is no need for a moment exchange device in this direction). Both mounts have a 3-inch-diameter hole bored through the vertical length while each face secures an accelerometer and the coil side of the LA40-52 actuator.

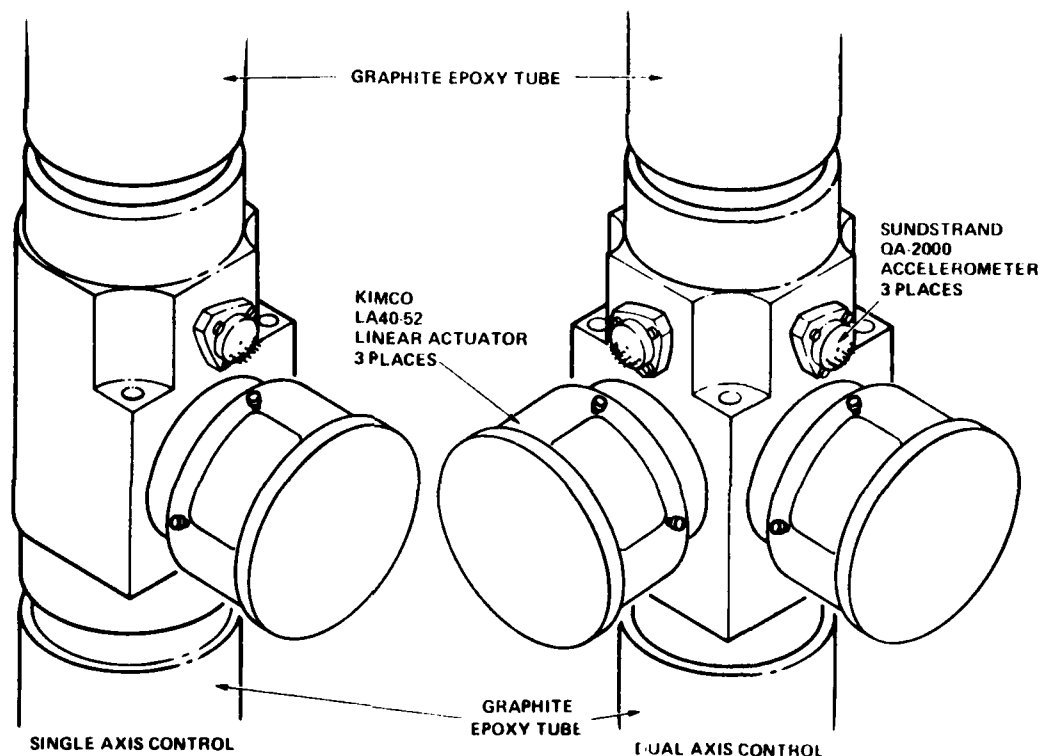


Figure 27. Momentum exchange device.

The simplicity of this design includes using the actuator's permanent magnet portion for the mass to be accelerated. This eliminates any additional weight which might have been added to achieve required force action. In other words, the 0.2 kg coil side of the actuator is attached to the structure while the 4 kg permanent magnet side of the actuator is accelerated in space to produce required force action.

#### 6. PERFORMANCE SUMMARY

The capability of actuator control devices versus system level requirements are summarized in Table IX. In all cases but two, the percent margins are fairly high and positive. This shows that the design meets and exceeds present system requirements. Should future alterations of the system be implemented, the present design should be able to absorb the altered set of constraints.

The two lowest percent margins of Table IX correspond with the momentum exchange device. The negative margin represents a bad initial guess on device weight which was minimized as intended. The lowest margin of +6% falls under the stroke minimum requirement of 30 mm. The high stroke requirement here is needed to accelerate the actuator mass through this distance.

Control parameters of weight, cost and power are given in Table X for the actuator devices. The total weight of all devices includes cable, hardware and mounts. The actuator costs were found from the manufacturer, whereas the remaining hardware was computed using present shop charges times estimated man hours required. Operating rms power estimations came from the electronics section and are also listed here along with a maximum procurement time of 16 weeks.

Major goals achieved from development of the VCOSS control device actuators are listed below.

- 1) All off-the-shelf actuators are used within design of the control devices for ease of the requirement changes.

TABLE IX. CAPABILITIES VS REQUIREMENTS

Device	Requirement, Capability, % Margin	Weight (kg) <sup>*</sup>	Power Needs (w) <sup>**</sup>	Force (N) <sup>**</sup>	Stroke (mm) <sup>**</sup>
Structure Isolator Control	Requirement	3	37	32	1.5
	Capability	2.5	47	49	2.1
Kimco LA20-26	% Margin	20%	27%	53%	40%
Truss Dampening Control	Requirement	3	15	18	0.12
	Capability	2.6	47	49	2.1
Kimco LA20-26	% Margin	15%	213%	172%	1650%
Momentum Exchange Device	Requirement	5	49	23	30
	Capability	5.4	315	133	31.8
Kimco LA40-52	% Margin	-7%	543%	478%	6%

$$* \% \text{ margin} = \frac{\text{requirement} - \text{capability}}{\text{capability}} \times 100$$

$$** \% \text{ margin} = \frac{\text{capability} - \text{requirement}}{\text{requirement}} \times 100$$

TABLE X. ACTUATOR CONTROL PARAMETERS

	Unit	Quantity	Actuator	Hardware	Mount	Miscellaneous	Total
Weight (kg)	Isolator	9	0.98	1.5	4.65/3		39.9
	Truss	12	0.98	1.6	--		34.0
	Med (Dual Axis)	2	4.2	1.3	--	10%	12.1
	Med (Single Axis)	6	4.2	1.1	--		35.0
Total Cost (\$)			54.18+	41.9+	13.95+	11.0	121.0
	Isolator	9	2000	1400	485		35,000
	Truss	12	2000	1600	--		43,900
	Med (Dual Axis)	2	2500	--	2960		10,900
	Med (Single Axis)	6	2500	--	1560		24,400
Total Power (W) Operating RMS Total			62,000+	32,520+	19,645		=\$114,200
	Isolator	9	12.3	--	--		111
	Truss	12	5.0	--	--		60
	Med	8	16.3	--	--		130.7 301.7
Procurement Time			12	16	16		16 wks

- 2) Selected actuators have been utilized in previous space applications. In one application, the system is used to maintain the alignment of a complex optical train that points and directs a laser beam at a dynamic target.

The Kimco actuator dynamically aligns the optical train consisting of a series of mirrors, by making rapid and minute changes in the position of one of the mirrors, the beam-steering mirror. Basic function of the overall system is to direct a laser beam. Accomplishing this requires extremely rapid and precise positioning since both the optical system and the target are in a dynamic environment and are often separated by great distances.

The magnetic assembly in the actuator is incorporated into a reactionless gimbal, and its wide bandwidth response makes the actuator an ideal candidate for this servo application. The response is up to almost 1000 Hz when fully driven and 10 kHz at low force levels. The Kimco actuator's high bandwidth capability enables it to correct large errors faster than a hydraulic counterpart.

- 3) The procurement schedule is compatible with VCOSS II goals.
- 4) Present actuator selections meet and exceed performance requirements initially set. As mentioned earlier, if for any reason future system requirements change, new actuators may be "catalog chosen" to meet these performance requirements.
- 5) Power consumption and weight were minimized using this catalog-type of actuator selection.

## SECTION VI

### SENSORS

#### 1. REQUIREMENTS

The requirements for sensor performance were established from system level analysis. Mission goals were incorporated into a system model. System performance based on this analysis established a set of higher level requirements for control. These requirements were tiered down to the component level where they were used to design or select the appropriate hardware. Table XI summarizes the requirements by control system element.

The degrees of freedom identify the number of directional measurements made by each device. In the case of the M-E sensors (accelerometers), each sensor measures translation along one axis only. There are, in some cases however, measurements made along two axes using two devices. The sensors for isolation control (TAS and accelerometers) measure decentration (2 DOF), tilts (2 DOF) and translation (1 DOF).

#### 2. SENSOR GOALS

The specific goals established for the VCOSS sensors are:

- o Must exceed the performance requirements.
- o Do not operate at the ends of the device's operational range - this minimizes the risk associated with hardware not performing to specification at its operational limits for whatever reasons.
- o Use off-the-shelf hardware whenever possible - reduces the cost and development time of new hardware.
- o Any technology development should be compatible with VCOSS II goals and schedule - the sensor for truss dampening requires development work. In Section 3.b a discussion of its development schedule is presented.
- o Minimize power consumption and weight.



TABLE XI. SENSOR REQUIREMENTS SUMMARY

● Truss elongation		
Bandwidth	DC - 1 kHz	
Resolution	0.4 micron rms	
Total excursion to be measured	0.4 mm	
Degrees of freedom	1	
● Structural displacement		
	<u>Momentum Exchange</u>	<u>Isolation</u>
Bandwidth	0.1-700 Hz	DC - 1 kHz
Resolution	0.4 micron rms	0.4 micron rms
Degrees of freedom	1	5

### 3. CANDIDATE SENSOR CONCEPTS

Three generic measurement techniques were considered for VCOSS: triangulation, trilateration and seismic.

a. Triangulation - This method, shown in Figure 28, measures the motion of a point with respect to a fixed reference. It is achieved simply by placing a luminous target at the point to be measured and a detector at a fixed reference. Measurements of angle at the detector determine the motion of the target in both centration and tilt. Placement of an appropriate number of targets and detectors allows determination of the required degrees of freedom. This concept has been incorporated in active isolation control. Figures 29 and 30 show typical hardware designs. A technical description of this measurement technique can be found in Appendix A.

There are several advantages of using the TAS for making LOS error measurements. First, it performs extremely well at the low end of its dynamic range, allowing for frequency response to the DC level. Second, TRW has previously developed this hardware under contract to NASA and considers it off the shelf for future (such as VCOSS) applications.

# TRIANGULATION

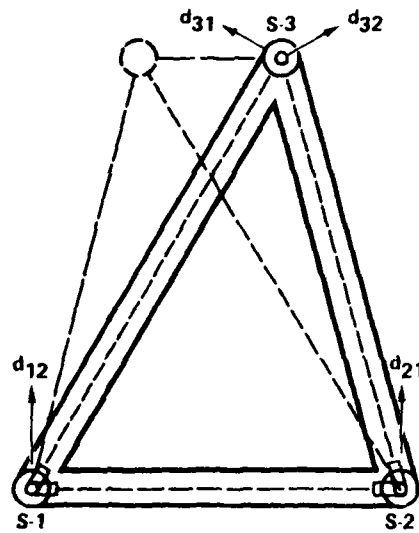


Figure 28. Triangulation sensing methodology.

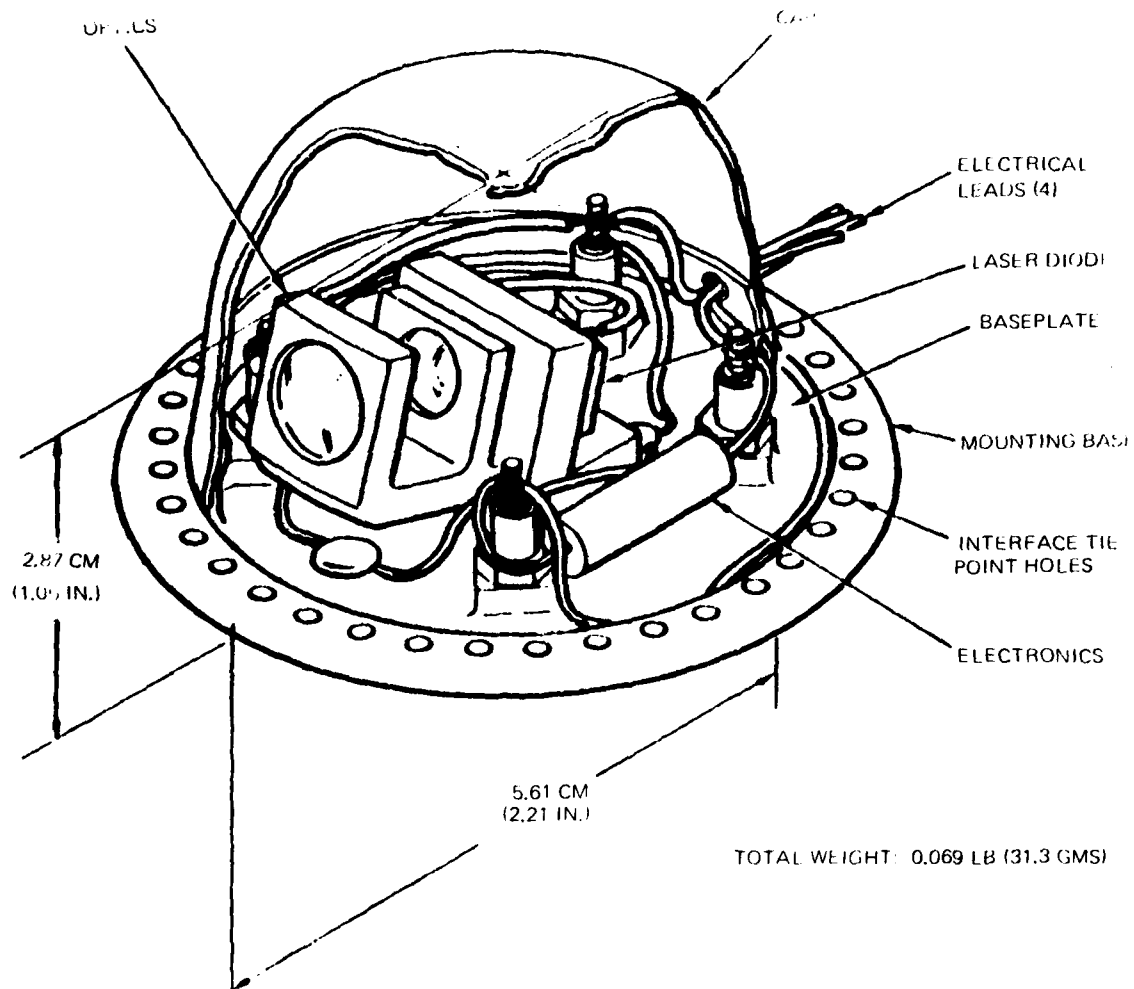


Figure 29. TAS target.

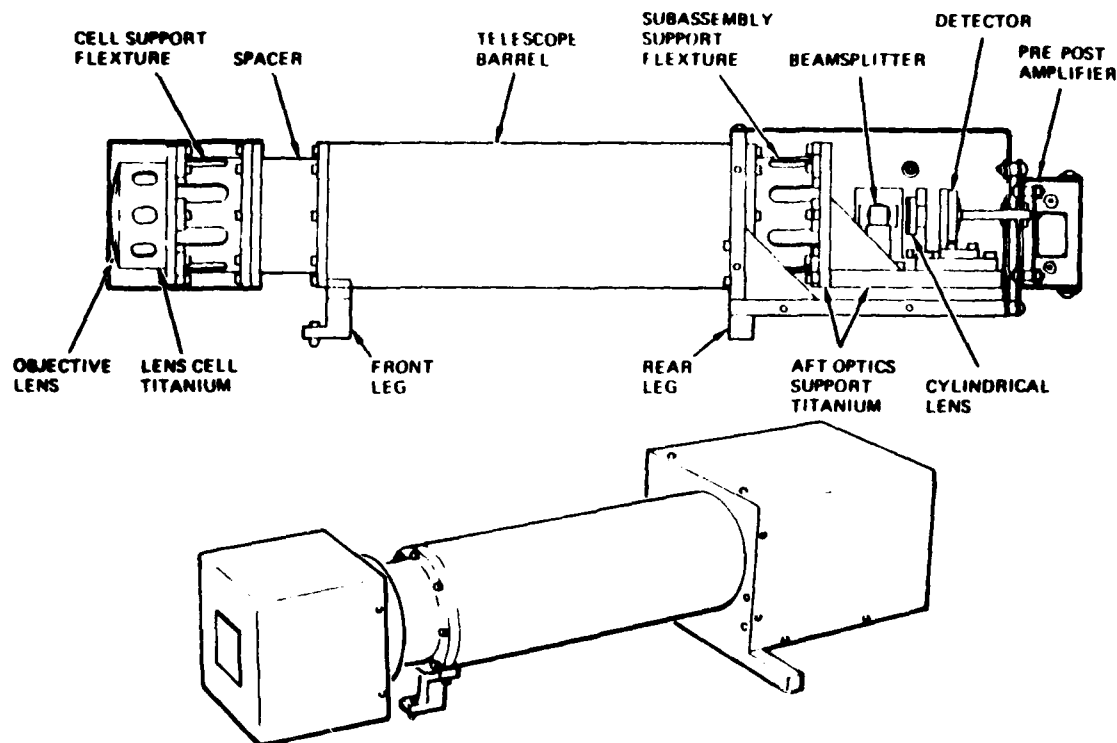


Figure 30. TAS detector.

Finally, because the detector is a telescope of large magnification, it is very sensitive to angular and decentration changes. Previous tests have verified performance to less than 0.1  $\mu$ rad accuracy.

b. Trilateration - This technique employs measurement of changing length between points to determine displacement. Figure 31 assumes the apex of L-2 and L-3 to be the reference. Measurement of distances L-1, L-2 and L-3 determines the location of the apex of L-1 and L-2. These measurements can be made by determining the change in length of the associated members.

The hardware to be employed is a TRW developed fiber optic interferometer. The fiber optic interferometer, for dynamic length measurements, is quite simple. It consists of a laser diode source feeding a coupler that splits the beam along two fibers. These fibers can be either stretched along the centerline of the strut or held in tension, cemented to the inner wall of the strut. At the opposing end cap, the beams are recombined by a coupler to feed a fringe counting detector. See Figure 32. By

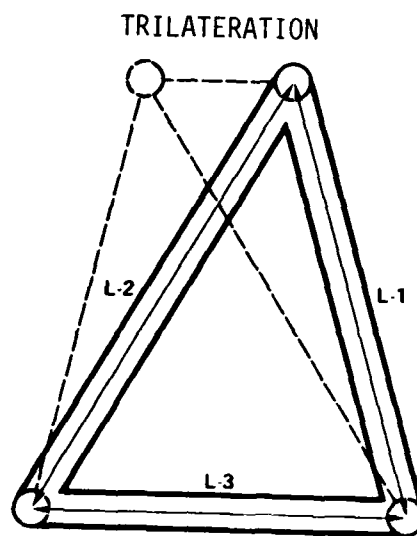


Figure 31. Trilateration sensing methodology.

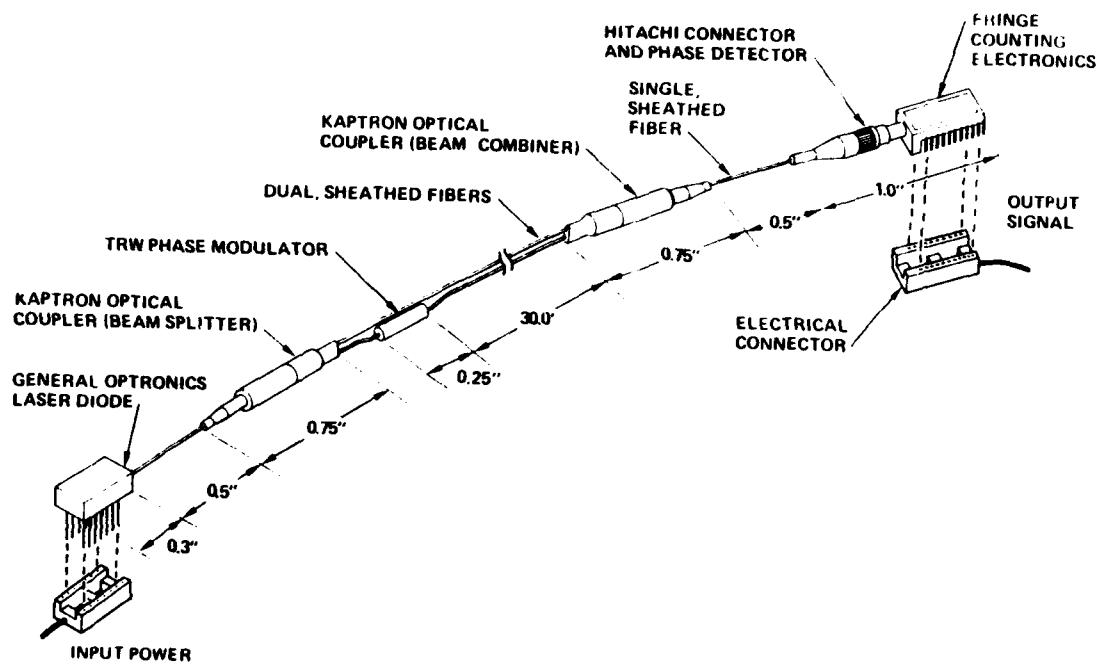


Figure 32. Fiber-optic interferometer.

appropriate selection of the elastic-mechanical and elastic-optical properties of each of the fibers, the wavefront difference of the beams arriving at the detector measures the elongation of the fiber pair.

Because this device operates on differences in path length at optical frequencies, its potential measurement accuracy is in the submicrometer range. With the addition of a third fiber, temperature drift errors can be compensated for. Specific details of the design can be found in Appendix B. Figure 33 shows the development plan established under a current IR and D program for the fiber optic interferometer.

c. Seismic - In contrast to the previously mentioned approaches to measurement, the seismic method is the simplest to implement in hardware. By measuring and recording accelerations on a body, a history (in real time) is maintained as to the location of the body. For both the isolation and the momentum-exchange control loops, accelerometers are applied as the primary axial translation sensors.

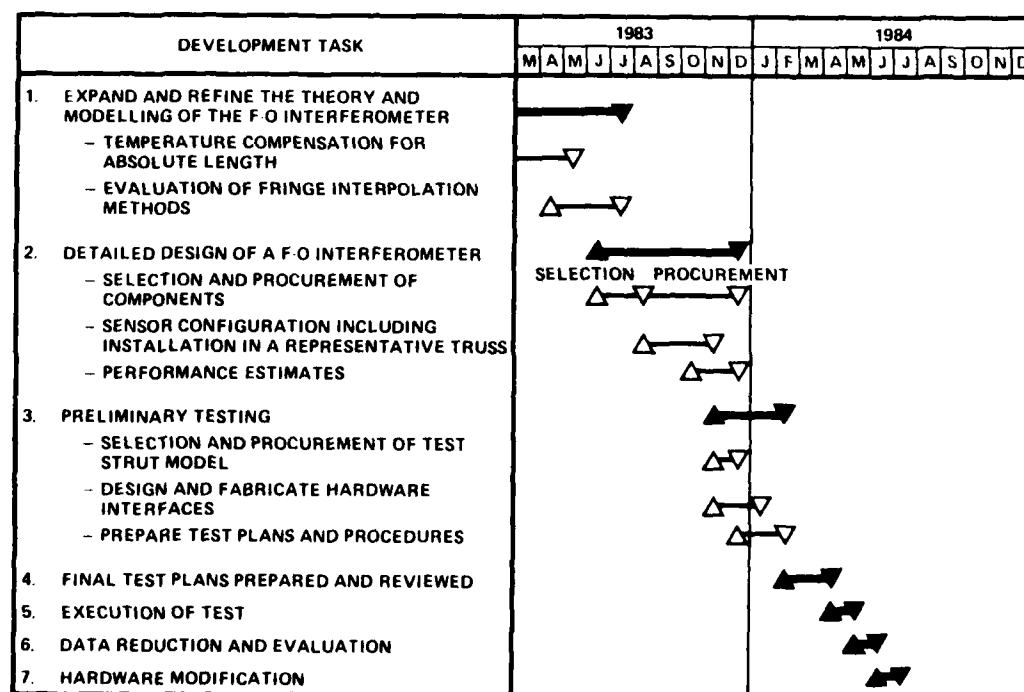


Figure 33. F.O.I. development schedule.

There are several advantages to this approach:

- o The selected accelerometer has a measurement resolution to 1  $\mu$ g. This meets the performance requirement of low bandwidth response for momentum-exchange control.
- o This component is a catalog item.
- o A feature of the chosen accelerometer is a temperature dependent electronic reference signal that can be used to correct thermal effects.
- o Demonstrated reliability, low weight and low power consumption.

#### 4. COMPONENT SPECIFICATIONS

Table XII summarizes the specifications of the selected components for each control method.

#### 5. RISK ASSESSMENT

An assessment of the hardware risks is presented in Table XIII. The only significant risk is in the cost estimate for the TAS. Although one unit has been previously fabricated, inadequate data was available to estimate the recurring costs under the scope of this program. It is felt, however, that the estimate presented in the previous section is accurate to within a factor of two.

TABLE XII. SELECTED COMPONENT SPECIFICATIONS

Per Unit	Triangulation Sensor (Isolation Control)		Accelerometer (Momentum- Exchange)	F-0 Interferometer (Truss Dampening)
	Receiver	Target		
Weight (gms)	560	17	70	450
Power Consumption (W) Max. Avg.	2.0	0.15	1.25	1.5
	1.4	0.11	0.8	1.1
Bandwidth	DC - 1 kHz	--	0 - 1 kHz	DC - 1 kHz
Resolution	0.1 $\mu$ rad	--	1 g	0.05 m
MTBF (hours)	80,000	80,000	8500	10,000
Procurement Time (weeks)	52	52	12	65
Cost (\$ x 1000)	12.5	12.5	3.0	1.5-2.0

TABLE XIII. SENSOR RISK ASSESSMENT

Prediction	Momentum-Exchange (Accelerometers)	Isolation Control (TAS)	Truss Dampening (F-0 Interfer- ometer)
Performance	Low	Low	Low-Medium
Weight	Low	Low	Low
Power Consumption	Low	Low	Low
Reliability	Low	Medium	Medium
Availability for VCOSS II	Low	Low	Medium
Cost	Low	High	Medium



## SECTION VII

### CONTROL ELECTRONICS

#### 1. ELECTRONICS REQUIREMENTS

Table XIV lists the principal requirements for the three VCOSS electronics boxes: the isolation control electronics (ICE), truss dampening electronics (TDE) and momentum exchange control electronics (MECE). Table XV lists the characteristics for these three boxes.

The input signals to each electronics box are different and dependent on the nature of the sensor. The ICE receives two axes of data from each of two photodiode position sensors. Each input consists of an analog

TABLE XIV. CONTROL ELECTRONICS REQUIREMENTS

Parameter	Isolation Control	Truss Dampening	Momentum Exchange
Quantity and type	One multi-axis controller	Hybrid controllers	Eight single-axis controllers
Input signals from sensors	Four sets of photodiodes, two sets of data from each	1. Digital pulse train 2. Signal bit to indicate polarity of fringe motion	1. Analog torquer current 2. Analog temperature signal (from accelerometer)
Signal processing	Complex, high-speed matrix operations	Position plus derived rate control	Gain only with a bias added for temperature compensation
Output drivers	Three set of three axis actuators	Single actuator	Single actuator
Drive capability	5.6 amps into 0.66 ohm	3.2 amps into 0.66 ohm	2.5 amps into 1.4 ohm
Bandwidth (kHz)	1.0	1.0	0.7
Sampling rate (kHz) (minimum)	2.0	2.0	2.0

TABLE XV. CHARACTERISTICS OF CONTROL ELECTRONICS

Parameter (Per Unit)	Isolation Control	Truss Dampening	Momentum Exchange
Quantity	1	12	9
Weight (kg)	5.9	1	1
Size (cm)	20.3 x 3.9 x 2.6	1.8 x 2.4 x 1.2	1.8 x 2.4 x 1.2
Power (W) (electronics)	49	4	4
Operating Drive Power (Peak)	37 W each axis 32 N (actuator force) @ 0.08 m/s (actuator velocity)	15 W each 18.2 N (0.006 m/s)	49 W each 22.2 N (1.5 m/s)
Bandwidth	TBD	Up to 2 kHz, limited by driver	Up to 2 kHz, limited by driver
Sample Rate	TBD	Up to 50 kHz	N/A

current that is amplified and A/D converted to provide digital data to the computer in the ICE.

The TDE receives a digital pulse train and a bilevel sign bit from the f-o interferometer (FOI). Each pulse represents one interference fringe. The pulses will be counted by a hardware counter. The counter will be sampled at a fixed rate. The delta count is accumulated for position and differenced with the previous count to derive rate data for the controller.

The MECE receives two analog inputs from its accelerometer. The first is an acceleration signal and the second is a temperature signal (thermistor) that is used to compensate for accelerometer calibration errors. The accelerometer errors are primarily a function of temperature.

The ICE requires complex, matrix mathematical processing at high speed to provide control for all nine actuators. The TDE signal processing consists of a hybrid (both analog and digital) control loop providing position plus derived rate control. The MECE signal processing consists of simple analog amplifiers plus the temperature compensation circuits.

The ICE drives three sets of actuators, each set consisting of three orthogonal actuators. Each TDE and MECE provides drive to only one actuator. The drive requirement for each type of electronics is tabulated in Table XV.

The requirements for bandwidth and sampling rate for each loop is derived from the system performance requirements. The derivation is presented in Section 3 and the resulting requirements for the electronics are tabulated in Table XV.

## 2. GOALS ESTABLISHED FOR VCOSS ELECTRONICS

The criteria established for selecting the type of electronics for each VCOSS application follow:

- o Use existing circuit designs wherever possible
- o Select best circuit technology for each application
- o Exceed performance requirements
- o Minimize development risk, cost, weight and power
- o Hardware/software flexibility for VCOSS II

Existing circuit designs will be used wherever they can be effectively applied. This reduces the development effort in terms of time and cost. It also minimizes risk of development problems. Selecting the most appropriate circuit technology for each application and including design margin will minimize problems and reduce development risks. Selecting designs that provide flexibility in both hardware and software areas will result in designs that can evolve and adapt to changes that arise during the course of the development and testing phases of the project.

## 3. CANDIDATES FOR ELECTRONICS

Several candidate designs and technologies were evaluated for each of the three electronics box designs. These are presented in Table XVI. Two different microprocessors were considered for the ICE. The first is the Texas Instruments SBP9989, which is a complete 16-bit processor on one chip using I<sup>2</sup>L technology. The second is a processor designed using the 2900 bit-slice family developed by Advanced Micro Devices Inc. This family of

TABLE XVI. ELECTRONIC CANDIDATES

- ISOLATION CONTROL ELECTRONICS  
TI SBP 9989 MICROPROCESSOR - COMPLETE 16 BIT PROCESSOR ON SINGLE CHIP.  
AMD 2900 MICROPROCESSOR - FAMILY OF CHIPS, FLEXIBILITY TO DESIGN THE PROCESSOR.
- TRUSS DAMPENING ELECTRONICS  
SBP 9989 MICROPROCESSOR  
SERIAL ARITHMETIC UNIT USING MSI/SSI
- MOMENTUM-EXCHANGE CONTROL ELECTRONICS  
SBP 9989 MICROPROCESSOR  
ANALOG CONTROLLER WITH PROM FOR TEMPERATURE COMPENSATION
- ACTUATOR DRIVE  
VOLTAGE DRIVE  
CURRENT DRIVE
- POWER CONVERTERS - +5,  $\pm$  15V REQUIREMENT  
CENTRAL CONVERTER  
DISTRIBUTED CONVERTERS

devices provides great flexibility to design a high-speed processor tailored to the specific requirements of the application at hand.

One of the two candidates considered for implementing the TDE is the SBP9989. The other is a simple serial arithmetic unit that would be designed using standard low power Schottky transistor-transistor logic/medium scale integration and small scale integration circuits.

Again, one of the candidates considered for the MECE is the SPP9989 microprocessor. The other is a fully analog processing loop with digital electronics in the form of a PROM to provide the required accelerometer temperature compensation.

Two other major electronic areas presented opportunities for competing implementations. The first is the area of actuator drive electronics. The first candidate is voltage drive and the second is current drive that will

compensate for actuator resistance tolerance, temperature variations and back emf that is proportional to the velocity of the actuator.

The second electronic area for tradeoff is the type of power converter to be used. Either one central converter that provides secondary power to all the electronics boxes can be used or separate small converters can be distributed and located with the electronics box being powered. Various combinations of central and distributed converters can also be considered.

#### 4. CANDIDATE SELECTION

Table XVII lists the selected candidates resulting from each tradeoff study and the reasoning that led to the particular selection that was made. The study quickly concluded that the SBP9989 would not be capable of meeting the processing speed requirements for the ICE. It would not be

TABLE XVII. CANDIDATE SELECTIONS

- Isolation Control — 2900 Family Microprocessor  
SBP 9989 cannot meet processing speed requirements ( 2 kHz).
- Truss Dampening — Serial Arithmetic Unit. SBP 9989 is overkill for simple processing needed. Saves parts, cost, power
- Momentum-Exchange Control — Analog Controller  
Analog controller uses proven, standard, low risk circuits  
Saves parts, cost, power
- Current Drive for Actuators  
Better temperature, provides compensation for resistance, back EMF and temperature variations (force proportional to current)  
Minimal increase in parts, power, cost  
Uses proven, low risk circuit technology (4 transistor bridge)  
Voltage drive not feasible for high velocities of momentum-exchange control electronics
- Distribution Power Converters  
Impractical to distribute +5 volts over long distance  
Saves cable weight  
Simplifies testing of electronics

able to perform all of the required complex high speed matrix operation, at a 2 kHz iteration rate. Thus, the AMD 2900 was selected.

The very simple processing performed by the TDE could be performed by either type of processor. Since each controller is completely independent, the demands placed on the accompanying electronics are minimal. The capability of the SBP9989 far exceeded that of the present task. Since the serial arithmetic unit required fewer parts and less power, this is the logical choice to implement the TDE.

Since the MECE receives analog inputs and provides an analog output, an analog controller is a logical candidate. Only if a microprocessor implementation is simpler, because of the complexity of the required processing, should it be the chosen approach. In this case, the processing is quite simple because of the independence of each controller. Thus, the logical choice is an analog controller.

Current drive was selected for all the actuators because improved performance is obtained for a minimal cost in hardware. The actuator force is proportional to drive current. The applied voltage is determined by the applied current times the coil resistance plus the back emf developed due to the motion of the actuator. The resistance is temperature dependent and includes an initial tolerance. The back emf, especially for the MECE, is a large portion of the total applied voltage. Current drive overcomes all of these variations. It has been used by a number of motor drives designed by TRW.

The structure size has a major impact on the converter trade-off study. All of the units use a substantial portion of their power from +5 V. Using a central converter requires distributing large +5 V currents over long distances. It is much more efficient to distribute the same amount of power at +28 V. The savings in cable weight is substantial. Not only will the +5 V current be much higher, but it needs to be better regulated than the +28 V converter input. Also, the allowable voltage drop for the +5 V is much smaller than for the +28 V. Each electronics box used three voltages (+5 V, +15 V and -15 V), resulting in a greater number of wires than providing one +28 V input to a dedicated converter.

Several other new TRW projects are planning to use distributed converters. It also eliminates the problems of switching secondary power

in a way that avoids single-point failures. It simplifies the manufacturing test equipment and procedures to provide one power supply rather than three. The problems of line drops associated with long test cables are also lessened. All these considerations led to the selection of distributed converters.

a. Truss dampening electronics - The truss dampening electronics (TDE) provide control of a single-axis truss actuator based on the output of a fiber-optic interferometer (FOI). Figure 34 is a block diagram of the TDE. Characteristics are given in Table XVII. It is anticipated that the FOI output will consist of a pulse train (each pulse representing one interference fringe) and a signal bilevel indicating the direction of motion. The TDE provides position-plus-rate control of the truss actuator. The rate signal is derived from the FOI signal by differencing successive samples.

FOI output pulses are accumulated over the sample interval in the pulse counter. At the start of a sample interval, the error register contents (old pulse count) are loaded into the accumulator and the pulse counter contents (new pulse count) are loaded into the error register.

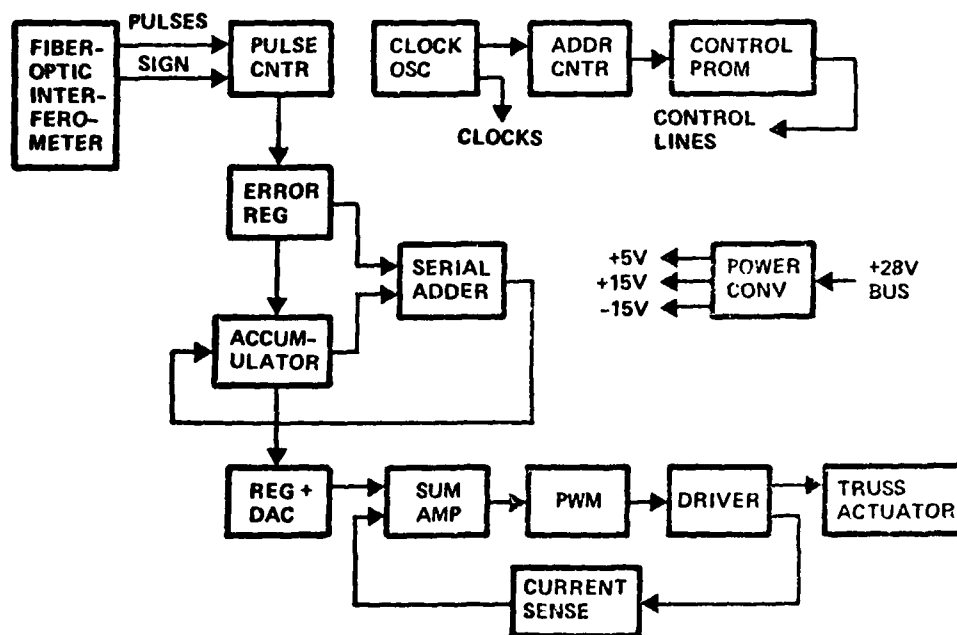


Figure 34. Truss dampening electronics flow diagram.

A simple serial adder is used to compute the composite error signal needed to control the truss actuator. The rate is computed as the difference between the old and new pulse counts by shifting them through the serial adder. The result from the serial adder is shifted into the accumulator. The rate data is then scaled by shifting the accumulator. The scaled rate is added to the new pulse count (position signal) and the sum is shifted into the accumulator. The accumulator contents are then loaded into a holding register that feeds a digital-to-analog converter (DAC).

The analog output of the DAC drives a pulsewidth modulator (PWM), similar to the one used in the MECE. The TDE drive provides up to  $\pm 3.2$  amps of bidirectional current drive to the truss actuator. Because of the low winding resistance and low actuator velocity, the required drive voltage from the TDE is quite low compared to the bus voltage. The TDE would operate more efficiently if the actuator were rewound to operate at higher voltage and lower current.

A single PROM contains a simple program to control the arithmetic operations. The PROM provides 8 outputs that are used to control loading and shifting of the registers and operation of the serial adder. The clock oscillator provides clocks to the counter that addresses the PROM, the shift registers and the PWM. The TDE used the same power converter as the MECE because the power requirements are similar.

It is anticipated that each TDE will be housed as a separate unit located near the actuator that it drives. It is expected to use many mechanical parts in common within the MECE, since they are about the same size.

b. Momentum exchange control electronics - The momentum exchange control electronics (MECE) provide control of a single-axis momentum exchange actuator based on the output of an accelerometer. Figure 35 is a block diagram of the MECE. Characteristics are given in Table XVII.

The accelerometer coil current of about 1.3 ma/g provides the MECE input signal to be processed to provide a bidirectional current drive of up to  $\pm 2.5$  amps to the actuator. The torquer current is applied directly to the summing junction of a current-to-voltage (I/V) amplifier. This technique reduces the output offset error.



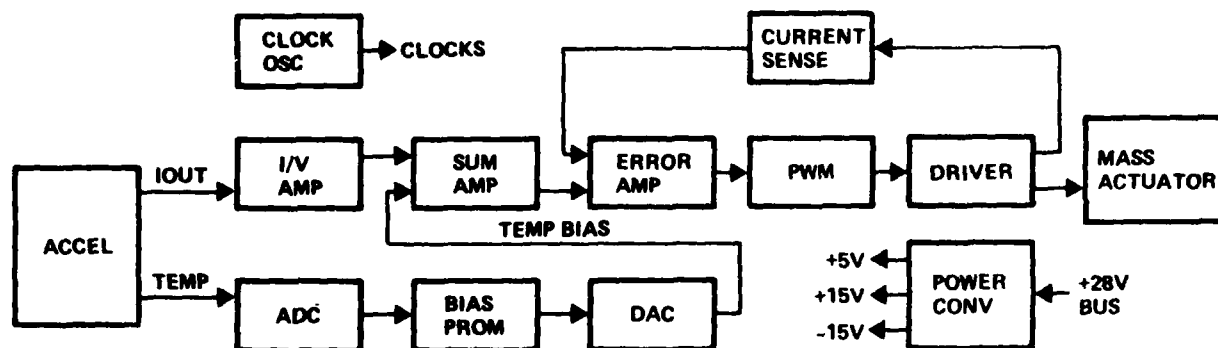


Figure 35. Momentum exchange control flow diagram.

The accelerometer provides an analog temperature output that is used to compensate for the null bias of the accelerometer. Each accelerometer is individually calibrated by the manufacturer. This calibration data is stored in a programmable read-only memory (PROM). An analog-to-digital converter (ADC) converts the temperature signal to a PROM address. The data in the addressed location in the PROM is converted to an analog signal that is summed with the I/V amplifier output to provide a corrected acceleration signal.

The driver output stage is derived from a classified project currently underway at TRW. It consists of an H-bridge driver operated in a switching mode to provide efficient bidirectional drive to the actuator. The lower legs use power FETs and the upper legs use PNP Darlington transistors. The driver stages are transformer-coupled to provide excellent isolation between primary and secondary grounds. The H-bridge is driven by a pulse-width modulator (PWM) stage.

The drive current to the actuator is sensed and fed back to an error amplifier to provide closed-loop regulation of the actuator drive current. Controlling actuator current (rather than voltage) eliminates errors in the actuator force resulting from variations in back emf, temperature and resistance tolerance.

The clock oscillator provides the clocks required by the PWM and ADC. The MECE operates from primary bus power and contains its own converter to generate the regulated +5 V, +15 V and -15 V it requires. It is one of a family of converters being developed at TRW, each with different output power capabilities.

It is anticipated that each MECE will be housed as a separate unit located near the actuator that it drives. It is expected to use many mechanical parts in common with the TDE, since they are about the same size.

c. Isolation control electronics - The isolation control electronics (ICE) provide the signal processing required to control these three-axis isolation actuators using signals from four TAS angle sensors as inputs. Figure 36 is a block diagram of the ICE and Figures 37a and 37b are detailed block diagrams for the sensor input amplifiers and output drive circuits. Characteristics are given in Table XVII. Each TAS provides four input currents, one from each quadrant of a quad-cell detector. The cell currents are individually converted to voltages by I/V amplifiers. These voltages are summed as shown to develop two error signals. Each TAS has two targets, so that the sensor amplifier outputs are scanned twice each sample period, once for each set of targets, resulting in a total of 16 error signals.

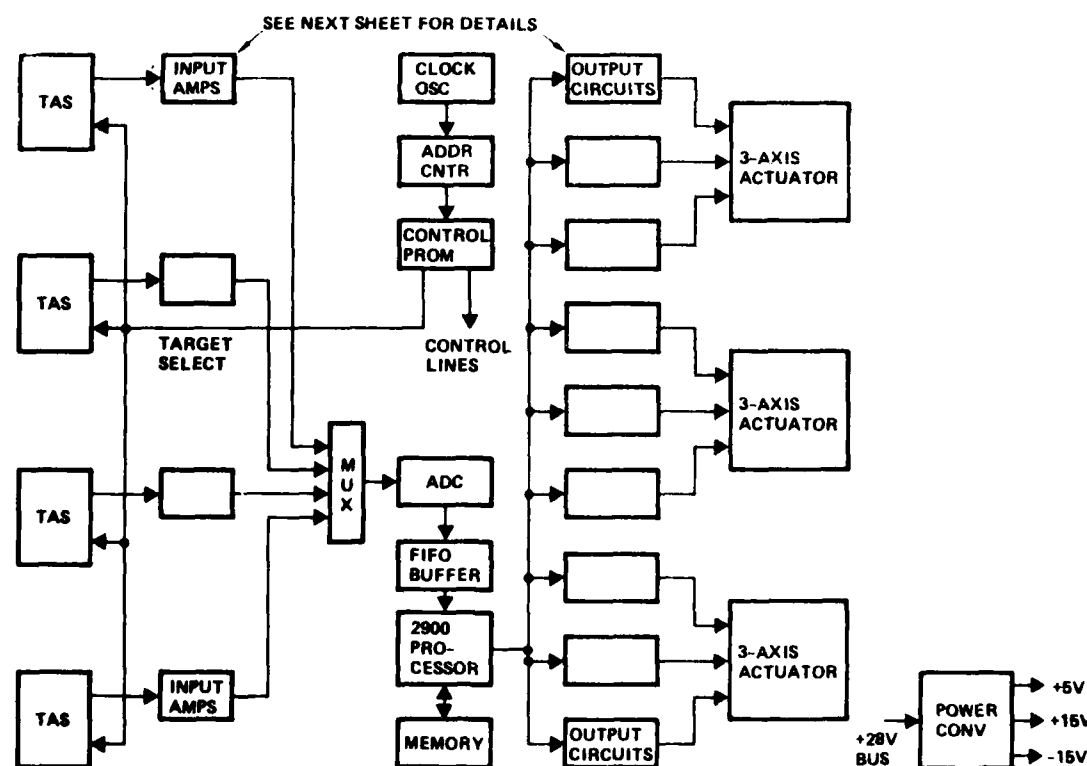


Figure 36. Isolation control flow diagram.

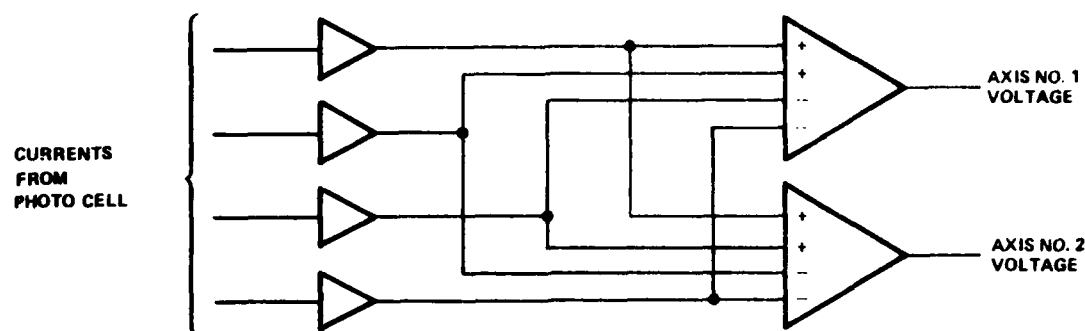


Figure 37a. Input amplifiers for each TAS.

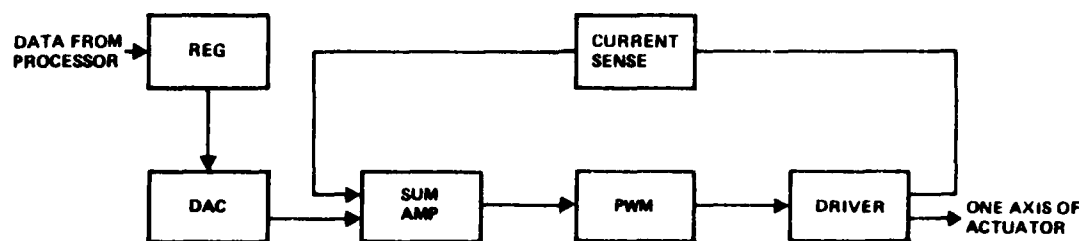


Figure 37b. Isolation control output circuits (1 of 4).

The error signals are selected one at a time by the MUX, converted to digital data by the ADC and stored in a first-in-first-out (FIFO) buffer. A simple program stored in PROM controls target selection, the MUX, ADC and FIFO. The PROM program also synchronizes the 2900 processor to the sensor processing.

The processing required to transform 16 sensor inputs to 9 actuator outputs involves an estimated 85 multiplications and 85 additions. The required program iteration rate is 2 kHz, for a maximum execution time of 500  $\mu$ s. A preliminary design of a high-speed processor using the 2900 family of ICs is underway at TRW. This machine has execution times of 0.3  $\mu$ s for register-to-register add, 0.9  $\mu$ s for memory-to-register add, 1.8  $\mu$ s for register-to-register multiply and 2.4  $\mu$ s for memory-to-register multiply. Assuming 50% register-to-register operations and adding a 50% allowance for shift and other operations, results in an execution time of 344  $\mu$ s, for a timing margin of 45%.

The ICE provides up to  $\pm 5.6$  amps drive to each of nine actuators. The ICE driver uses the same topology as the MECE and TDE drivers, but with a higher current drive capability. Because of the low winding resistance and

low actuator velocity, the required drive voltage from the ICE is quite low compared to the bus voltage. The ICE would operate more efficiently if the actuator were rewound to operate at higher voltage and lower current. The ICE requires a much larger power converter than the MECE or TDE. This converter is part of the same family of TRW-designed converters as the ones used in the MECE and TDE.

It is anticipated that the ICE will be housed in a five slice stack. The slices will be stacked on top of each other, rather than in the more traditional side-by-side arrangement. The bottom slice will house the processor and converter. It is mounted flat and at the bottom of the stack to minimize its temperature rise and the power density at the mounting interface. One slice will contain the sensor processing electronics and ADC. The three remaining slices will be identical and contain three output drivers each.

#### 5. ELECTRONICS RISK ASSESSMENT

Tables XVIII and XIX summarize the assessment of the risks associated with the proposed approaches and selections made in the electronics area. As can be seen from Table XIX, the emphasis has been on making those selections that minimize technical risk. Especially in the TDE and MECE, standard proven analog and digital circuit technology will be used. The 2900 family chosen for a flight version ICE is a relatively low risk development. For VCROSS II a commercial minicomputer may be substituted for a specially developed processor. By the time of a flight program, TRW will probably have a processor available to be used in the ICE.

The actuator current driver technique has been used extensively, so that it is a proven current technology. Considerable design and development work is underway on distributed converters here at TRW. They are planned for a current project and have been proposed on other future work.

TABLE XVIII. ELECTRONICS RISK ASSESSMENT

Prediction	Momentum-Exchange (Analog Controller)	Isolation Control (Microprocessor)	Truss Dampening (Serial) Arithmetic)
Performance	Low	Low	Low
Weight	Low	Low	Low
Power Consumption	Low-Medium	Low-Medium	Low
Reliability	Low	Low-Medium	Low
Availability for VCOSS II	Low	Medium	Low
Cost	Medium-High	Medium-High	Medium-High

TABLE XIX. ELECTRONICS RISK ASSESSMENT

- 2900 family processor development based on several previous TRW designs (TDRSS, DSP).
- Commercial minicomputer may be used for VCOSS II.
- Electronics for truss dampening and momentum-exchange use standard analog and digital circuit technology.
- Actuator driver used existing circuit design.
- Distributed converters are being used on most new TRW projects.

## SECTION VIII

### CONCLUSIONS

The main purpose of this program was to compare an active controlled design to a stiffness controlled design. Table XX summarizes the performance and cost associated with active vibration control.

Meeting the LOS and defocus requirements placed demands of an additional 460 watts of power and 425 kg of weight at a cost of \$1.25M.

TABLE XX. SUMMARY OF ACTIVE CONTROL SYSTEM PERFORMANCE

	Program Goal	Baseline Design	Active Control Design
LOS Error (RSS)			
X,Y Tilts ( $\mu$ rad)	0.05	1075.0	0.052
Defocus ( $\mu$ M)	25	136.0	2.0
Average Power Consumption (W)	Minimize	--	
Actuators			301
Sensors			29
Electronics			129
Total			459
System Weight (kg)	Minimize		
Baseline		7200	7200
Actuators and Hardware			121
Sensors			7
Electronics			26
Solar Cells			68
Total			7422
Cost (\$X1000)	Minimize		
Actuators			114
Sensors			148
Electronics			1000
Total			1262

Table XXI summarizes the performance of a stiffness controlled model. The additional spacecraft weight required to achieve this level of performance was 7800 kg. No cost data was generated for this model.

TABLE XXI. STIFFNESS CONTROLLED PERFORMANCE\*

LOS X ( $\mu$ rad)	LOS Y ( $\mu$ rad)	LOS (RSS)	Defocus ( $\mu$ m)
59.27	167.31	196.46	4.73

---

\*This table was generated from data supplied by Draper Labs, who developed the stiffness model.

APPENDIX A

SENSOR CONFIGURATION, GENERAL CONSIDERATIONS



## APPENDIX A

### SENSOR CONFIGURATION, GENERAL CONSIDERATIONS

The function of the optical angle sensor is to provide continuous measurements of the targets line-of-sight coordinates relative to a central reference frame. In this section, the approach toward the optical angle sensing system is described, and then design tradeoffs including multiple target handling are touched on.

#### A.1 Elements of the Sensor System

The elements of the sensor system are (1) modulated, bright "point" targets; (2) automatic angle measuring receivers; and (3) electronic processors. Typically, the target is a light emitting diode attached to a structural section of the optics.

Shown in Figure A-1, the basic receiver consists of a long focal length telescope, a beam splitter, anamorphic relays and single axis, image position detectors. The relays perform coordinate separation, producing X-only image motion at the X-detector, and Y-only image motion at

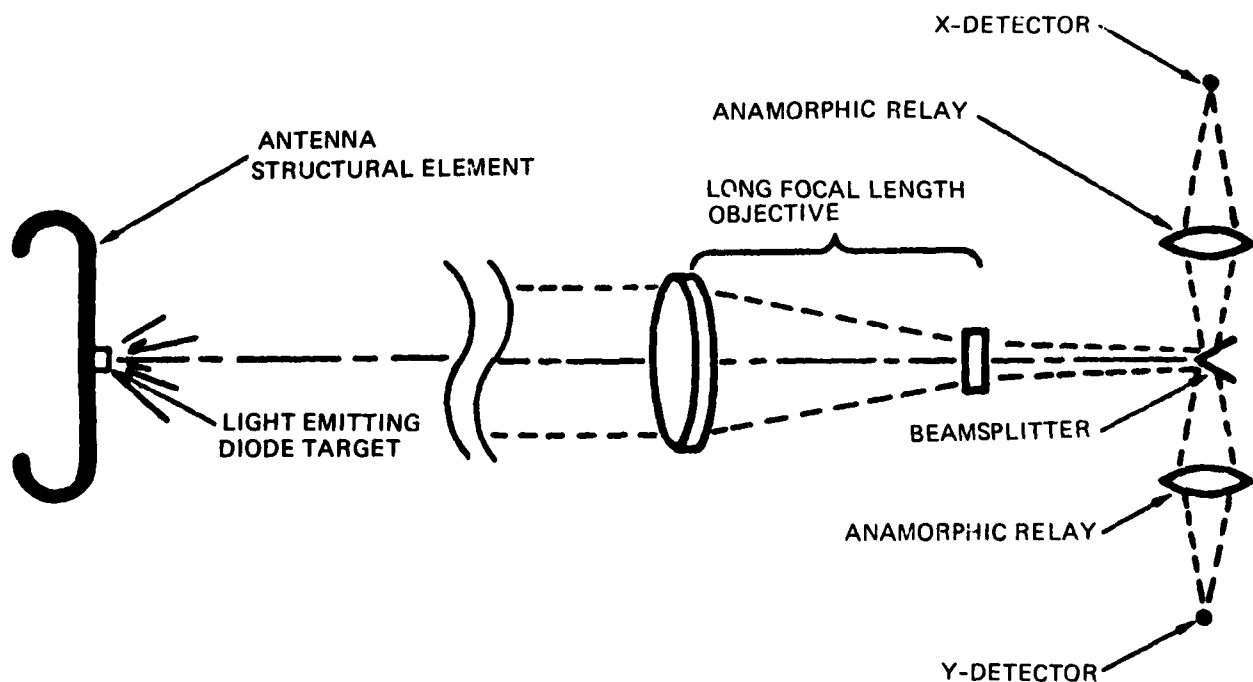


Figure A-1. Receiver Optics Schematic

the Y-detector. By the optical multiplexing techniques (not shown in the figure) the receiver capability can be expanded to accommodate, simultaneously, several targets.

Signal processing is shown in Figure A-2. The detector, a lateral effect planar diffuse silicon photodiode, produces output current signals,  $I_1$  and  $I_2$ , whose relative magnitudes depend upon the position of the image along the detector. Since the target source is modulated, the current signals are square wave, with the waveform somewhat retained during preamplification and postamplification. At the multiplexer, a sample is taken at the square wave peak (e.g.,  $x_1^+$ ) and at the trough (e.g.,  $x_1^-$ ) for both channels and the samples are converted to digital values. If the modulation frequency is  $f_m$ , then  $f_m$  pairs of values are generated each second for each channel.

The first process is to determine the peak-to-peak value of the square wave, and the second process (see Figure A-2) is to compute, for each pair

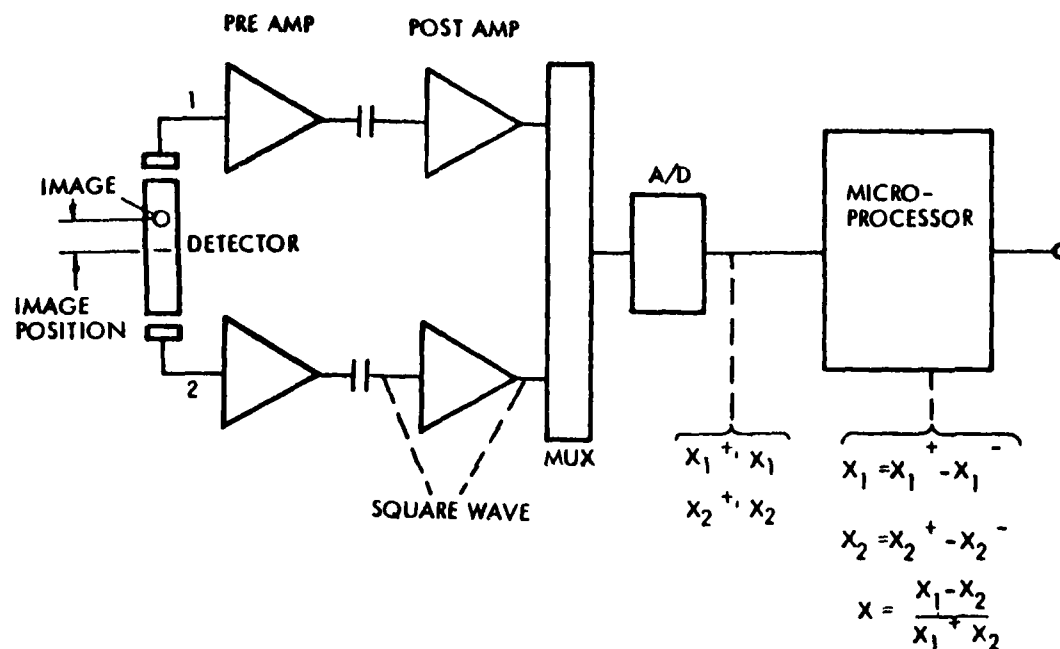


Figure A-2. Detector Signal Processing

of peak-to-peak numbers, the measured image coordinate,  $X$ . Identical processes are carried on at the  $Y$ -detector to find image coordinate,  $Y$ . These coordinates are converted to angular target excursion by a conversion constant, and then to target displacements  $(x,y)$  by multiplying by the range,  $z$ .

#### Signal Processing

- Process 1:

$$\begin{aligned} x_1 &= x_1^+ - x_1^- & y_1 &= y_1^+ - y_1^- \\ x_2 &= x_2^+ - x_2^- & y_2 &= y_2^+ - y_2^- \end{aligned}$$

- Process 2:

$$x = \frac{x_1 - x_2}{x_1 + x_2} \quad y = \frac{y_1 - y_2}{y_1 + y_2}$$

- Process 3:

$$\begin{aligned} x \text{ (target displacement)} &= k X z \\ y \text{ (target displacement)} &= k Y z \end{aligned}$$

Here,  $k$  is the conversion constant, changing the calculated  $X$  and  $Y$  values to angles,  $\phi_x$  and  $\phi_y$ . The resultant target displacements can be digitally filtered, and then transformed to normal and tangential surface deformations.

#### A.2 Conceptual Design Tradeoffs

The following conceptual design tradeoffs have been considered:

- (1) Target Maximum Excursion versus Measurement Accuracy
  - (2) Target Range versus Power at the Detector
  - (3) Target-Receiver Geometry
  - (4) Methods of Ranging
- Target Maximum Excursion versus Measurement Accuracy: The maximum deformation accepted by the sensor system has a

direct bearing upon the measurement accuracy. This dependency is invoked by the image position detector.

- Receiver: The receiver is to consist of a long focal length telescope terminated by a beamsplitter, and two anamorphic relays imaging upon single axis detectors. The relays and detectors are crossed, so that one relay-detector measures the X, or horizontal, position of the image, and the other the Y, or vertical, position of the image.
- Pre- postamplifiers: The pre- postamplifiers provide analog signal processing for the four signal channels (two from each single axis detector). These electronics are encased in a shielded housing integral with the receiver. The electrical interface is:

Signal Output:

Number of Lines: 4

Signal Voltage Range: +5 volts, at modulation frequency

Output Impedance: Less than 100 ohms

Supply: +15 volts to signal ground at +20 mA (typical)

- Targets: One active target, an LED with beam shaping optics, and one passive target, are supplied.
- LED Drive: LED drive electronics capable of driving the active target and the illuminator are supplied. The drive is controlled by a square wave control unit, and has the following output characteristics:

Frequency Range: 40 to 200 Hz square wave

Drive Current Range: 0 to 1 ampere, peak

Drive Impedance Compatible with the TI ES16C LED

In the following sections we first establish the optical configuration of the receiver and the consequent assignment of tolerances, and then describe the design accepting these tolerances.

### A.3 Receiver Optical Configuration and Tolerancing

The heart of the device is the receiver, and the driving demand upon the receiver is its optical performance. Therefore, the receiver optical design and the design tolerances are defined to become a specification for the optomechanical design of the receiver.

The receiver optics are shown schematically in Figure A-3. Note that the receiver must be set up for a specific target throw distance. If this is changed, then the objective-detector spacing,  $D_1$ , must be adjusted; and consequently the cylinder-detector spacing,  $D_2$ , must be changed to image lens L on the detector. Since a continuous adjustment capability for  $d_1$  is not feasible, the base telescope can be made with a 400 mm spacing (infinity focus), with a 40 mm spacer that provides the closeup 4.2 meter object distance. Should other object distances be required, appropriate spacers can be made. At the cylinder-detector, continuous adjustment of the spacing is available.

#### A.4 Linearity and X-Y Coupling

To ensure that the optical train, using commercially available components, performs as expected, a ray trace analysis was made. This shows that the deviation from a linear response (comparing target position to image centroid position) is less than 0.5 micrometers at the detector for the total excursion range of the target. In the central accurate measurement region, the deviation is estimated to be less than 0.1  $\mu\text{m}$ . If the axis along which the target coordinate is to be measured is termed the sensitive axis, and the axis normal to this, the insensitive axis, then the image shift in the insensitive direction (from a centerline) is a maximum of 9 micrometers for a target in any position in the total field.

#### A.5 Assignment of Tolerances

Although the receiver can be nonenvironmental, initial consideration was given to tolerances and the difficulty of maintaining measurement

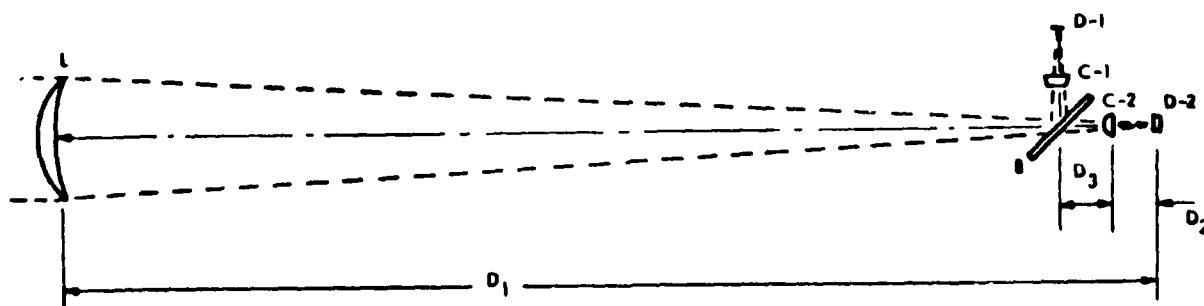


Figure A-3. SAMS DRA Phase 3 Receiver Optics

accuracy in an environment less benign than that of the laboratory. To this end, a complete sensitivity analysis of the receiver optics has been made and a tolerance budget prepared.

- Lens L: Lens axially adjustable to focus the object at detectors D-1 and D-2. Once this adjustment is made, stability should be (all values 3 signal):
  - Decenter: 0.3 m
  - Tilt: 0.3 mrad
  - Spacing: 0.1 mm
- Beamsplitter B: Beamsplitter spacing  $D_3$  to cylindrical lens is arbitrary, design optimization. After installation and alignment, stability should be:
  - Position (normal to beamsplitter surface): 0.2  $\mu\text{m}$
  - Tilt: 0.01 mrad
- Cylinder Lenses C-1 and C-2: After lens L is adjusted to image object on detector, cylinder is adjusted to image L on detector (in one axis). This is a critical, absolute adjustment, resolution better than 0.1 mm. Once the adjustment is made, stability should be:
  - Decenter: 0.3  $\mu\text{m}$
  - Tilt: 0.1 mrad (both axes)
  - Twist: 0.1 mrad
  - Spacing to Detector: 0.1 mm
- Detectors D-1 and D-2: These pair of detectors are single axis silicon photodiodes, having sensitive areas 5 mm (sensitive axis) by 2 mm (insensitive axis). Critical spacing  $D_2$  can be adjusted optionally either by moving cylindrical lens or detector.

In this budget, the centration requirements upon critical elements are unusually demanding. To maintain the optical reference axis of the receiver, the allowable lateral shift of lenses and beamsplitter is less than one wavelength of visual light.

#### A.6 Design Description

The components of the surface accuracy measurement system breadboard are (1) the receiver, (2) the passive and active targets with illuminator,

and (3) pre- and post-amplifiers and the target LED driver. This describes first the principal features of the receiver design, then touches on the target elements, and concludes with a description of the electronic support units.

#### a. Receiver design

A layout of the receiver is shown in Figure A-4. At the forward end, the meniscus objective lens is cemented to a thin-wall titanium lens cell, that in turn is supported by a multifingered aluminum support structure. The spacer shown is used for a target range of 4.2 meters. Without the spacer, the focus range is infinity. Aft of the telescope tube, a support structure similar to the lens cell support carries a miniature titanium bench on which the channel, splitting and relay optics are mounted. The Y-channel through beam illuminates a vertical axis cylindrical lens and immediately behind this a vertical axis, silicon image position detector. A similar X-channel (not shown) folded into the plane of the paper, contains a horizontal axis cylinder lens and a horizontal axis detector. Each of the detectors is connected via a short EMI shielded lead to its thermally isolated pre- post amplifier.

The SAMS breadboard hardware incorporates special mechanical features in several areas which will be critical to flight model on-orbit optical performance. The hardware includes bonded lens elements, flexural subassembly support, a thermally symmetric telescope barrel, and thermally isolated preamplifiers.

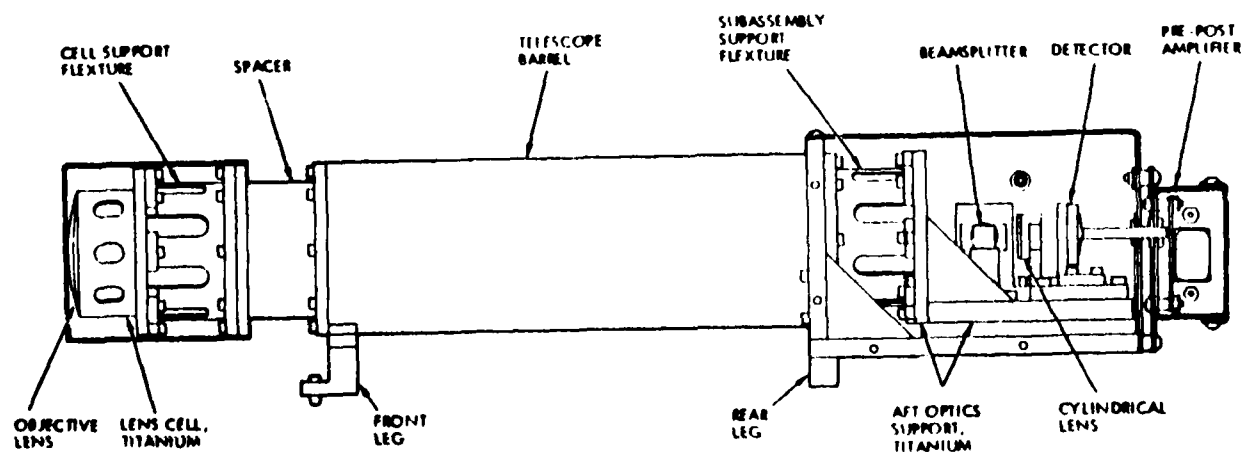


Figure A-4. Layout, Receiver, SAMS DRA Breadboard

A prime concern for flight model hardware will be to preserve optical alignment. SAMS requires each lens element to be stable in lateral position to approximately 0.3 micrometers after calibration. The design assumes that there will not be any on-orbit calibration updates. Within the limits of the program scope, the hardware has been designed to maintain the accuracy.

b. Objective lens mount

The degree of centration accuracy in supporting the long focal length objective lens places an exceedingly difficult set of requirements upon the lens support. The more conventional lens support techniques must be disqualified:

- **Adhesive-Glass Mount:** Typically the glass lens is retained in a metal support by a peripheral bond of soft adhesive cement. Through effects of thermal cycling and aging, the supporting cement will cold-flow causing decentering.
- **Metal-Glass Close-Fitting Mount:** A glass-metal fit precise to the tolerance needed will induce unacceptable stresses at the lens when the mount is thermally cycled. The thermal coefficients of the retainer and the glass cannot be precisely matched, and the thermal impedance between the glass-metal contacts is undesirably high, preventing temperature equilibration of the elements.
- **Metal-Glass Cleat Mount:** The objective lens can be retained by three or more flexible metal retainers; however, the configuration is fragile, particularly under a harsh vibration (e.g., launch environment) exposure. Moreover, the thermal impedance between the mount and the lens is undesirably high.

As a result of these considerations, a novel and somewhat unorthodox approach toward lens retention has been developed. A multifinger titanium cell (see figure A-5) provides the mechanical and thermal transition from the lens to the telescope. Since the objective lens of a flight telescope will be subjected to thermal transients due to its view of space and solar illuminated objects, transient stresses in the lens bond have been reduced by minimizing the thermal time constant between the lens and cell.

The objective lens is bonded to a titanium cell with a "rigid" thermally conductive epoxy in order to eliminate vibration induced misalignment. The coefficient of expansion of the lens matches that of the



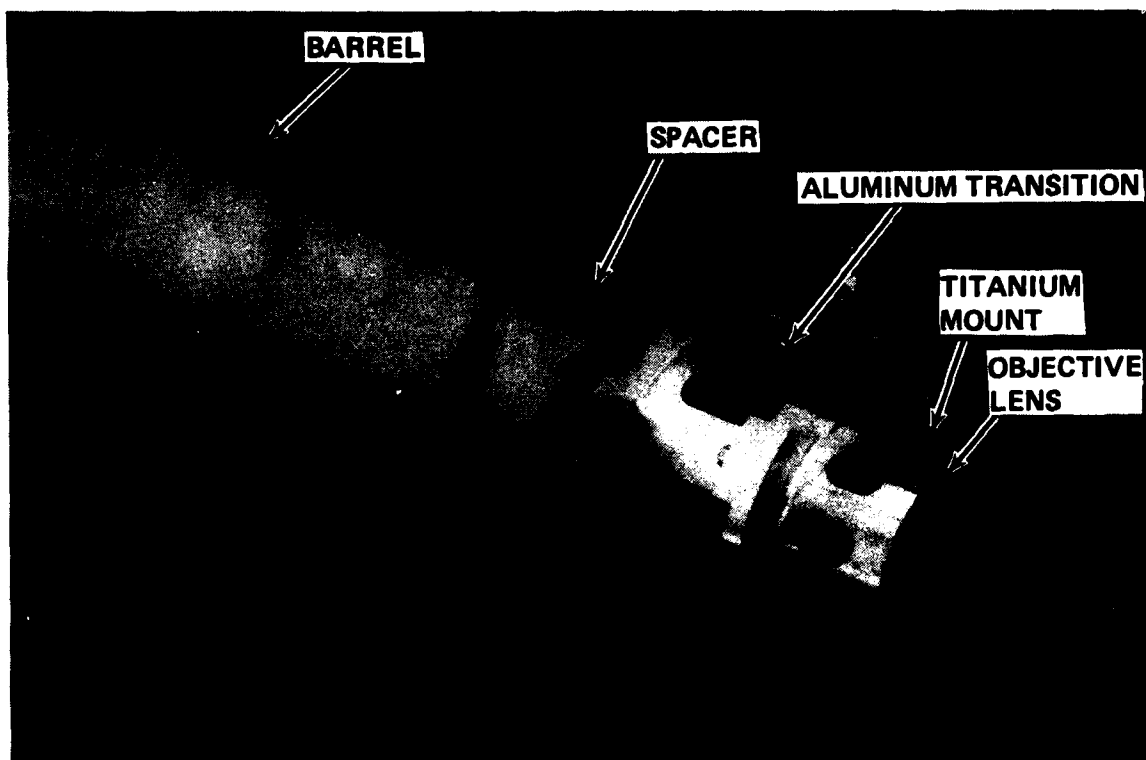


Figure A-5. SAMS Breadboard Objectives Lens Holder

titanium to reduce steady-state stresses which would otherwise result from on-orbit shifts in system mean temperature.

c. Telescope Barrel

An aluminum flexure (see Figure A-5), bolted to a focus spacer, supports the objective lens cell. The flexure provides stiff objective cell centration while accommodating thermal strain differences between the titanium cell and the aluminum telescope barrel. The flexure is designed to be thermally and elastically symmetric about the telescope optical axis.

The telescope barrel (Figure A-6) is the longest piece of hardware along the optical axis. It defines the major portion of system alignment sensitivity to lateral thermal gradients. Therefore, the barrel wall thickness has been maintained at 0.95 millimeters for the uninsulated breadboard. The resulting high lateral thermal conductivity of the aluminum tube will minimize breadboard pointing drifts due to asymmetric heat inputs such as nearby electronics, lights, etc.

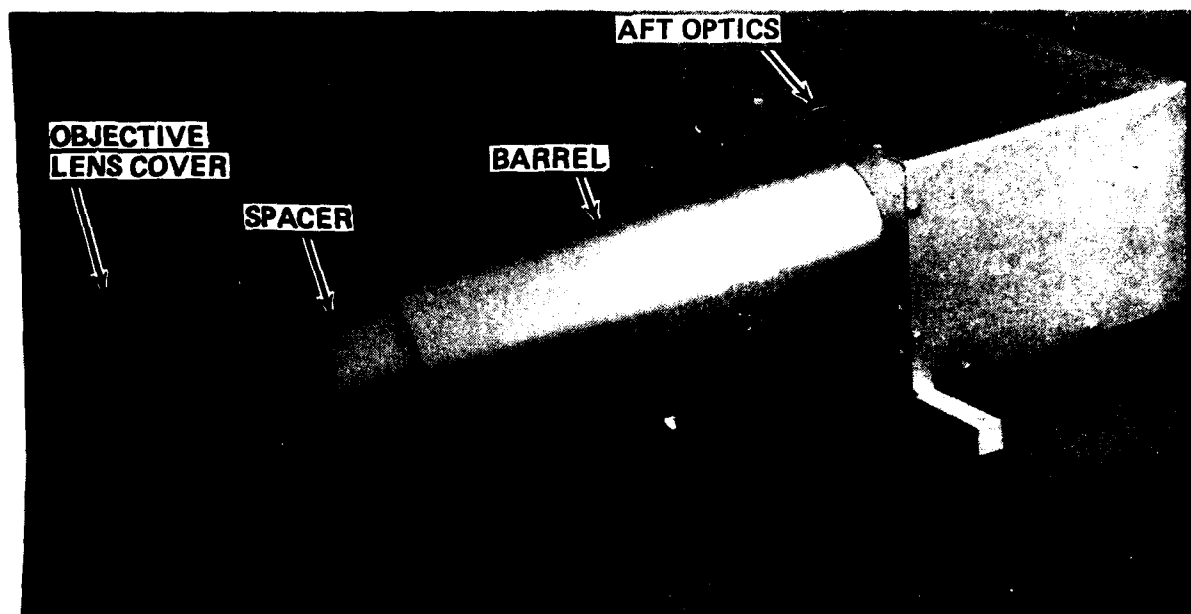


Figure A-6. SAMS DRA Breadboard Receiver

d. Aft optics

The aft optics (Figure A-7) consists of a cube beamsplitter and a pair of cylinder lenses and detectors. All of the optical elements are bonded to titanium holders. A titanium plate forms a supporting platform. The entire subassembly is bolted to the telescope barrel through an aluminum flexure.

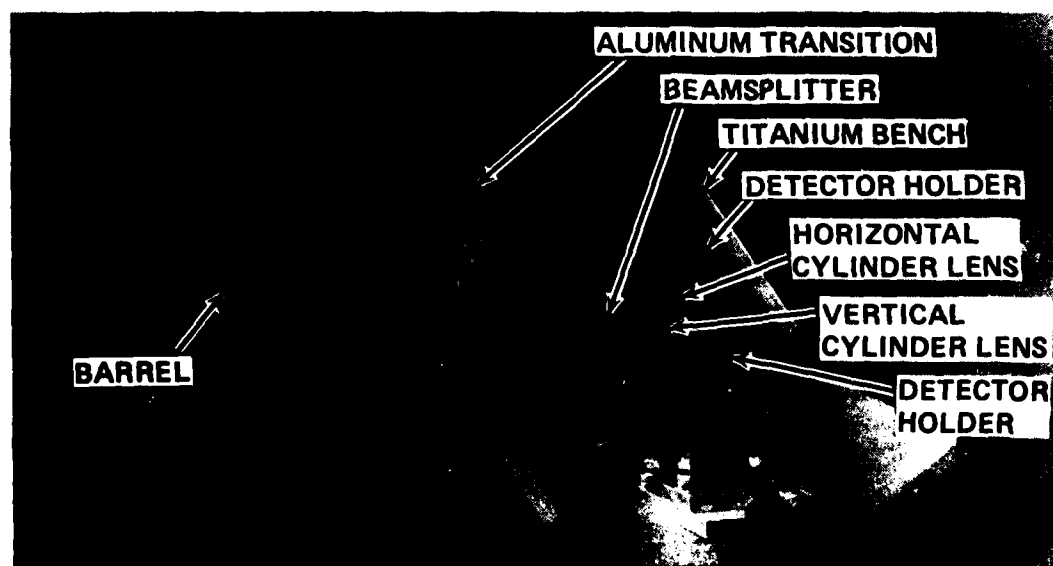
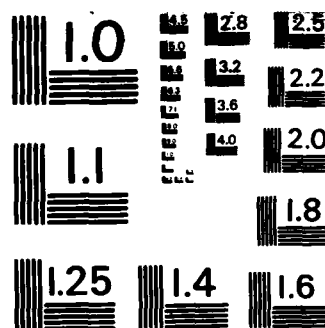


Figure A-7. SAMS DRA Breadboard Receiver Aft Optics

AD-A139 910 VIBRATION CONTROL OF SPACE STRUCTURES VCOSS B: MOMENTUM 2/2  
EXCHANGE AND TRUS. (U) TRW SPACE AND TECHNOLOGY GROUP  
REDONDO BEACH CA L BRADY ET AL. JUL 83  
UNCLASSIFIED AFMIL-TR-83-3075 F33615-81-C-3235 F/G 20/11 NL





MICROCOPY RESOLUTION TEST CHART  
NATIONAL BUREAU OF STANDARDS-1963-A

A pair of preamps are located within two shielded containers mounted on a fixed portion of the aft optics cover. The preamp containers and boards are thermally isolated from the cover.

e. Target

The operating mode target is an active LED with a beam shaping cone.

- Active Target: The active LED target is a TI ES16C component coupled to a TI 200 beam shaping cone.

f. Electronics design

Electronics designed for the device consists of (a) two dual channel pre- postamplifiers mounted at the aft end of the receiver, and (b) a LED driver.

- Pre- post-amplifier: Nominal operating frequency is 40 to 80 Hz. Since the gain of the post-amplifier pair (1556s) is unity, the overall transimpedance of the pre- post-amplifier is  $1.47 \times 10^6$  V/A. Filtering time constants introduced by the channel are:

$$t_1 = (1.47 \times 10^6) \times (100 \times 10^{-12}) = 1.47 \text{ ms (Lo Pass)}$$

$$t_2 = (200 \times 10^3) \times (1 \times 10^{-6}) = 0.2 \text{ sec (Hi Pass)}$$

$$t_3 = (15 \times 10^3) \times (0.1 \times 10^{-6}) = 1.5 \text{ ms (LOS Pass)}$$

At 40 Hz square wave input, the output waveform is essentially flat from the 50% half period to the end of the half period.

APPENDIX B

FIBER ELONGATION SENSOR

## APPENDIX B

### FIBER ELONGATION SENSOR

The purpose of the multiple fiber elongation sensor is to measure the length of strut members of high precision structures. These measurements can then be used either to monitor the structure behavior or actively control the structure. Features of the described approach are:

- Measurement accuracy to submicrometers
- Measurement rates substantially above natural frequencies of the structure
- Complete temperature compensation
- Specific compatibility with typical hollow beam, composite material members
- Use of simple, conventional, fiber optic components.

Although the approach relies upon optical interferometry, (1) unlike current absolute distance measurement techniques, it does not require a reference leg, and (2) unlike current differential distance measurement techniques, it produces absolute distances.

In the following sections we first describe the approach, and then illustrate the technique with an example.

#### B.1 Approach

The approach is shown schematically in Figures B-1 and B-2. In Figure B-1, the structural member is shown as a hollow beam, with the multiple fiber strung in tension between the beam end fittings. The fiber group consists of three or more fibers (see Figure B-2) each having different optical-mechanical-thermal characteristics. At the first end fitting, a coherent (nearly monochromatic) source introduces light into each of the fibers. At the second end fitting, the transmitted light is introduced into two interferometers measuring the relative phase between fibers #1 and #2 and between #2 and #3. Data from the interferometers is processed to yield the separation distance,  $L$ , of the end fitting stations.

In a quiescent state (say, when the sensor and member are calibrated), the measured phase shift in a given fiber is denoted here as  $\phi_0$ . The fiber



Figure B-1. Structural Member Containing F.O.I.

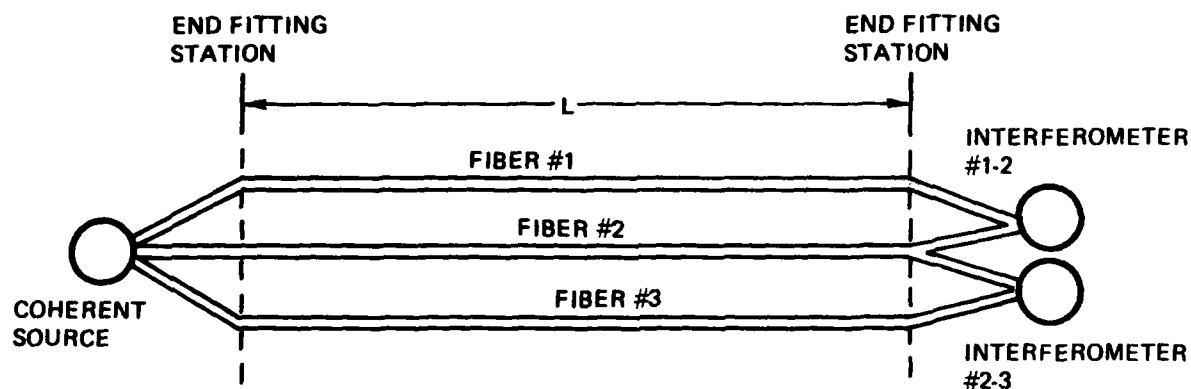


Figure B-2. F.O.I. Schematic

is at uniform temperature  $T_0$  and at stretched length  $L_0$  (calibrated length). Now the sensor-strut is exposed to a more realistic environment in which the strut length is other than  $L_0$  and the temperature may vary along the length of the strut. The phase shift through the fiber is now:

$$\begin{aligned} \phi &= \phi + \Delta\phi = \phi_0 + a \sum_i^n \Delta L_i + b \sum_i^n \Delta L_i (T_i - T_0) \\ &= \phi + a \Delta L + b \sum_i^n \Delta L_i (T_i - T_0) \end{aligned}$$

where  $a$  and  $b$  are constants that include the mechanical, optical, and thermal properties of the fiber.



The fiber length,  $L$ , is divided into a number of segments ( $\Delta L_i$ ) sufficiently fine grain to ensure that the temperature can be assumed to be constant along each segment.

For three factors with different materials characteristics, the resultant phases (assuming the same temperature distributions along each fiber) are:

$$\text{Fiber \#1: } \phi_1 = \phi_{01} + a_1 \Delta L + b_1 \Delta L - T$$

$$\text{Fiber \#2: } \phi_2 = \phi_{02} + a_2 \Delta L + b_2 \Delta L - T$$

$$\text{Fiber \#3: } \phi_3 = \phi_{03} + a_3 \Delta L + b_3 \Delta L - T$$

where

$$\Delta L - T = \sum_i^n \Delta L_i (T_i - T_0)$$

Interferometer 1-2 reads the phase difference between fiber #1 and #2; that is:

$$\Delta\phi_{12} = \phi_1 - \phi_2 = (\phi_{01} - \phi_{02}) + (a_1 - a_2) \Delta L + (b_1 - b_2) \Delta L - T$$

And interferometer 2-3 reads,

$$\Delta\phi_{23} = \phi_2 - \phi_3 = (\phi_{02} - \phi_{03}) + (a_2 - a_3) \Delta L + (b_2 - b_3) \Delta L - T$$

It is apparent that if the coefficients are nonzero, the equations can be solved for  $L$ . Since the initial  $L = L_0$ , represented by the terms is shown by calibration, the member length is determined:

$$L = L_0 + \Delta L$$

## B.2 Example Performance

An example application is given here, in which the strut length is 20 meters, the fiber diameters are all 2 micrometers, and the fiber materials are fused silica ( $\text{SiO}_2$ ), dense flint glass ( $\text{SF}_4$ ), and titanium crown glass (TiK1). Characteristics assumed for these materials are:

Material	Index	Poisson's Ratio	Strain-Optics Coefficients		Temp. Coef. of Index
			P11	P12	
$\text{SiO}_2$	1.455	0.17	0.121	0.270	$10 \times 10^{-6}$
$\text{SF}_4$	1.740	0.241	0.232	0.256	$6.4 \times 10^{-6}$
TiK1	1.472	0.254	0.25	0.30	$-3.7 \times 10^{-6}$

For working wavelength of 0.8 micrometer, the estimated outputs from the interferometers are:

$$\Delta\phi_{12} = -1.837 \times 10^6 \Delta L + 28.274 \Delta L - T$$

$$\Delta\phi_{23} = 1.25 \times 10^6 \Delta L + 79.33 \Delta L - T$$

And by processing,

$$2.806 \Delta\phi_{12} - \Delta\phi_{23} = -6.4 \times 10^6 \Delta L$$

That is, one micrometer change in length causes 6.4 radians, or about one fringe change. This is readily measurable.

## B.3 Discussion

While the sensitivity to length change as illustrated by the example is adequate, it is noted that the temperature effects are large and compensation, therefore, must be precise. The term  $79.33 \Delta L - T$ , for instance, amounts to about  $1590 \Delta T$  for a length of 20 meters. That is, a temperature change of  $0.01^\circ$  causes 15.9 radians phase change, or the equivalent of about 2.5 micrometer length. This aspect of the approach will have to be evaluated by experiment.

#### B.4 Dimensional Characteristics of a Single Fiber

For this analysis, we assume that the single fiber is unclad and stretched the length of the strut. Its length is thereby determined by the strut length. The diameter of the fiber will change with both stretched length and with temperature, and this change will affect the propagation of the light through the fiber. Here, we define the effect of temperature and stretching upon the fiber diameter; the importance of this effect will be evaluated later.

In the initial benign condition, before installation within the strut, the fiber is assumed to have these properties:

Length:	$L_0$
Diameter:	$D_0$
Temperature:	$T_0$
Poisson's ratio:	$\mu$
Young's modulus:	$E$

The coordinates are X-axis along the fiber length and Y- and Z-axes symmetrical lateral to the length. Fiber cross section is taken to be circular.

#### B.5 Change in Diameter with Length, at Constant Temperature

When the fiber is stretched and installed at the strut, the resultant strain is:

$$\epsilon_x = \frac{L - L_0}{L} = \frac{\Delta L}{L}$$

The resultant fiber diameter is:

$$D = D_0 (1 - \mu \epsilon_x)$$

Consequently, the initial conditions for the installed fiber are:

$$\text{Length} = L = L_0 + \Delta L = L_0 (1 + \epsilon_x)$$

$$\text{Width} = D = D_0 (1 - \mu \epsilon_x)$$

$$\text{Temperature} = T_0$$

After installation, the fiber propagation is calibrated, so these become the base conditions from which changes are to be determined. If the strut does not expand by  $\Delta L = \epsilon_X L$ , then the corresponding change in fiber diameter is  $\Delta D' = -\mu \epsilon_X D$ .

#### B.6 Change in Diameter with Temperature, Constant (Length)

If, prior to installation, the fiber's temperature is changed to  $T_0 + \Delta T$ , then its benign dimensions are:

$$\text{Length} = L''_0 = L_0 (1 + \alpha \Delta T)$$

$$\text{Width} = D''_0 = D_0 (1 + \alpha \Delta T)$$

where  $\alpha$  is the fiber temperature coefficient of expansion.

In the strut, this fiber is constrained to length  $L$ ,

$$L = L_0 (1 + \epsilon_X'' + \alpha \Delta T)$$

Obviously, the mechanical stretch, or strain, is less with the expanded fiber. The effect of this temperature change on the fiber diameter is:

$$D''_0 = D_0 (1 + \alpha \Delta T - \mu \epsilon_X'')$$

For the base condition, at temperature  $T_0$ ,  $L = L_0 (1 + \epsilon_X)$ ,

$$\epsilon_X'' = \epsilon_X - \alpha \Delta T$$

and

$$\begin{aligned} D''_0 &= D_0 (1 + \alpha \Delta T + \mu \alpha \Delta T - \epsilon_X) \\ &= D_0 (1 + \alpha \Delta T (1 + \mu) - \epsilon_X) \end{aligned}$$

The second term is the change in fiber diameter with change in temperature.

### B.7 Propagation Characteristics in a Single Fiber

We assume that the fiber is unclad and stretched to a confined length,  $L$ . If the propagation constant within the fiber is  $\beta$ , then the phase change of light traversing the fiber is,

$$\phi = \beta L \text{ radians}$$

The propagation constant is determined by the fiber index of refraction (i.e., the velocity of light in the medium) and the fiber diameter (defining the waveguide dispersion). Therefore, the change in phase with change in fiber length and propagation constant is:

$$\Delta\phi = L \Delta\beta + \beta \Delta L$$

where

$$L \Delta\beta = L \cdot B_n \Delta n + L B_D \Delta D$$

Both the index ( $n$ ) and the fiber diameter ( $D$ ) are sensitive to strain and to temperature. The purpose of this analysis is to define these effects on phase and to estimate their magnitudes.

### B.8 Effect of Optical Index on Phase

The phase change due to variation in the index of refraction is  $LB_n \Delta n$ , where the phase coefficient is  $B_n = d\beta/dn$ . Neglecting waveguide dispersion the propagation constant  $B = k_0 h$  where  $k_0$  is the propagation constant in vacuum and  $n$  is the index of refraction. Therefore,

$$B = d\beta/dn = k_0 = 2\pi \nu/c$$

$$\nu = \text{frequency of the light}$$

$$c = \text{velocity of light in a vacuum}$$

The change in index,  $\Delta n$ , occurs with a change in fiber length (photo-elastic effect) and with a change in fiber temperature:

$$\Delta n = \frac{dn}{dL} \Delta L + \frac{dn}{dT} \Delta T = \Delta n_L + \Delta n_T$$

From the strain-optic tensor, it can be shown that

$$\Delta n_1 = -\frac{1}{2} n^3 \epsilon_X \left[ (1 - \mu) P_{12} - \mu P_{11} \right]$$

$\mu$  = Poisson's ratio

$\epsilon_X$  = strain in X-direction

$P_{11}, P_{12}$  = strain-optics tensor coefficients

And the change in index with temperature is simply,

$$\Delta n_T = C_{nT} \Delta T$$

$C_{nT}$  = temperature coefficient of refractive index

In summary, the change in phase due to index change is

$$\Delta \phi_n = L B_n \Delta n = L k_o \left\{ -\frac{n^3 \epsilon_X}{3} \left[ (1 - \mu) P_{12} - \mu P_{11} \right] + C_{nT} \Delta T \right\}$$

#### B.9 Effect of Fiber Diameter on Phase

The change in diameter of the fiber due both to strain and temperature is:

$$\Delta D = -\mu D \epsilon_X + D \alpha (1 + \mu) \Delta T$$

where

$\mu$  = Poisson's ratio

$\epsilon_X$  = strain along fiber axis

$\alpha$  = temperature coefficient of linear expansion

The phase change induced by the diameter is,  $\Delta\phi_D = L B_D \Delta D$ . The phase coefficient,

$$B_D = \frac{d\beta}{dD} = \frac{V^3}{2\beta D^3} \left( \frac{db}{dV} \right)$$

where  $b$  and  $V$  are normalized parameters describing the waveguide mode, and  $db/dV$  is the slope of the  $b, V$  dispersion curve at the operating point.

In summary, the phase change from fiber diameter is:

$$\Delta\phi_D = L \left[ \left( \frac{V^3}{2\beta D^3} \right) \frac{db}{dV} \right] \left[ -\mu D \epsilon_x + D \alpha (1 + \mu) \Delta T \right]$$

#### B.10 Estimate of Magnitudes

Phase change due to  $\Delta L/L = \epsilon_x$  has three contributions: (a) from the physical length change of the fiber, (b) from the index change, and (c) from the diameter change:

$$(a) \quad \Delta\phi = L k_0 n \epsilon_x$$

$$(b) \quad \Delta\phi = L k_0 n \epsilon_x \left\{ -\frac{n^2}{n} \left[ (1 - \mu) P_{12} - \mu P_{11} \right] \right\}$$

$$(c) \quad \Delta\phi = L k_0 n \epsilon_x \left[ \left( -\frac{V^3}{2\beta^2 D^2} \right) \frac{db}{dV} \mu \right]$$

Assigning the following typical glass values to the above parameters, we can arrive at approximate phase conditions:

$$n = 1.5$$

$$db/dV = 0.5$$

$$\mu = 0.25$$

$$\lambda = 0.8 \times 10^{-6} \text{ m}$$

$$P_{11} = P_{12} = 0.25$$

$$K_0 = 7.85 \times 10^6 \text{ m}^{-1}$$

$$D = 2 \times 10^{-6} \text{ m}$$

$$\beta = 1.15 \times 10^7$$

$$V = 2.5$$

$$\Delta\phi = 1.0 (L k_0 n) \epsilon_x$$

$$\Delta\phi = -0.14 (L k_0 n) \epsilon_x$$

$$\Delta\phi = 0.0017 (L k_0 n) \epsilon_x$$

As can be seen, the effect of diameter change causes less than 0.5% of the total contribution, and can, for purposes of this analysis, be neglected.

The temperature contributions to phase change are: change due to index and change due to fiber diameter.

$$\Delta\phi = L k_0 (C_{nT}) T$$

$$\Delta\phi = L k_0 \left[ \left( \frac{V^3}{2k_0^2 n D^2} \right) \frac{db}{dV} \right] [\alpha (1 + \mu)] \Delta T$$

Using the approximate parameters for glass assumed above and letting the temperature coefficient of expansion be  $5 \times 10^{-6}$ , we get the phase sensitivities as:

$$\Delta\phi_d = 10^{-5} (L k_0) \Delta T$$

$$\Delta\phi_e = 1.3 \times 10^{-7} (L k_0) \Delta T$$

Again, the contribution from diameter change is small; here about a percent of the total change.



### B.11 Summary

The phase behavior of the fiber can, thus, be expressed as:

$$\Delta\phi = Lk_0 n \left\{ 1 - \frac{n^2}{2} \cdot \left[ (1 - \mu) P_{12} - \mu P_{11} \right] \right\} \epsilon_x + Lk_0 (C_{nT}) \Delta T$$

With the acknowledgement that the conversion constants for  $\Delta T$  will be modified by a percent or so by the inclusion of waveguide dispersion effects.

## REFERENCES

1. R.P. Iwens, et al, "ACOSS-8, Phase II - TRW," RADC-TR-81-242, September 1981.
2. R.B. Benhabib, et al, "ACOSS-14 Final Technical Report," RADC-TR-83-51, November 1982.
3. M.H. Gran, et al, "Vibration Control of Space Structures (VCOSS) Interim Technical Report", July 1, 1982.
4. A.G.J. MacFarlane, et al, "Complex Variable Method for Multi-variable Feedback System Analysis and Design," Alternatives for Linear Multivariable Control, NEC, Illinois, 1978.
5. A.G.J. MacFarlane, and B. Kouvaritakis, "A Design Technique for Multivariable Feedback Systems," Int. J. Control, 25, 837-874, 1977.
6. T. Henderson, "VCOSS Design Model — NASTRAN Printout," The Charles Stark Draper Laboratory, Inc., November 12, 1981.
7. T. Henderson, "VCOSS Design Model and Disturbance," The Charles Stark Draper Laboratory, Inc., November 12, 1981.
8. R. Strunce, et al, "VCOSS PSD Disturbance," The Charles Stark Draper Laboratory, Inc., March 1982.
9. H.W. James, N.B. Nichols and R.S. Phillips, Theory of Servomechanisms, MIT Rad, Lab. Series, Vol. 25, McGraw-Hill, New York, 1947.

END

FILMED

5-84

DTIC